A MICRO SEAFLOOR MARINE CURRENT ENERGY CONVERSION SYSTEM

MD NAHIDUL ISLAM KHAN

A MICRO SEAFLOOR MARINE CURRENT ENERGY CONVERSION SYSTEM

A thesis presented to the School of Graduate Studies of Memorial University of Newfoundland in partial fulfillment of the requirement leading to the award of a Master of Engineering in ELECTRICAL ENGINEERING

By

© MD NAHIDUL ISLAM KHAN

Department of Electrical Engineering

Faculty of Engineering & Applied Science

Memorial University of Newfoundland

July 17, 2008

Abstract

The Seaformatics project is a five year AIF project that intends to develop to a proof-of-concept seafloor array of wireless marine sensors for use in monitoring seabed processes, including applications such as geological imaging and earthquake detection. Individual low cost sensor pods will be self-powered through ocean bottom currents and will be able to communicate with each other and to the Internet through surface master units to facilitate observation of the ocean floor from shore.After examining the available systems, it was decided that the Savonius rotor was most appropriate. Models were constructed and tested in the wave tank and the wind tunnel at MUN.Scaling Laws that could be used to predict full scale or prototype behaviour were developed.

A micro sea-floor power generation system has been designed and developed at Electrical Energy System Lab of Memorial University of Newfoundland to extract few watts electrical power. The proposed power generation system consists of a drag type Savonius rotor, a gear box, a permanent magnet generator, a controlled DC-DC converter, batteries for energy storage, instrumentation and a micro controller based control system for the turbine. Micro controller will control the DC-DC converter to extract the maximum power from the system. Such a control scheme will be based on the voltage, current and speed measurement of the system. Maximum power algorithm based control scheme will ensure that the system is always extracting the maximum power from the water current. This thesis aims to develop a technical and economical viable marine current energy conversion system.

Dedication

I would like to dedicate my thesis
to my beloved grandparents

Acknowledgements

Several people were instrumental in the completion of this work and the least I can do to show them my appreciation is to acknowledge them. This research has been supported by an Atlantic Innovation Fund and 'Seaformatics'.

I would like to thank my supervisor, Dr.Tariq Iqbal for introducing me to the field of Marine Energy Technology, keeping me on the right track and also helping me in this research work when I was facing some unexpected challenges.Dr.Iqbal has been a wonderful mentor and role model and is very generous to share his seemingly endless knowledge and experiences in the field.He initiated the founding ideas behind this thesis and provided insight and valuable information into many of the problems that were encountered. I am grateful to him for always being kind and patient with his suggestions, and I thank him for all of his support during this thesis.

I would like to thank my co-supervisor, Dr.Michael Hinchey for his advice, encouragement and unwavering optimism. Dr.Hinchey is another individual whose encouragement was instrumental in my pursuing of this degree. His growing research interests and his will to share his knowledge and experience with me were motivational towards the accomplishment of my task. His positive attitude throughout the duration of this thesis always put things into perspective whenever difficulties arose.

I would like to thank the technical service staff who manufactured the 'prototypes' turbines'. Thanks to Paul Bishop and Brian Pretty assisted me to test it in the Tow Tank and Wind Tunnel. I had the opportunity to meet and work with these two great

individuals and I learnt so much during that time. In addition I would like to express my appreciation to Dr. Vlastimil Masek for the immense support and encouragement during my work.

There are many other people that have contributed directly or indirectly to this thesis. Some acting as sounding boards, sources of information, or providing resources that contributed to the development of my electronics. While their individual contributions have been small, their efforts have still been greatly appreciated.

I would like to thank my parents Nusrat Khan and G.K.M Nazrul Islam Khan, my loving younger sister Farzana Khan, my grandfather Abdul Majid Khan, and the rest of my family for their endless love, support and encouragement throughout my entire academic career. My father has given me lot of mental support and guidance to go ahead during my hard time. His scientific comments helped me a lot to recover the obstacles. Finally, I would like to thank my wife Israt Jahan Khan for being so understanding and patient while I followed this dream. The year that we were apart was challenging, and I can only hope that she knows how much her moving to Newfoundland for me has meant. Both of our families have been far away from us these past two years, but they are closer than ever in my mind and heart.

Table of Figures

List of Tables

List of Symbols

Mechanical Parameters

$A = DH$	swept area of the rotor
H	height of rotor
$Power = T\,\omega$	hydrodynamic power
$C_P = \frac{Power}{\frac{1}{2}\times\rho\times A\times V^3}$	power coefficient
N	rotational speed
T	torque
$U = \omega R$	peripheral velocity
V	water current
$\lambda = \frac{U}{V}$	velocity coefficient
ω	angular velocity
d	bucket diameter
D	diameter of the rotor
D_f	diameter of the endplate
e	gap between the two bucket
H	height of the rotor
R	radius of the rotor: R = D/2
$\alpha = \frac{H}{D}$	aspect ratio
$\beta = \frac{e}{d}$	overlap ratio
$C_S = \frac{S}{ND}$	flow coefficient

$C_P = \frac{Power}{\rho D^5 N^3}$	power coefficient
ρ	density of the medium
Q	volumetric Flow

Electrical Parameters

I	Current
V	Voltage
P	Power
L	Inductance
C	Capacitance
R	Resistance
D	duty cycle
f	frequency
n	efficiency
p	number of poles

A Micro Seafloor Marine Current Energy Conversion System

Table of Contents

Chapter 1

Introduction

1.0 Background

Currently most of the world's energy demand is met by fossil fuels with their attended devastating effects on the environment, most notably the emission of carbon dioxide (CO_2) leading to climate change. According to Kyoto agreement countries agreed to reduce the emission of greenhouse gases to the atmosphere [1]. Also according to the *International Panel on Climate Change* (IPCC), atmospheric concentrations of CO_2 resulting from burning of fossil fuels and deforestation have increased by more than one third in the past 150 years and are at the highest levels for at least the past 420,000 years (Singer 2003). Fossil fuels that took 200,000 years to be formed by geological processes are now being burned in one year. Therefore, efforts should be made to meet the present and future energy demands cleanly and efficiently. To provide a sustainable power production in the future and at the same time respecting the Kyoto protocol, there is a growing demand for energy from renewable sources such as wind, geothermal, solar and ocean.

The oceans cover 75% of the world surface and as such ocean energy is a global resource. There are different forms of renewable energy available in the oceans: waves, currents, thermal gradients, salinity gradients, the tides and others. Ways to exploit these high energy densities resources are being investigated worldwide. Renewable energy sources, most notably, wind energy, solar energy and small scale hydro power schemes have undergone major developments. Their potential to meet the world's energy demand for

the 21st century and beyond, cleanly, safely and economically is high. However the intermittency and weather dependency of most of them still poses a challenge and calls for extensive and diligent research and development effort. One other form of renewable energy which has attracted some interest is marine current or tidal stream energy. This energy resource has a potential to be exploited on a large scale because of its predictability and intensity. It is most likely to be the new clean energy alternative for the 21st century.

1.1 Marine Current Energy

Energy conversion from marine currents is quite similar to that of wind energy conversion but there are also several differences between them. The underwater placement of a marine current energy converter (MCEC) gives some advantage such as no noise disturbance for the public, low visual exposure and little use of land space but also adds some challenges like the need for water and salt proof technology, difficult and costly maintenance etc. Ocean current speeds are much lower than wind speeds. This is important because the kinetic energy contained in flowing bodies is proportional to the cube of their velocity. However, another more important factor in the power available for extraction from a flowing body is proportional to the density of the material. Water is about 900 times denser than wind, so for the same area of flow being intercepted, the energy contained in a 12 mph water flow is equivalent to that contained in an air mass moving at about 110 mph. Thus, ocean currents represent a potentially significant, currently untapped, reservoir of energy. The total worldwide power in ocean currents has been estimated to be about 5,000 GW, with power densities of up to 15 kW/m^2. Ocean-

current generated energy technologies have many favourable characteristics, including the following:

- Water currents have a relatively high energy density.
- Some ocean currents are relatively constant in location and velocity, leading to a large capacity factor (fraction of time a system is actively generating power) for the turbines.
- Because they are installed beneath the water's surface, water turbines have minimal visual impact.

There are also some challenges associated with higher density e.g. turbulence which gives high strain on the turbine. A final characteristic to highlight is the relatively high degree of utilization, tidal streams are likely to have a utilization factor up to 40-50 % and currents of more constant nature are likely to have a utilization factor up to 80 % [2]. For wind power the corresponding utilization factor is usually between 25-30% in most places. The utilization factor is defined as the actual annual energy output divided by the theoretical maximum and is dependent on the rated power of the installed device [3]. A high utilization factor is important to achieve an economically viable power production [4,5]. A drawback with marine currents as an energy source is that the water currents usually have a low velocity that rarely exceed 5 m /s [6-10]. Lower current velocities results in low turbine speeds, thus, if a conventional generator were used to produce electricity, a gearbox becomes essential to achieve higher rotor speeds. It is important to note that gearboxes contribute to mechanical losses and require maintenance regularly to avoid power generation failures. From the perspective of reliability and economics, a

simple energy conversion system with minimum maintenance is desirable when the device is placed off-shore.

1.2 Modes of Operation

Underwater Turbines are used to harness the kinetic energy in moving water. Basically three steps are involved in the energy transformation as in Figure 1.1.

The turbine rotor is driven by the current. This converts the energy of the current into rotational energy of the shaft. The output power of turbine is optimized by adjusting the angle between the rotor blades and the current vector (pitch control).

The gearbox converts the low rotational speed of the turbine shaft to the desired higher speed of the generator shaft.

The generator converts its shaft rotational energy to electric energy which is transmitted to the shore via a cable on the seabed or used to power underwater equipment.

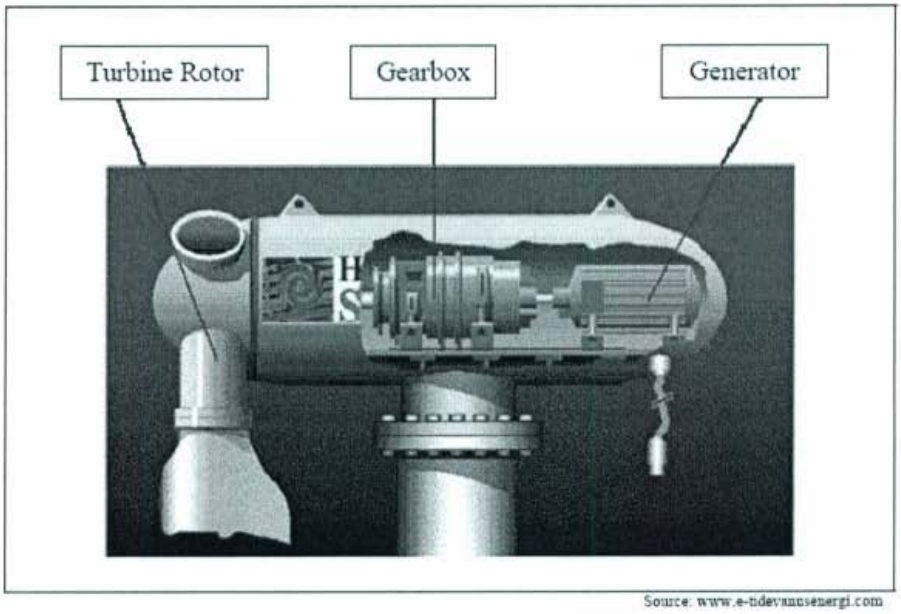

Figure 1.1 Principal components of a marine current turbine

1.3 Support Structure Concepts

A key requirement for the turbines is to hold them reliably in place taking into consideration the harsh marine environment. Currently there are three options as shown in Figure 1.2 which is under consideration. The types of turbines being considered are propeller.

Gravity Structures are substantial steel or concrete mass attached to the base of the units to achieve stability by their own inertia.

Piled Structures are pinned to the seabed by one or more steel or concrete beams. The beams or piles are fixed to the seabed by hammering if the ground conditions are sufficiently soft or by pre-drilling, positioning and grouting if the rock is harder. The simplest form of piled structures is a single pile penetrating the seabed with the turbine fixed to the pile at the desired depth of deployment. The pile may stick out on the water surface or below.

Floating Structures provide a more credible solution for deep water locations. In this case the turbine unit is attached to a downward pointing vertical beam rigidly fixed to a barge. The barge is then moored to the seabed by chains or wire or synthetic ropes which may be fixed to the seabed by drag, piled or gravity anchors, depending on the seabed condition.

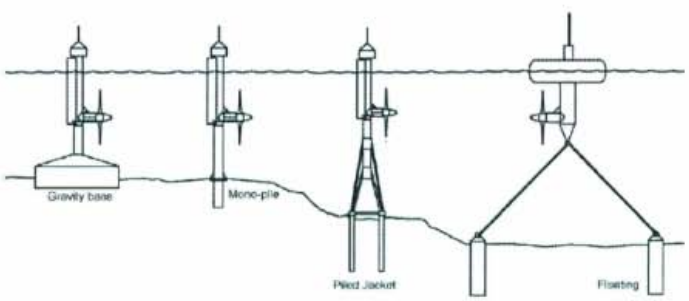

Figure 1.2 Support structure concepts

Monopile Installation is an already established technique and seems to be the most favored option. However this is currently limited to depths less than 50 m considering the capabilities of available jack-up barges (Fraenkel, 2004).

1.4 Study of Ocean Current in Atlantic

The circulatory system of the surface waters of the Atlantic can be depicted as two large gyres, or circular current systems, one in the North Atlantic and one in the South Atlantic. These currents are primarily wind driven, but are also affected by the rotation of the earth. The Atlantic receives the waters of many of the principal rivers of the world, among them the Saint Lawrence, Mississippi, Orinoco, Amazon, Paraná, Congo, Niger, and Loire, and the rivers emptying into the North, Baltic, and Mediterranean seas. Nevertheless, primarily because of the high salinity of outflow from the Mediterranean, the Atlantic is slightly more saline than the Pacific or Indian oceans.The Atlantic Ocean may be described as a bed of water colder than 9°C (48° F)-the cold-water sphere-within, which lays a bubble of water warmer than 9° C-the warm-water sphere. Data of current flows at various depths in Atlantic Ocean for more than one year collection is analyzed to determine the change in flows as shown in Fig. 1.3.

Figure 1.3 also shows histograms of one-year hourly water current speed data recorded at four depths of Atlantic Ocean in east of St. John's. The average speed is very low and its variations over a year are significant. This makes it really challenging to extract sufficient amount of electrical power from ocean floor current.

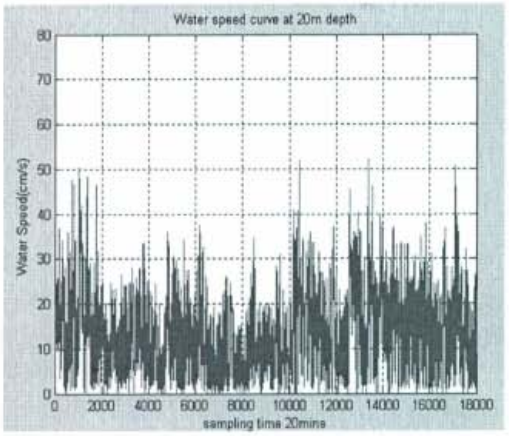
Water speed curve at 20m depth
Water Speed(cm/s)
sampling time 20mins

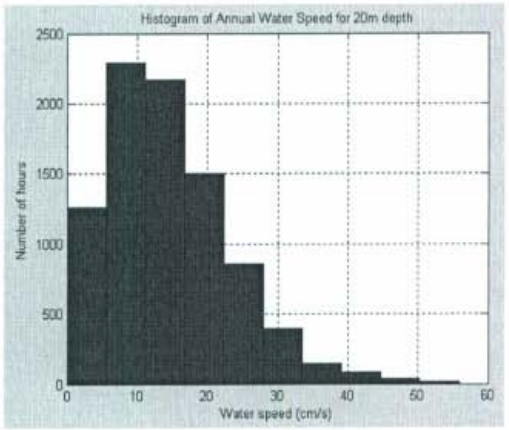
Histogram of Annual Water Speed for 20m depth
Number of hours
Water speed (cm/s)

(a)

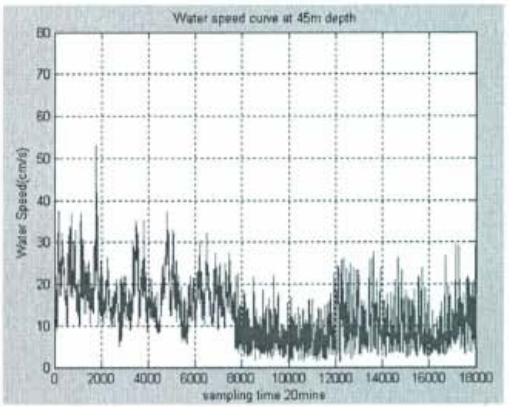
Water speed curve at 45m depth
Water Speed(cm/s)
sampling time 20mins

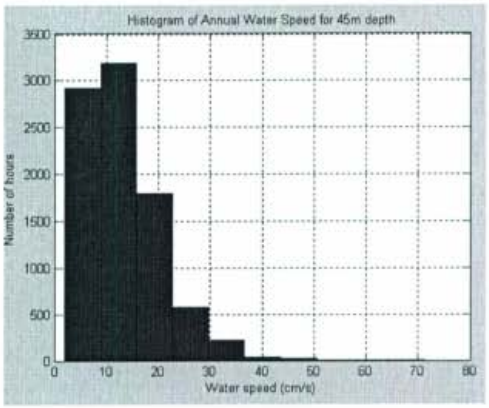
Histogram of Annual Water Speed for 45m depth
Number of hours
Water speed (cm/s)

(b)

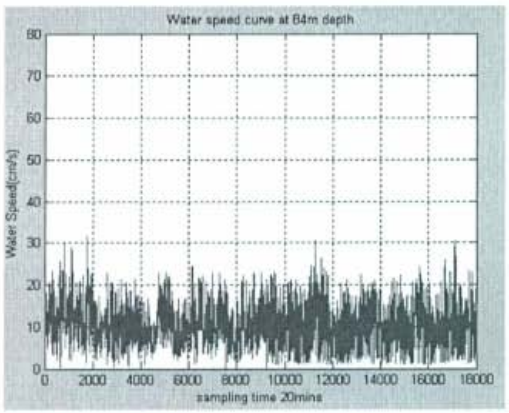
Water speed curve at 84m depth
Water Speed(cm/s)
sampling time 20mins

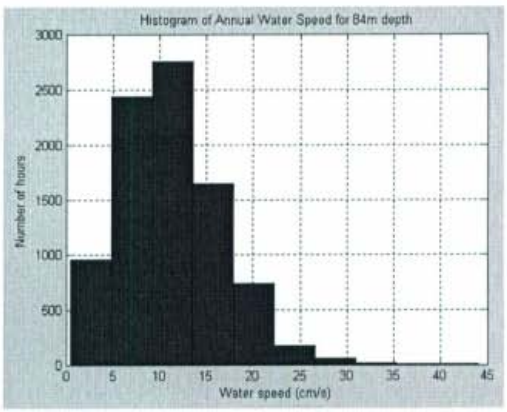
Histogram of Annual Water Speed for 84m depth
Number of hours
Water speed (cm/s)

(c)

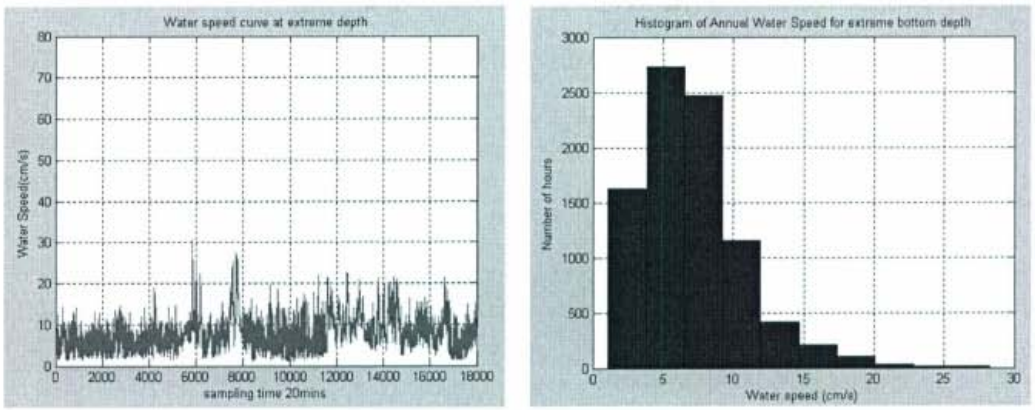

(d)

Figure 1.3 (a, b, c &d) Water current speed variations and histogram at four depths over a period of more than a year.

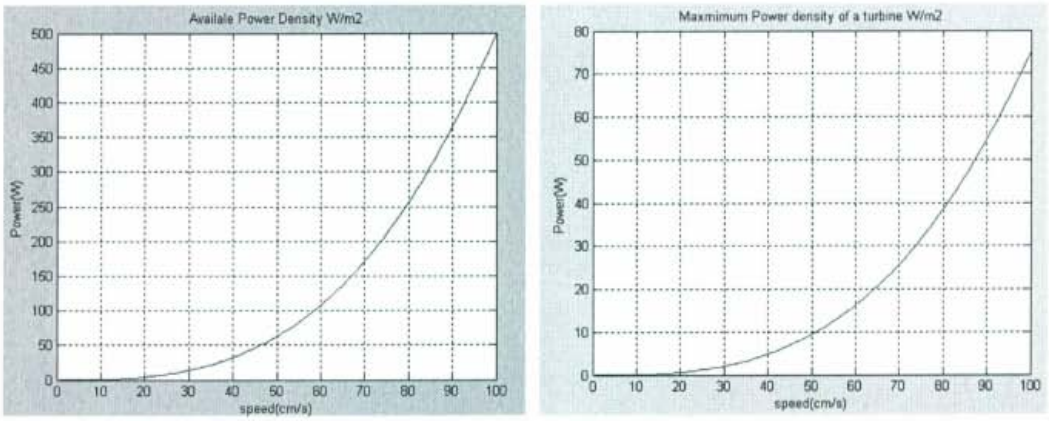

Figure 1.4 Available and maximum extractable power density from water current

Figure 1.4 shows available power density of water current as a function of flow speed. It also shows how much maximum of available power density can be extracted. It is based on a reasonable assumption that turbine power coefficient will be about 0.15 because the efficiency of turbine is usually less than 20%.

Table 1.1 Expected Output of Power Generation System

Depth(m)	Average Flow Speed (cm/s)	Maximum available power density (W/m^2)	Extractable Power with a turbine (W/m^2)	Maximum available energy density in a year (Whr/m^2)	Extractable energy density in a year (Whr/m^2)
20	14.6070	1.5583	0.2337	152195.0	23169.0
45	13.2005	1.1501	0.1725	44045.0	5954.0
84	11.2233	0.7069	0.1060	109590.0	15906.0
Near Bottom	7.0555	0.1756	0.0263	98465.0	14268.0

It is observed that extractable power per square meter is very small due to the low water current speed. The average speed is very low and its variations over a year are significant. From table 1.1, we can say that, to produce say 1W output at a depth of 84m we need a turbine with an apparent area of $10m^2$. In addition it is not possible to design a direct driven system in such a low flow of water. Based on the above analysis we can conclude that either we use turbine at a site where flow speed is higher or reduce power consumption in signal conditioning circuits to a minimum possible.

1.5 Marine Current Energy Conversion System

Power generation in harsh seafloor conditions is the major challenge. Batteries cannot store power for a long time. Closed cycle engines need storage of fuel and oxygen for a long time that is not possible in seafloor conditions. Temperature differential is nominal therefore; ocean thermal energy cannot be exploited. Only remaining options are wire linked floating wave energy converter and ocean current converter.A fundamental

requirement for the success of the power system is the presence of ocean currents of sufficient velocity near the seafloor to permit self-contained energy generation.

The objectives of this research is to design, fabricate and test an autonomous, lightweight, low-cost, pressure-resistant energy generation system that can optimize power 'harvesting' from ocean current sources and deliver few watts of electric power to the 'Seaformatics' pod. This assumes year-long average marine currents of 0.5m/s are available: ocean current movement near the seafloor is limited, but existing studies indicate it might be as high as 0.5m/s on the Grand Banks. While it would add cost and weight to the units, the contingency plan is to use batteries suitable for a marine environment. The system should also coordinate power-using resources and direct the activity sequences in real time. Risk is further mitigated by the intent to source and modify off-the-shelf components and the research plan to evaluate and select the best options for the turbine and the generator components.

1.6 Environmental Impacts of Marine Current Development

A system that generates electricity needs to be assessed in its entirety to pinpoint any energy, environmental, social or economic implications. The environmental impacts of marine current energy have been branded as benign even though no detailed Environmental Impact Assessment (EIA) studies have been conducted yet. Past studies state that the impacts are likely small, however they need quantification to make informed judgments. However a few studies (DTI 2001, 2002) have identified the possible and likely environmental impacts. These impacts can be grouped into two main categories namely:

(i) Effects common to other construction projects (e.g. offshore wind)

- Visual impact
- Noise and construction
- Installation of cables
- Onshore power lines and substations
- Land access for construction and maintenance
- Pollution (e.g. oil spillage)

(ii) Effects unique to marine current power schemes

- Physical Impacts- The influence of tidal energy extraction on coastal processes, tidal flows, seabed scouring and sediment transport.
- Ecological Impacts- Possible interaction between moving submerged rotor blades and marine creatures.
- Antifouling- The need to have moving parts within the seawater environment is likely to lead to a need for regular maintenance action or the use of antifouling paints.

Table 1.2 gives a summary of the comparison of the renewable energy system and the marine current has been found be the most promising.

Table 1.2 Comparison of Renewable Energy

	Renewable resource	Low capital cost	Low running cost	Minimal environmental impact	Predictable	Minimal visual impact	Modular
Fossil	✗	✓	✗	✗	✓	✗	✗
Nuclear	✗	✓	✗	✗	✓	✗	✗
Wind	✓	✗	✓	✓	✗	✗	✓
Solar	✓	✗	✓	✓	✗	✗	✓
Hydro	✓	✓	✓	✗	✓	✗	✗
Wave	✓	✗	✓	✓	✗	✓	✓
Marine Current	✓	✗	✓	✓	✓	✓	✓

1.7 Objective of this Thesis

The energy conversion system studied in this thesis consists of a vertical axis turbine and a permanent magnet generator with gear box. This concept has few moving parts and is constructionally simple. Such a construction will reduce a maintenance requirement which is desirable once the device is placed under water. The combined turbine-generator system is intended to be placed on the ocean floor in such a way that the generator and the turbine have the same axis of rotation. A controlled DC-DC converter, instrumentation and a microcontroller based control system has been implemented. System will produce the power required for battery charging and signal conditioning circuits. Microcontroller will control the DC-DC converter to extract the maximum power from the system. Such a control scheme will be based on the voltage, current and speed measurement of the system. Maximum power algorithm based control scheme will make sure that system is always extracting the maximum power from water current.

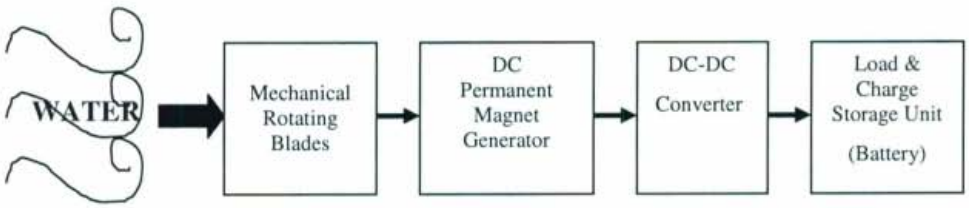

Figure 1.5 Block diagram of Marine Power Conversion System

Fig. 1.5 represents the block diagram of the proposed model. The main issues of research to develop such a system are:

1. System sizing based on the year round seafloor marine current data.

2. Design and development of an efficient turbine.

3. Integrating a multiple pole slow speed generator.

4. Design and development of energy storage system.

5. Design of DC-DC converter control system.

6. Selection and testing of maximum power algorithm.

7. System testing in deep-sea conditions.

1.8 Thesis Report

This thesis is made up of seven chapters.A brief description of the content of each chapter is as follows:

Chapter one gives a background to marine current energy. The need to meet increasing energy demand cleanly and safely was highlighted. The marine current resource, the technology status and challenges as well as the need for environmental impact studies were briefly discussed resulting in the definition of objectives of this thesis.

Chapter two focuses at more detailed study of the marine current resource dynamics and estimation making reference to past studies. The modes of operation of the technologies are then highlighted with particular reference to marine current turbines. Prototypes undergoing testing and refinement were also discussed briefly and the enumerating engineering challenges facing them. A summary of the environmental impacts of these developments and the importance of three physical factors of the marine environment which are likely to be affected is discussed.

Chapter three discusses the different types of turbines and its efficiency.The scaling laws for the turbines is derived and its importance is discussed.

Chapter four presents the design and constructional aspects for the building of laboratory experimental different types of suitable turbines for marine current energy conversion system and the dimensionless analysis .It also discusses the experimental setup to study of the performance of the marine current turbine and the validation of scaling laws.

Chapter five explains the design of a suitable dc-dc converter to maintain a constant voltage at the output. It also explains the technique of removing the voltage ripple of the converters.

Chapter six discusses the experimental set up of a low rpm generator, batteries for energy storage, a controlled dc-dc converter, instrumentation and a micro controller based control system for the turbine. The algorithm of maximum power point tracking theorem for the system and its implementation is discussed. The chapter also presents the results and analysis of the system. In this case results the output power, efficiency of the system was presented.

Chapter seven presents the overall research conclusions and also some suggestions for future work that could be carried out for a better understanding of the various aspects involved in the marine current energy conversion process.

Chapter 2

A status review of marine current systems

2.0 Introduction

Tidal currents are recognized as a resource to be exploited for the sustainable generation of electrical energy. As with all energy generation developments they have to be considered and analyzed in entirety; energy, economics and environmental concerns. This chapter looks at the nature of the marine current resource and the technology required exploiting it. Prototypes which have been developed and undergoing testing have been highlighted as well as possible environmental impacts. Focus is placed on three physical factors of the aquatic environment which are likely to be affected.

2.1 Marine Currents

Oceans of the world can be regarded as an abundant source of energy. A portion of the total energy from the oceans is due to the marine currents (including tidal currents, currents caused by salinity or temperature gradients, and/or the Coriolis effect caused by the earth's rotation [11]). Generally the water current movements are slow but the seabed topography can increase the current velocities up to 7 m/s [12], particularly between islands and the mainland, around ends of headlands and in river estuaries.

The current velocity is an important factor in the design of a marine current power plant, because it sets the limits for both the power output as well as the forces acting on the turbine and support structures. The available power from the ocean increases rapidly

with increasing current velocity. The velocity varies with the depth and the velocity profile approximately follows [13]:

$$V(h) = \left(\frac{h}{H}\right)^{\alpha} V_{peak} \tag{2.1}$$

where h is the total water depth and H is any height above the seabed, α is a constant and V_{peak} is the current velocity at the surface. The factor α is generally taken equal to 1/7 and is different for different locations. It must be noted that Eq. (1) is approximate and the vertical profile will vary at different sites due to local seabed and coastal topography. For example equation (1) is not applicable in case of river estuaries and for currents due to salinity or thermal gradients [12]. It can be assumed that approximately 75 % of the energy is found in the upper 50 % of the flow [6].

2.2 Tidal Currents

The global marine current energy resource is generally driven by the tides and to a lesser extent by thermal and density effects. The tides cause the water to flow inwards twice each day (high tide) and seawards twice each day (low tide) with a period of approximately 12 hours and 24 minutes (a semi-diurnal tide), or once both inwards and seawards in approximately 24 hours and 48 minutes (a diurnal tide). In most locations the tides are a combination of the semi-diurnal and diurnal effects, with the tide being named after the most dominant type.

Tides are generated by gravitational forces of the sun and moon on the ocean waters of the rotating earth. The proximity of the moon and sun relative to earth has a significant effect on the tides. The magnitude of the tide-generating force is about 68% moon and 32% sun due to their respective masses and distance from earth (Open University, 1989).

The sun's and moon's gravitational forces create two "bulges" in the earth's ocean waters: one directly under or closest to the moon and other on the opposite side of the earth. These "bulges" are the two tides a day observed in many places in the world. Unfortunately, this simple concept is complicated by the fact that the earth's axis is tilted at 23.5 degrees to the moon's orbit; the two bulges in the ocean are not equal unless the moon is over the equator. This difference in tidal height between the two daily tides is called the diurnal inequality or declinational tides and they repeat on a 14 day cycle as the moon rotates around the earth [14].

Where the semi-diurnal tide is dominant, the largest marine currents occur at new moon and full moon (spring tides), which is when the sun and moon's gravitational pull is aligned as shown in Figure2.1. The lowest, occurs at the first and third quarters of the moon (neap tides), where the sun and moon's gravitational pull are 90 degrees out of phase.

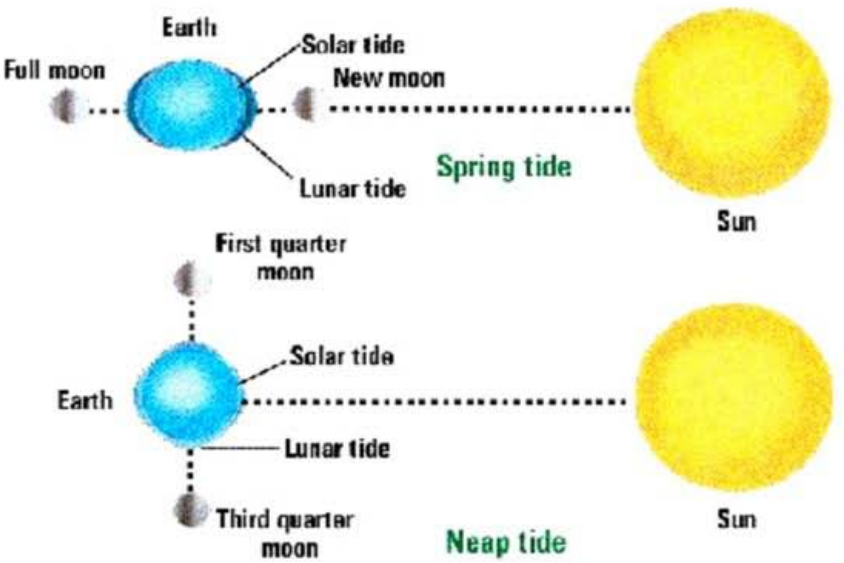

Source: www.jochemnet.de/fiu/tide2.jpg

Figure 2.1 Spring and Neap tides

When diurnal tides happen then the current strength varies with the declination. Generally the largest and lowest currents occur at the extreme declination of the moon and zero declination respectively. Thus the differences in currents occur due to changes between the distances of the moon and sun from Earth, the relative positions with reference to Earth and varying angles of declination. This phenomenon happens with a periodicity of two weeks, one month, and one year or may be longer and is predictable entirely. This means that the strength of the marine currents generated by the tide varies, depending on the position of the site on the earth. The other factors such as the shape of the coastline and the bathymetry (shape of the sea bed) are also responsible to affect the strength of marine currents. Along straight coastlines and in the middle of deep oceans, the tidal range and marine currents are typically low. Another factor that has impact upon the magnitude of marine currents is the presence of narrow passages or straits between islands and around headlands. These passages result in a narrowing and concentration of tidal flow. The flow through a passage is affected by the loss of energy due to friction. The entrances to lochs, bays and large harbours cause high marine current flows.

Generally, but not always, the strength of the currents is dependent on the tidal height of the location. Large marine currents do not necessarily require a large tidal range or height. In land-locked seas such as the Mediterranean, where the tidal range is small, some sizeable marine currents exist (BC Hydro, 2002). Some of the largest tidal flows are found on the east side of the Philippines where the tidal range is small.

Generally the marine current resource follows an approximate sinusoidal pattern with the largest currents generated during the mid-tide. The flood tide often has slightly larger currents than the ebb tide. The flood and ebb flows are generally 180 degrees out of face

with no flow at the turn of the tide (slack tide). However there are some locations where the water flows continuously in one direction only, the strength being largely independent of the moon's phase. These currents are dependent on large thermal movements and run generally from the equator to cooler areas. A not too far fetching example is the Gulf Stream, which moves approximately 80 million cubic metres of water per second (BC Hydro, 2002). Another example is the Strait of Gibraltar where in the upper layer, a constant flow of water passes into the Mediterranean basin from the Atlantic and a constant outflow in the lower layer (BC Hydro. 2002).

2.3 Ocean Currents

The more constant water movements are also found in the oceans. There is a dynamic relationship between constant ocean movements and the slope of the mean sea level (MSL) surface. The MSL is the average level of the sea surface measured relative a fixed level on land . The greatest surface slopes and deviation from the MSL surface are found in areas of great ocean currents for example the Gulf Stream, the Kuroshio Current and the Antarctic Circumpolar Current shown in Figure 2.2. The relationship between the current velocity and the mean sea level surface slope [14] for a steady current is given in (2.2).

$$vf_c = g.\beta \tag{2.2}$$

where v is the current velocity, β *is* the slope of the MSL, g is the gravitational acceleration and f_c is the Coriolis parameter given by:

$$f_c = 2\omega_s \sin\Phi_l = 1.459\times10^{-4}\sin\Phi_l \tag{2.3}$$

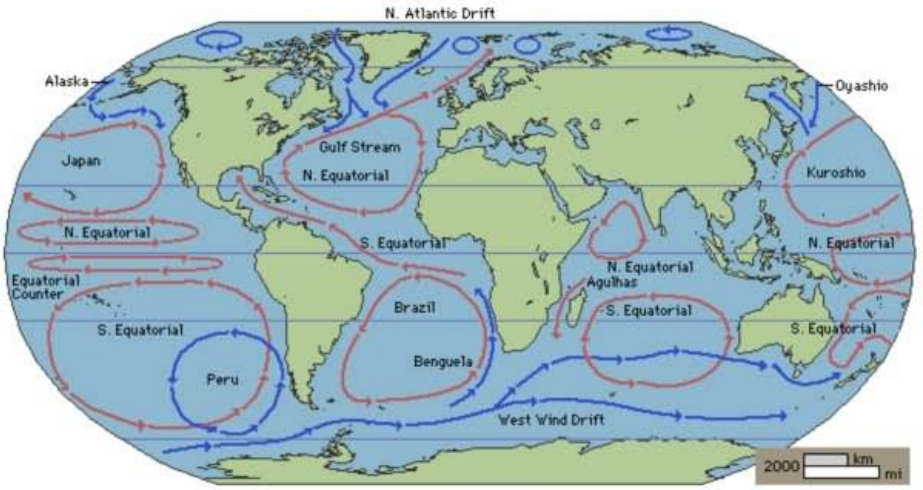

Figure 2.2 The major ocean currents, the red arrows illustrate warm water currents and the blue are cold water currents.

In equation (3) ω_s is the angular speed of earth's rotation and Φ_l is the latitude [14]. In the Gulf Stream an average current velocity of 2.1 m/s has been measured [15] and the Kuroshio Current has a maximum velocity of 1 m/s around Taiwan and slightly higher outside Japan [16, 17].

2.4 Other Currents

In some places nearly constant currents occur due to density differences caused by salinity or temperature gradients. These types of currents exist for example in the Mediterranean in the strait of the Dardanelles and in the sites of Samos, Kafirea, Kea and Kithos in Greek waters [6].

In Skagerak/Kattegatt current velocities of up to 1.4 m/s have been measured. These currents are mainly due to barotropic flows and salinity gradients when the brackish water from the Baltic Sea meets the Atlantic Ocean. According to [18] the currents in this area are strongest along the Danish coast.

2.5 The Marine Environment

Many benefits of aquatic ecosystems can be preserved if the ecosystems are protected from degradation. Aquatic ecosystems comprise a body of water, biological community (animals, plants and micro-organisms), and the physical and chemical characteristics and climatic regime with which they interact. It is predominantly the physical characteristics (e.g. temperature, salinity, light, flow) and chemical characteristics (e.g. organic and inorganic carbon, oxygen, nutrients) of an ecosystem that determine lives , breeding , and the structure of the food web.

The exploitation of marine current energy is likely to be in areas of high current speeds, typically with peak speeds at spring tides of 2 to 3 m/s or more. These areas include narrow straits, between islands and around headlands. By reversing four times a day tidal currents cause the mixing of waters of different salinity, temperature and nutrients. The physical characteristics are described briefly in this section.

2.5.1 Salinity

Salinity is a measure of the salt content in seawater. The principal elements present in ocean's salinity are chlorine (55 %) and sodium (31 %), which combine to produce table salt. Salinity levels fluctuate with the penetration of tidal flows, and with mixing of fresh water and marine water by wind and currents. In estuaries overall salinity levels decline in the spring when snowmelt and rain produce elevated freshwater discharges from streams and groundwater. Salinity levels grade from fresh water which has less than 1 part per thousand (ppt) to oceanic water which has greater than 30 ppt as freshwater entering from rivers and streams mixes with seawater. Seawater has a global average salinity of 35 kg/m^3 or 35 ppt .

2.5.1.1 Salinity Profiles

Generally salinity levels in the ocean tend to vary vertically (high saline water is denser than low saline water) but due to the penetration of tidal currents in estuaries horizontal variation is common there. The degree of vertical and horizontal variation depends on the strength of the marine current. Moreover the distance up to which the tidal effect is felt depends on amongst others, the slope of the channel, the tidal range, the volume of fresh water discharge and the configuration of the river. This leads to three different salinity regimes as in Figure 2.3.

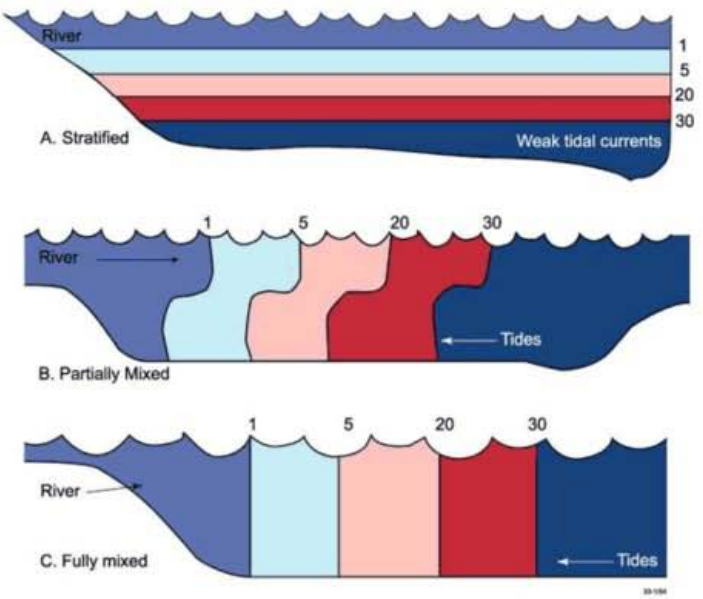

Figure 2.3 Salinity regimes (unit is ppt)

Stratified Conditions can be described as increase in salinity with water depth. It happens when river flow is sufficient to produce a plume of low-density freshwater (1000 kg/m3 at 20 °C) which can flow over higher-density seawater (1025 kg/m3 at 20°C), and where

marine currents and waves are not strong enough to mix the water column (e.g. in wave-dominated estuaries).

Partially mixed condition can be characterized as marine currents having turbulence which cause vertical mixing but they are of insufficient strength to fully mix the water column as salinity varies both vertically and horizontally.

Fully mixed conditions occur in coastal waterways in which tide, river or wave energy produces enough turbulence to mix the water column. In this case, salinity is uniform through the water column, but varies between the riverine and oceanic ends.

2.5.1.2 Importance of Salinity

Most aquatic organisms function optimally within a narrow range of salinity. When salinity goes above or below this range, an organism may lose the ability to regulate its internal ion concentration. Variations in salinity therefore results in changes in species composition, distribution and abundance. Salinity also affects chemical conditions especially within an estuary, particularly dissolved oxygen levels. It is known that the amount of dissolved oxygen in water decreases with increasing salinity.

2.5.2 Water Temperature

Water temperature is a measure of the heat (or kinetic energy) in water. Change in water temperature can be regarded as an indicator of water quality and the state of environment. It is therefore a critical factor in determining marine organisms' survibility. Water temperature in coastal areas changes naturally, as part of daily and seasonal cycles, with variations in air temperature, currents and local hydrodynamics.

2.5.2.1 Temperature Profile

Most of the solar radiation (i,e light and heat) that hits ocean is absorbed in the first few tens of meters of water. Waves and turbulence mix this heat downward quickly leading to a gradual decrease in temperature followed by a sharp decrease in the thermocline region and a gradual decrease in the deep zone. Generally as the depth increases the variation in temperature decreases.

Measurements by Coastal Laboratory, Liverpool Bay, in the Irish Sea have shown little departure of the trend in channels, however the temperature difference is small (1 degree for the graph shown in Figure 2.4) . These levels are nonetheless variable in both time and space, partly due to the seasonal and daily variations in the tides and solar radiation.

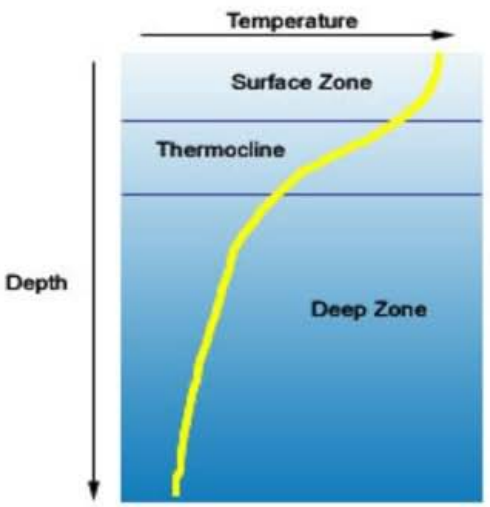

Fig. 2.4 Typical temperature profile of the sea

2.5.2.2 Significance of Temperature

Water temperature regulates ecosystem functioning both directly through physiological effects and indirectly as a consequence of habitat loss. Indeed, the rates of biochemical reactions usually double when temperature is increased by 10^{o}C within the given

tolerance range of an organism. This is called the Q_{10} rule, and it also applies to microbial processes such as nitrogen fixation, nitrification and denitrification. If temperature goes too far above or below the tolerance range for a given organism (*e.g.* fish, insects, zooplankton, phytoplankton, microbes), its ability to survive may be compromised. Temperature is also an important factor influencing viral persistence in estuarine environments. Generally water temperature influences the density, conductivity, pH and the saturation states of minerals of seawater.

2.6 Sediment Transport

Sediment transport is the movement of seabed material from one location to another. It is caused by the action of seabed currents. These seabed currents are mainly caused by the ebb and flood of the tides (over periods of hours) and by surface-waves passing overhead in shallow water (over periods of seconds). The waves break up the bed structure, lifting sediment into the water column. The faster the current, the greater the size of sediment particles a stream can move. Since the sand and mud take a finite time to fall back to the bed, the tidal currents sweep them away from their starting point to towards areas of quieter conditions, where they accumulate, (e.g., into a harbour, where they must be removed by dredging). Alternatively, sediments can be concentrated into areas where they are constantly moving about a fixed point. The marine environment, especially those areas with high tidal currents have complex sediment transport dynamics. Deposition outside the natural variability of an area will cause changes to the local seabed and sediment dynamics of the area. All consequence pathways could cause potential impacts with regard to marine ecology, whether positively or detrimentally.

2.7 Turbidity

Turbidity is a measure of the ability of light to transmit down through the water column. As suspended solids increase in the water, the amount of light traveling through the water column is reduced. Turbidity therefore gives an indication of water clarity or murkiness. This can influence the populations of organisms that are directly dependent upon light (phytoplankton and aquatic plants) and those that in turn depend on them for food. The suspended solids include particles of organism (e.g. algae), clay and silt (e.g. suspended sediment), detritus or solid waste. Since sunlight is the basic energy source for most life forms, the degree of turbidity of the water has an important effect and hence is used as an indicator of the state of the aquatic environment.

2.7.1 Significance of Turbidity

Water clarity is a major determinant of the condition and productivity of an aquatic system because increased turbidity can therefore change an ecosystem significantly. The most obvious effects are:

- A reduction in light available for photosynthesis.
- Smothering of organisms and habitats.
- Promotion of the growth of pathogens and waterborne.
- Obscuring of the vision of fish as they hunt for food

Therefore high turbidity levels can lead to a reduction in the production and diversity of species.

2.8 Marine Current Energy Extraction Technologies

The simplest and oldest technology involves building a dam, known as a barrage, across a bay or estuary that has large differences in elevation between high and low tides. When

the tide comes in, the water fills the area behind the barrage. When the tide starts to ebb, the gates of the barrage shut to hold back the water at its maximum height. Once the tide is out, the water is allowed to flow through holes near the bottom of the barrage where the turbine is located. The water, now running with great energy, turns the blades of the turbine that, in turn, generate electricity.

The first commercial scale tidal generating barrage rated at 250MW was built in La Rance, France in 1960.The plant continues to operate today just as another smaller plant constructed in 1984 in Nova Scotia, and Canada rated at 20MW. All these first generation tidal power plants have faced the hash marine environment and have been in continuous emission-free operation for many years. The high capital and environmental problems from accumulation of silt within the catchments area of the dam (which requires regular, expensive dredging) makes it no longer feasible for energy generation. Two new developed concepts can be described as follows:

- The first and the most advanced, adapted from wind energy industry can be considered as an underwater turbine. It can be categorized into horizontal and vertical axis turbines, depending on the orientation of the rotating shaft.
- The second one adapted from the oil industry is a system of oscillating hydroplanes linked to a hydraulic motor and generator arrangement.

Presently these concepts and the prototype are being undergoing to commercialize. Most of them are still now in the experimental stages.

2.9 Prototypes

In general technology development in the marine current energy sector has been slow worldwide. Ocean current energy is at an early stage of development, with only a small

number of prototypes and demonstration units having been tested to date. The high costs coupled with the harsh nature of the marine environment made it difficult to develop the technology. Recent advances in offshore installations and innovation have translated into real prototypes or field trial models. But still these technologies are not well developed into full commercialization. The focus is to prove the technologies can be made to work reliably. Some of the most promising ones are described in this literature. As these developing technologies are being commercialized so there is reluctance to release information due to competitive advantage.

2.9.1 Seaflow

The unit consists of a two-bladed rotor mounted on a steel pile set into a socket drilled in the seabed. The dimension of rotor diameter is 11 m with full span pitch control thereby making it capable of generating power for both directions of flow. It is currently being operated in one direction of flow and a dump load is being used instead of grid connection due to economic reasons. The power train consists of a gearbox and an induction generator. It makes the unit an integral, sealed, watertight unit. The system operates at variable speed and the control system and power conditioning, together with the dump load ballast are located in the housing above the pile. An important feature of this technology is that the rotor and drive train (i.e. gearbox and generator) can be raised completely above the surface as shown in Figure 2.5. In this position easy maintenance can be carried out.

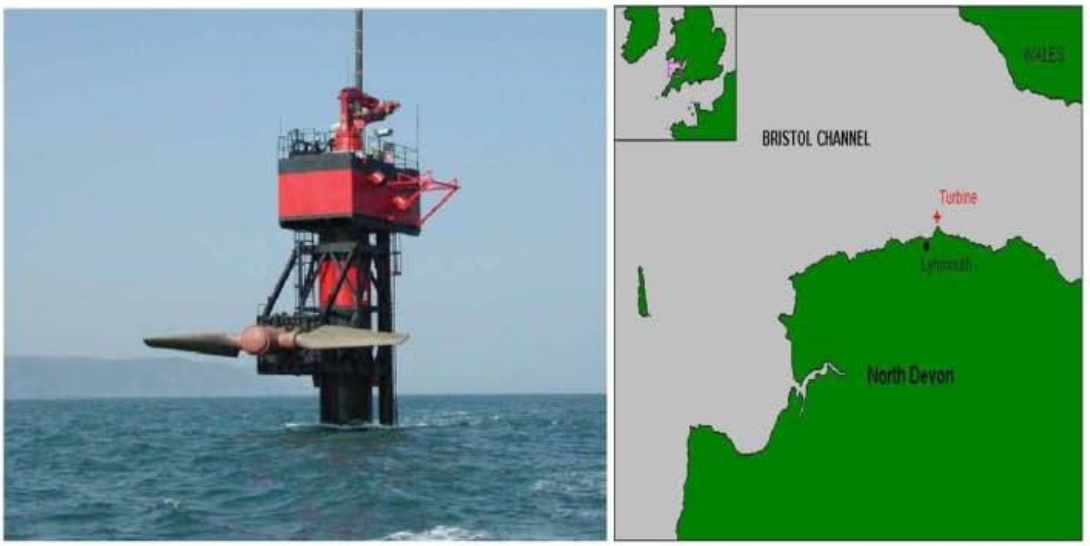

Source: www.marineturbines.com

Figure 2.5 Seaflow in position for maintenance and location in Bristol Channel, UK

The prototype (experimental unit) is installed between the channel between Foreland Ledge and Foreland Point on the North Devon coast, 3 km to the North-East of Lynmouth, UK which is rated at an output power of 300 kW in a current speed of 2.7 m/s. The Foreland Point was chosen due to favorable tidal stream speeds. According to Coastal Research, an independent consultancy in marine environmental science, this location has tidal streams in excess of 2.5 m/s during spring tides.

2.9.2 Tidal Stream Turbine

The prototype is expected to supply 700 MWhr energy per year shown in Fig.2.6. The submerged structure weighs 120 tonnes. Its a three-bladed turbine made up of glass fiber-reinforced plastic measured 10 meters from hub to tip. By rotating the blades around their own axis by 180 degrees at slack water, the machine is ready for the reversing current keeping. The average current velocity at this location is 1.8 m/s. The strait has a width of

400 m at its narrowest cross section and a maximum depth of 50 m allowing a sailing depth of 19 m.

Source: www.e-tidevannsenergi.com

Figure 2.6 Deployment of the first grid connected tidal turbine in Kval Sound, Norway

2.9.3 Tidal Fence (Davis Hydro Turbine)

Blue Energy has over two decades developed a floating vertical axis turbine known as Davis Hydro Turbine.

The Blue Energy Ocean Turbine acts as a highly efficient underwater vertical-axis windmill. Four fixed hydrofoil blades of the Blue Energy Ocean Turbine are connected to a rotor that drives an integrated gearbox and electrical generator assembly. The turbine is mounted in a durable concrete marine caisson, which anchors the unit to the ocean floor, directs flow through the turbine further concentrating the resource supporting the coupler, gearbox, and generator above it. The hydrofoil blades employ a hydrodynamic lift principal that causes the turbine foils to move proportionately faster than the speed of the surrounding water. Prototypes ranging form 4 kW to 100 kW have been tested mostly in rivers.

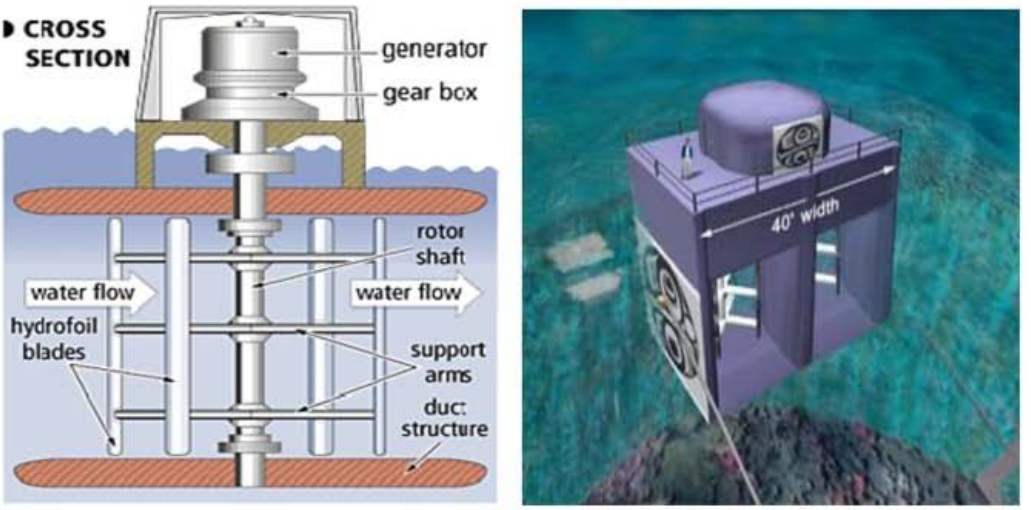

Source: www.bluenergy.com

Figure 2.7 Computer rendering of the twin (2 x 250 kW) floating units[13]

Blue Energy is currently pursuing the development of a 500kW pre-commercial demonstration project off the coast of British Columbia, Canada. The project is comprised of two floating 250kW units as shown in Figure 2.7. The unit will be viable in ocean currents of 1.75 m/s.

2.9.4 The Stingray Tidal Stream Generator

The stingray generator converts the kinetic energy of moving water into hydraulic power and turns an electrical generator by means of a hydraulic motion. It consists of a stack of large hydroplanes attached by a linkage. The hydroplanes change its face relative to the approaching water stream by a simple mechanism. The lift and drag force causes the arm to oscillate vertically (shown in Figure 2.8). A hydraulic cylinder attached to the main arm is forced to alternately extend and compress, producing high-pressure oil and delivered to the hydraulic motor to drive the generator. The whole structure is fully submerged and is fixed rigidly onto the sea bed.

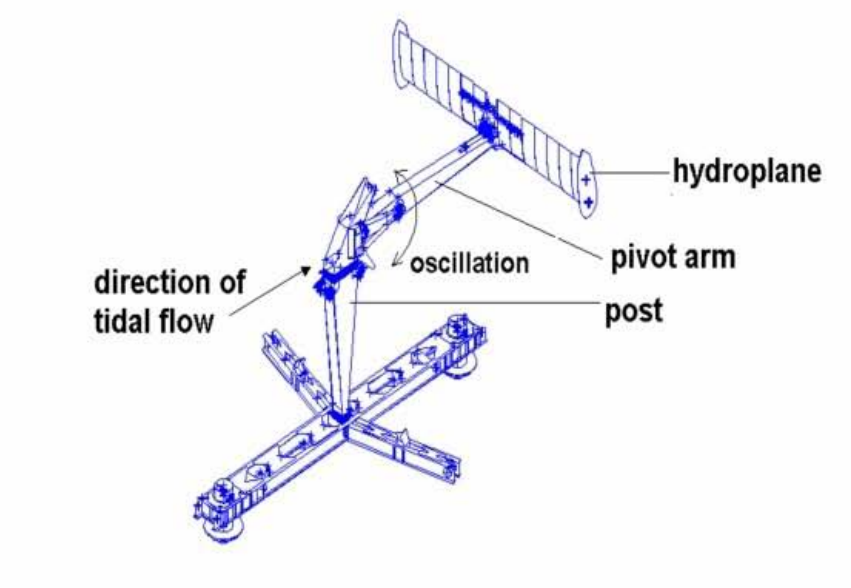

Source: www.smdhydrovision.com

Figure 2.8 Principle of operation of the Stingray Generator [6]

Initial power cycles completed with 'manual' control of the hydroplane angle produced a peak hydraulic power of 250kW and a time averaged electrical power output of 90kW in a 1.5 m/s measured current. Figure 2.9 shows the deployment of Stingray in Scotland.

Source: www.engb.com

Figure 2.9 Deployment of Stingray in Yell Sound, Scotland [6]

2.9.5 MOOS Power System

The MOOS power system is designed to collect and store energy from the buoy environment, transmit power to distant loads over the riser and seafloor cables, and make clean power available to buoy and seafloor loads via a standardized electrical interface. The system block diagram is shown in Figure 2.10.

The capability of the power system was made based on goals established during the user requirements survey. These goals included a continuous-average power delivery capability between 10 and 100 watts, the ability to transmit power of 300 W peaks down a 4-km mooring riser, and the ability to transmit power of 10 W peaks to the end of a 10-km benthic extension cable. The power system was physically constrained to operate on a buoy and riser cable. The MOOS system was thus designed to exploit, or to be able to exploit, energy naturally occurring in the ocean environment, in the form of solar and wind power

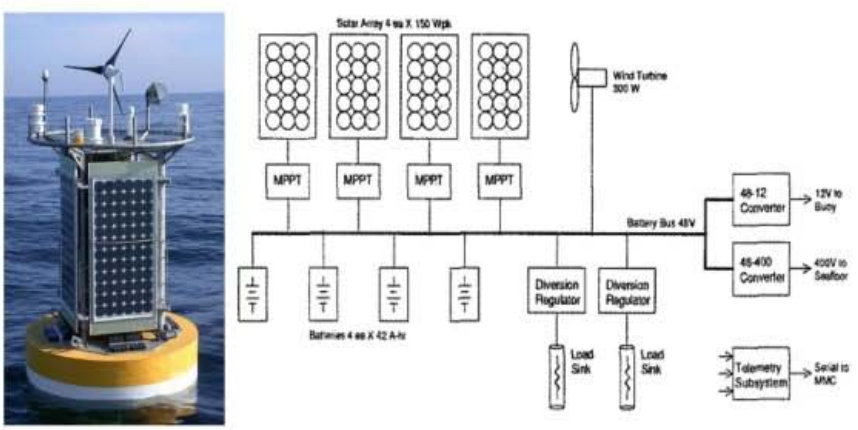

Source:www.mbari.org

Figure 2.10 MOOS Power System[13]

2.10 Emerging Technologies

There are a couple of additional concept variants currently in development. Some of them are worth noting as they may emerge as strong options for future.

2.10.1 TidEI Tidal Stream Generator

The TidEI concept is a pair of contra-rotating turbines, mounted on a single crossbeam. It is buoyant and tethered to the seabed by a series of mooring chains. The floating system allows the turbines to align in the direction of the tide automatically, i.e. following the tide backwards and forwards as it changes direction. The turbine blades are fixed pitch and variable speed operated.

Source: www.smdhydrovision.com

Figure 2.11 1/10th scale TidEl tidal stream generator

A commercial size, 1000 kW (2 x 500 kW), prototype with 15 m diameter is at the development stage for offshore testing to be carried out in 2005 and 2006. It is likely to be tested in an offshore environment with peak tidal speed of 2.5 m/s or more and a water depth of 30 m. This will help to prove its viability and numerous perceived advantages.

Meanwhile a 1:10 scale system (Figure 2.11), partly funded by DTI, and has undergone a seven week trial program at the New and Renewable Energy Centre (NaREC) in Blyth.

2.10.2 Lunar system

This technology being developed by Lunar Energy features a ducted turbine, fixed to the seabed by a gravity foundation. The blades are bi-directional rather than variable pitch, and there is no yaw mechanism which maximizes the energy from the water flow, even when flow is not parallel to the turbine axis. This reduces complexity and allows improved reliability. Moreover it is likely to be deployed in deep waters without impacting shipping traffic.

2.11 Technology Challenges

In early stage all new technologies challenges are bound to be faced .Some of the most pressing ones are being discussed here. As prototypes are being tested and the technology matures most of them, if not all, are bound to be addressed. Though some of them may be unique to certain technologies, most of them are common to most if not all the technologies under development.

***Foundation and Moorings Installation*:**

The installation of marine current generators will present their own unique difficulties. The constructions of foundations and installation during water movement is challenging. Slack water can be expected each day only for few minutes. Scouring around the base of temporary support structures can be significant even over very short periods. Most devices may have similar installation, foundation and mooring problems and so there is scope for generic research in this area.

***Maintenance Requirements*:**

It is very important to have easy access to the unit for maintenance. Two concepts have been proposed so far. The first is a hoist system based on a hydraulic unit, similar to the system used to raise marine platform legs. The second one is a semi-submersible system which allows the rotor and power train to float on the water surface for access. Due to economic reasons it will be wise to design the turbines in such a way that it requires minimum level of maintenance.

***Cavitation*:**

Relatively high velocities at the tips of the rotor blades cause formation of cavities along the blade. To avoid this different approach is needed for marine current turbines because of its larger plane or rotor area. Cavitation is sensitive to water depth and can be avoided by placing units in deeper water at potential cavitation sites. Hence, research is needed to understand the problems of cavitation and whether selection of blade profiles and materials can bring a difference in cavitation efficiency loss and damage problems.

***Packing Density*:**

A good understanding of the impact of quantity and size cause on the marine environment and flow pattern can be a basis of design guidelines for system sizing. Some of the factors to be taken into consideration include seabed structure, depth, flow pattern and available area. This will help designers to locate suitable sites, and investor to understand the implications of these farms.

***Turbulence*:**

The velocity of the flow at a given location can sometimes vary across the actuator area. This can cause significant variations in loading across the actuator and associated fatigue

and vibration problems. The study of turbulence levels is important for installation of individual units in an area with strong flow. The turbulent structure of the flow field is another important factor design affecting the design of components to resist fatigue. Design codes for marine current devices considering turbulence levels is important in setting realistic limits to design.

***Biofouling*:**

Many devices installed in the sea become artificial reefs, attracting a wide variety of marine organisms. These cover the structures and can cause significant fouling. Fouling of moving parts could affect the performance of devices. Several methods for preventing fouling have been proposed. These include the use of antifouling paints and sonic and ultra sonic systems. Both methods have their challenges and drawbacks calling for further research.

2.12 Conclusion

The environmental impacts of marine current development are site specific. The production, distribution and diversity of species depend on the level and variation of these physical characteristics. The extent of the impacts will depend on the extent of exploitation of the resource. A high level of exploitation may result in significant reduction of current speeds and its attended effects on adjacent aquatic environment. This decrease in current speed may also attract fishes. In short it be said that marine current developments are likely to have positive and negative impacts on the environment. The levels however need quantification to make informed judgement.

Chapter-3

Micro Marine Current Turbine

3.0 Introduction

This chapter discusses the types of turbines and its efficiency. The scaling laws of turbines have been derived and its importance for the analysis of the dimension of turbine has been discussed.

3.1 Horizontal and Vertical Axis Turbines

There are two types of turbines, horizontal axis (propeller type) and vertical axis (eggbeater type). Horizontal axis turbines are the most popular geometry for two primary reasons. The blades of a horizontal axis turbine can produce constant positive torque from the flow. Horizontal axis turbines also operate at higher rotational speeds. A faster rotating rotor is more conducive for electrical power generators, which operate on an order of hundreds if not thousands of revolutions per minute.

Turbines may be anchored to the ocean floor in a variety of ways. Mechanisms such as posts, cables, or anchors are required to keep the turbines stationary relative to the currents with which they interact. They may be tethered with cables, with the relatively constant current interacting with the turbine used to maintain location and stability. In some areas with powerful currents, it would be possible to install water turbines in groups or clusters to create a "marine current facility," similar in design approach to a wind

turbine farm. Two possible arrangements are shown in figure 3.1. Turbine spacing would be determined based on wake interactions and maintenance needs.

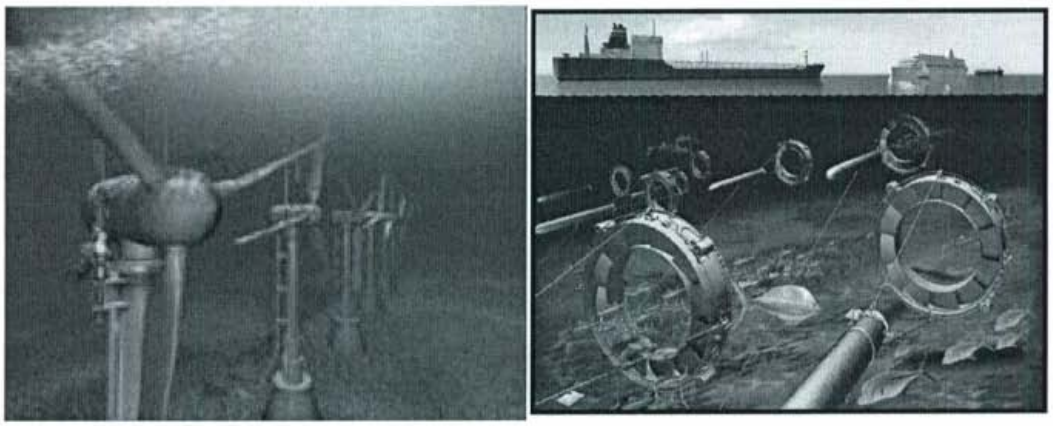

Figure 3.1 Visualization of two possible turbine and anchor technologies

The turbines used for the first Marine Current Energy Converters (MCEC) have shorter, thicker blades than wind turbines to withstand the larger stresses due to higher density of water. The axial flow rotors always require facing the incoming current and thus need a mechanism that allows the turbine to operate with the flow in both directions. This can be achieved by pitch control of the rotor blades through one hundred eighty degree at turn of tide. Common to all different designs are that they have the axis of rotation along the flow. Most of the turbine designs have been adapted from the applied wind turbine geometry [20]. The characteristic for the vertical axis rotor is that it does not need to be oriented to the flow. This design also allows with ease to mount the gearbox and generator above or below the rotor avoiding interference with the flow across the rotor. Regardless of the design a turbine can only harness a fraction of the available power in the free flowing water.

3.2 Drag and Lift Turbines

Blade designs are based upon either the principle of drag or lift. In drag type turbines the blade shape is employed to have a higher drag coefficient on one side of the incident current than on the other. Drag powered turbines are designed to produce high torque capabilities. The downward drag force on the retreating blades is greater than the retarding force on the advancing blades and thus a net torque is produced. The speed of the rotor is inherently limited because the retreating blades cannot travel faster than water speed. They generally said to operate at low tip speed ratio (TSR) less than one. It is a limitation of drag type turbines that higher speeds and higher peak efficiencies can never be achieved. Moreover, relatively large amount of material are required for a given swept area. The construction is very simple and inexpensive compared to other turbines.

Lift type turbines incorporates aerofoil section blades to produce lift. The blades can turn sufficiently fast relative to free stream flow and converts the lift into positive torque. These turbines can operate at TSR up to ten and can achieve better efficiencies than drag turbines. The following table 2.1 shows a comparison study of lift and drag type turbines.

Table 3.1: Lift and Drag Horizontal and Vertical axis Turbines

Rotor Type	Hydrodynamic	Axis	Self-start	Cp	Keynotes
Propeller	Lift	HAWT	Good	High	Noisy,Turbulence,Low torque, High speed
Darrieus	Lift	VAWT	Poor	High	Low torque
Savonius	Drag	VAWT	Good	Low	High torque, Low speed, Poor efficiency

3.3 Turbine Efficiency and the Betz limit

Turbines are usually defined by performance curve, which gives power coefficient(C_P) as a function of velocity coefficient(λ). The pressure exerted by the fluid upon the turbine is given by the following equation [22]:

$$\text{Pr}essure = \frac{\rho U_{\infty}^{2}}{2} \tag{3.1}$$

The volume of the fluid striking the blades can be expressed as:

$$Q = AU_{\infty} \tag{3.2}$$

The power in a free-flowing stream tube is given by combining Eq.(3.1) and Eq.(3.2):

$$P_{\infty} = \frac{\rho U^{3}{}_{\infty} A}{2} \tag{3.3}$$

where U_{∞} is the freestream velocity of the fluid, and A is the cross stream area or the swept area of the rotor. When a turbine extracts power from the flow, it needs to reduce the energy of the fluid around it. This energy loss manifests itself as a pressure drop across the turbine rotor and can be considered as an increase in pressure at the leading edge and a decrease at the trailing edge of the turbine. The local high pressure area causes some of the upstream fluid to divert around the turbine, thus decreasing the amount of fluid passing through the turbine, which in turn reduces the amount of power available to the turbine. As more power is extracted from the fluid, the pressure disturbance increases, further reducing the amount of fluid passing through the turbine. Therefore, there is a theoretical maximum to the total power that can be extracted from a fluid. This was proven in 1926 by Albert Betz and is known as the Betz limit[22].

It can be assumed that the velocity at the rotor is the average of the velocity in the wake and the freestream velocity:

$$U_t = \frac{1}{2}(U_W + U_\infty) \tag{3.4}$$

The assumption can be proved using a one-dimensional momentum and energy balance. The mass flow rate through the rotor can be expressed as:

$$\dot{m} = \rho A U_t = \frac{1}{2}\rho(U_W + U_\infty) \tag{3.5}$$

where A is the area swept by the rotor blades. Power is related to velocity changes by

$$\mathrm{P} = \frac{1}{2}\dot{m}(U_\infty{}^2 - U_W{}^2) \tag{3.6}$$

Substituting (3.5) into (3.6) gives the amount of power extracted by the turbine,

$$P = \frac{\rho A}{4}(U_\infty{}^2 - U_W{}^2)(U_\infty + U_W) \tag{3.7}$$

Finally, the Betz limit becomes apparent when this is compared with the power in the freestream, P_∞. That is, dividing (3.7) by (3.3), we get

$$\frac{P}{P_\infty} = \frac{1}{2}\left[1 - \left(\frac{U_\infty}{U_W}\right)^2\right]\left[1 + \frac{U_\infty}{U_W}\right] \tag{3.8}$$

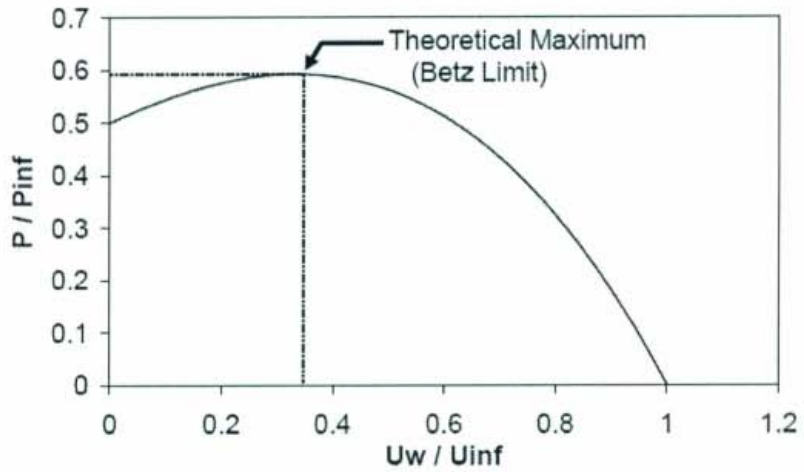

Figure 3.2 Power Ratio versus Velocity Ratio

The maximum of this function is the maximum power an ideal turbine will be able to extract from water. This limitation is generally expressed by adding an efficiency term Cp to (3.9).

$$P = \frac{1}{2} \times C_p \times \rho \times A \times V^3 \tag{3.9}$$

3.4 Scaling Laws of Turbines

An important benefit of dimensional analysis is that the results of a model studied, analyzed and plotted may then be used to predict performance of a full scale system. Established dimensional analysis methods or scaling laws [30] can also be applied to water current turbines. This chapter gives an overview of scaling laws for Savonius rotor based water current turbines. Dimensional analysis and scaling laws for a single rotor turbine are derived. Two rotor prototypes are built and tested in the lab to prove the validity of scaling laws.

Turbo machines consist of machines such as pumps, turbines and fans and each of these contains a rotor, or rotating member. Rotor in turbines is similar to rotor in pumps.

If the transfer of energy is from rotor to fluid then the machine is a pump, fan or compressor on the other hand if the flow of energy is from the fluid to the rotor the machine is a turbine. There are very few problems in the field of fluid mechanics that are solved using the differential and integral equations only. It is often necessary to resort to experimental methods in order to establish relationship between the variables of interest. Since experimental studies are usually quite expensive, it is necessary to keep the required instrumentation to a minimum. This can be done using a technique called dimensional analysis which is based on the notion of dimensional homogeneity. While plotting the results of turbine tests and in the analysis of performance characteristics, it is necessary to use dimensionless groups of variables. Appropriate groups of variables for a turbine can be found using dimensional analysis. There are generally two approaches that can be used in the study of dimensional analysis. Firstly we can use the Buckingham-pi theorem which organizes the steps of ensuring dimensional homogeneity [30]. From Buckingham-pi theorem it is known that the dimensionless groups maintain a functional relationship and nature of the relationship is unknown without experimentation. Secondly we can extract dimensional parameter that is required to analyze the performance of scaled models.

3.5 Dimensional Analysis

Two turbines that come from a common design is said to share a geometrical similarity. Kinematic similarity holds if the flow fields are approximately similar and there is no cavitation. The ultimate goal is to obtain the dynamic similarity where the scaling of force distributions are similar as well as other performance characteristics. To achieve dynamic similarity both geometric and kinematic similarity are required. In such a case, it

can be shown that kinematics similarity is obtained when the flow coefficient is held constant for two turbines of the same design. Therefore, from the normalization procedure above, dimensional analysis indicates that, the condition of dynamic similarity is achieved when the flow coefficient is matched between two machines X and Y of the same family. It is very useful for the analysis of data from full-sized machines, when it is desired to predict the performance of other full-sized machines of different size than those tested or to operate under different conditions.

The important variables in turbo machine performance are shown in Table 3.1.

Table 3.1 Turbo Machine Variables

Variable	Symbol
Energy Transfer	P
Volume flow rate	Q
Angular speed	N

3.6 Derivation of Scaling Laws

In this section two different approach of calculating the power coefficient of turbine is derived.

A. First Approach

Dynamic pressure in a turbo machine can be scaled as $\frac{\rho U^2}{2}$ where ρ denotes the density of fluid and U is some characteristic speed of the machine. In turbo machine U scales as DN [30] where D is the diameter of the rotor and N is its rotational speed.

$$\text{Pressure} = \frac{\rho U^2}{2} \qquad 3.11$$

Non dimensionlizing pressure by dynamic pressure of rotor one can form the pressure coefficient as:

$$C_P = \frac{P}{\rho D^2 N^2} \qquad 3.12$$

Volumetric flow Q is the product of a speed and an area. In a turbo machine speed scales as ND. Area can be scaled as D^2. Thus one can write the flow coefficient:

$$C_Q = \frac{Q}{ND^3} \qquad 3.13$$

$$= \frac{AV}{ND^3} \qquad 3.14$$

$$= \frac{V}{ND} \qquad 3.15$$

The power P transmitted through the fluid is PQ. Thus the fluid power coefficient is:

$$C_P = C_P C_Q \qquad 3.16$$

$$= \frac{PQ}{\rho D^5 N^3} \qquad 3.17$$

$$= \frac{Power}{\rho D^5 N^3} \qquad 3.18$$

These coefficients applies for a similar geometrically turbo machines which can be plotted in a non-dimensional way. For a point on a C_P versus C_Q characteristic the equations for C_P and C_Q represents the following relationship:

$$\frac{P_2}{P_1} = \left(\frac{\rho_2}{\rho_1}\right)\left(\frac{N_2}{N_1}\right)^3\left(\frac{D_2}{D_1}\right)^5 \qquad 3.19$$

$$\frac{P_2}{P_1} = \left(\frac{D_2}{D_1}\right)^2\left(\frac{N_2}{N_1}\right)^2 \qquad 3.20$$

$$\frac{Q_2}{Q_1} = \left(\frac{N_2}{N_1}\right)\left(\frac{D_2}{D_1}\right)^3 \qquad 3.21$$

Where D1, D2 are diameters of first and second model respectively

N1 and N2 are rev/min of first and second model respectively

P1 and P2 are power of first and second model respectively

Case 1:

Two turbines with fixed size and operating at variable speed can be related as follows:

$$\frac{P_2}{P_1} = \left(\frac{\rho_2}{\rho_1}\right)\left(\frac{N_2}{N_1}\right)^3 \qquad 3.22$$

$$\frac{Q_2}{Q_1} = \left(\frac{N_2}{N_1}\right) \qquad 3.23$$

Case 2:

Two turbines of different size running at constant speed can be related as follows:

$$\frac{P_2}{P_1} = \left(\frac{\rho_2}{\rho_1}\right)\left(\frac{D_2}{D_1}\right)^5 \qquad 3.24$$

$$\frac{Q_2}{Q_1} = \left(\frac{D_2}{D_1}\right)^3 \qquad 3.25$$

B. Second Approach

Alternatively the standard way of finding the power coefficient is described below briefly:

The pressure exerted upon the turbine blade is expressed as:

$$\text{Pressure} = \frac{\rho V^2}{2} \qquad 3.26$$

Volumetric flow of the fluid can be represented as:

$$Q = AV \tag{3.27}$$

Therefore the output power of the turbine can be written as:

$$\text{Power} = \frac{1}{2}\rho A V^3 C_P \tag{3.28}$$

3.7 Relationships of Dimensions

The first step in dimensional analysis is to turn various performance parameters into non-dimensional parameters. For similitude to hold, the flow coefficient, $C_Q = \frac{Q}{ND^3}$, the pressure coefficient, $C_P = \frac{P}{\rho N^2 D^2}$, and the product of both is the power coefficient, $C_P = \frac{Power}{\rho D^5 N^3}$, must remain the same between model and actual turbine. Thus, we can say (if the efficiency doesn't change):

$$\left(\frac{P}{\rho N^2 D^2}\right)_{actual} = \left(\frac{P}{\rho N^2 D^2}\right)_{model} \tag{3.29}$$

$$\left(\frac{\rho g H}{\rho N^2 D^2}\right)_{actual} = \left(\frac{\rho g H}{\rho N^2 D^2}\right)_{model} \tag{3.30}$$

$$\left(\frac{H}{\rho N^2 D^2}\right)_{actual} = \left(\frac{H}{\rho N^2 D^2}\right)_{model} \tag{3.31}$$

$$\left(\frac{Power}{\rho N^3 D^5}\right)_{model} = \left(\frac{Power}{\rho N^3 D^5}\right)_{actual} \tag{3.32}$$

From the two equations 3.30 and 3.31 it can be shown:

$$\left(\frac{N_a}{N_m}\right)^6 = \left(\frac{P_a}{P_m}\frac{D_m^5}{D_a^5}\right)^2 \qquad 3.33$$

$$\left(\frac{N_a}{N_m}\right)^6 = \left(\frac{H_a}{H_m}\frac{D_m{}^2}{D_a{}^2}\right)^3 \qquad 3.34$$

Equating (3.23) and (3.24) the following relation holds

$$\left(\frac{P_a}{P_m}\right)^2\left(\frac{D_m}{D_a}\right)^{10} = \left(\frac{H_a}{H_m}\right)^3\left(\frac{D_m}{D_a}\right)^6 \qquad 3.35$$

The size of the prototype estimated is 87% to have an output power which is half of the full scale prototype from above Eq.(4.24).The dimensionless analysis is based both upon the dimensions and as well as density of the fluid. The study was carried out for two similar prototypes of different size in the wave tank and wind tunnel. Both the experiments were carried out to consider the size of the turbines and the type of medium. It can be also proved from Eq. (3.35) that an 87% model is needed to have an output which is half of the first prototype.

3.8 Conclusions

The turbine efficiency and the importance of scaling laws has been discussed .In the next chapter different types of prototypes have been tested to find out the efficiency of the turbines. Also the validity of scaling laws have been justified for two prototypes of same geometrical shape and different dimension in the next chapter.

Chapter 4

Water Current Turbine Experiments

4.0 Introduction

This chapter starts with discussion of the performance of various kinds of water current turbines. It selects the Savonius rotor as a candidate for a micro seafloor power generation system. Test results in a tow tank and wind tunnel are presented.

4.1 Advantages of Savonius Rotor

When designing a rotor for marine current generation there are two types of rotors to consider. These are the Savonius rotor and the propeller rotor each with its own unique characteristics. The reasons to choose Savonius rotor over other types are stated below:

- Simple and low cost to build.
- A Savonius rotor cannot rotate any faster than the fluid rotating it. On the other hand the propeller type rotor gains momentum and can exceed the water speed. It can cause mechanical stress on motor due to overvoltage in the windings and can cause rotor damage. In order to prevent this a separate braking system must be designed to compensate this. It is suitable for low power application to choose Savonius rotor for simplified design.
- A Savonius rotor accepts flow from any direction and they are easier to install.
- Generator can be easily mounted on the top of vertical turbine. Another aspect of rotor design is to consider the connection method between generator and turbine to extract power. The propeller rotor needs to have a strong connection in order to compensate for the weight of the rotor itself. In a Savonius system the rotor

actually stands atop the motor. For this reason one could use a strong pin locked clip, which would act as the connection between the axle of the rotor and the motor shaft. When considering which option to choose, either the Savonius or propeller rotor, it is important to figure in the flexibility of each option, and plan accordingly. Due to the fact that the Savonius rotor does not actually have to be welded into place on the generator shaft, but rather pinned, it could be replaced easily, thus adding the flexibility desired for low power applications

- High starting torque helps to start at lower speed.
- Relatively low operating speed and may require a gearbox.
- Maintenance to maintain a clean leading edge is not necessary.

The above advantages outweigh its low efficiency and slow running speed makes it an ideal economical choice to meet small-scale power requirement [22]. This is essentially due to the low hydrodynamic performances of such rotors, based on the difference between the drag forces on the paddles. Agreement on the efficiency of the Savonius turbine apparently has finally been reached a half century after its development [19, 20]. Savonius claimed an efficiency of 31 per cent in the wind tunnel and 37 per cent in free air. However, he commented [21] "The calculations of Professor Betz gave 20 % as the highest theoretical maximum for vertical air wheels, which under the best of circumstances could not produce more than 10% in practical output." The theoretical and experimental results failed to agree. Unfortunately, Savonius did not specify the shape and size of his turbine well enough for others to try to duplicate his results. In fact, the best modern machines hardly reach this maximal value of the power coefficient. Expected performance curves of different turbines are shown in Figure 4.1.

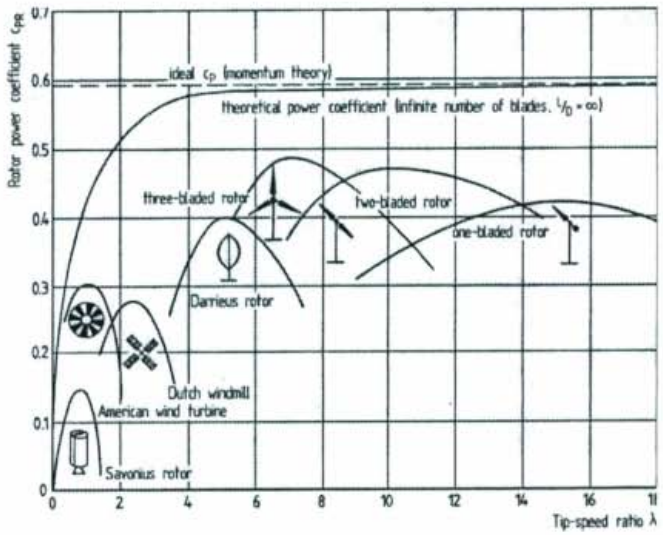

Figure 4.1 Expected performances of different types of turbines

The concept of the Savonius rotor was based on the principle developed by Flettner. Savonius used a rotor that was formed by cutting the Flettner cylinder into two halves along the central plane and then moving the two semi cylindrical surfaces sideways along the cutting plane so that the cross-section resembled the letter "S."

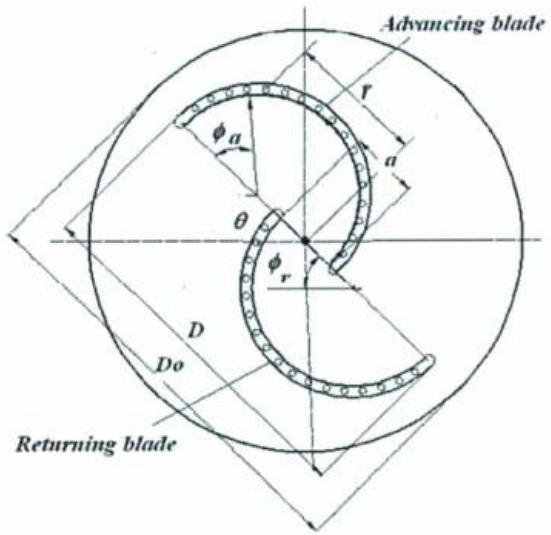

Figure 4.2 Typical stationary Savonius rotor with round edge

By the use of a new comparison method, namely the L-sigma criterion, Menet et al. have shown that the Savonius rotors are in fact more resistant to mechanical stresses than all fast running wind turbines [23,24]. The basic idea is to compare the mechanical power obtained by a vertical axis turbine with the one produced by a horizontal turbine. The comparison is done by considering the same front width of fluid (i.e. diameter of the rotor) and the same mechanical stresses produced due to the centrifugal forces on the paddles for the two turbines. The L-sigma criterion [25] shows that Savonius rotor is a better machine than all the fast running horizontal axis turbines.

Savonius turbine relies on stagnation principles to convert current into rotational energy. The Savonius rotor uses stagnation pressure on one side to promote rotation around a central vertical axis. The blade turning redirects water around itself with its rounded shape. Any tangential flow of water will produce a positive force on the rotor; vertical axis turbines operate in turbulent water better than horizontal designs. A Savonius design relies on the pressure of the current against the rotor blade to produce torque. As such, a Savonius design cannot exceed the speed of the water and operates at a lower RPM range than would a horizontal axis turbine. It has the benefit of producing a larger torque.

4.2 Optimum Savonius Design

If C_p were the power coefficient [2] of a turbine then the power P can be obtained from water:

$$P=\frac{1}{2} C_p A\rho V^3 \qquad (4.1)$$

where P is the output power (W)

ρ is the density of water (kg/m^3)

A is the swept area of rotor (m^2)

V is the speed of water (m/s)

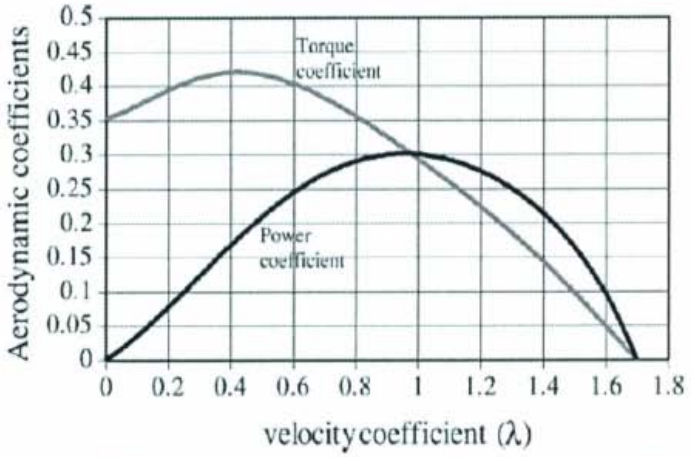

Figure 4.3 Expected performances for Savonius rotor [22, 26].

The tip peripheral velocity of the rotor U = ω R (ω is the angular velocity of rotor and R is the radius of the rotor).

Now the velocity coefficient of the turbine is defined as:

$$\lambda = \frac{U}{V} \tag{4.2}$$

The value of the velocity coefficient has been chosen 1.0 from Figure 3.5. The expected RPM of the turbine can be calculated from the above equation. The aspect ratio α is the height of the rotor divided its diameter, this is a very important criterion for the performances of a Savonius rotor:

$$\alpha = \frac{H}{D} \tag{4.3}$$

Generally the value of α is taken higher to improve the efficiency. Values more than 1.0 seem to improve the power coefficient for a conventional Savonius rotor [26]. It is known that end plates also lead to better hydrodynamic performances [27]. The influence of the diameter D_f of these end plates relatively to the diameter D of the rotor has been experimentally studied. The higher value of the power coefficient [27] is obtained for a value of D_f around 10% more than D, whatever the velocity coefficient. The overlap ratio β is given by the following equation:

$$\beta=\frac{e}{d} \tag{4.4}$$

where e is the overlap between two bucket and d is the diameter of each bucket shown in Fig.4.4. Ushiyama *et al.* [26] reported an increase in the coefficient of starting or static torque as the overlap ratio increases from 0 to 0.2 and a decrease as the overlap ratio increased from 0.3 to 0.5. Fujisawa [27] observed a monotonic increase in the coefficient of static torque with an increase in the overlap ratio from 0 to 0.5.

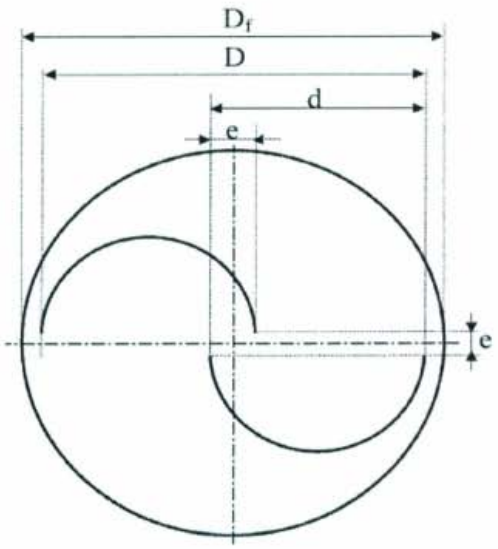

Figure 4.4 Top view of a single-step Savonius rotor

Figure 4.4 shows top view of a Savonius rotor, where e is the overlap and d is the diameter of each cylinder constituting the paddles. The best efficiencies [25] are obtained for values of β between 15 and 20%. The number of paddles should not more than two in order to achieve the maximum torque or power coefficient [26].

This configurations allow the best power coefficient (i,e efficiency) to be obtained but the starting torque for few directions of the water velocity would be so low that the rotor could not start alone. It is the reason why many authors have chosen to use a double-step Savonius rotor, where the upper and the lower paddles pairs are set at 90° to each other [26]. Also it has been mentioned that with three stages and each stage having a 60° phase shift can reduce the pulsation in torque. In this thesis three different types of prototypes have been tested [28].

4.3 Design Consideration

1. ***Choice of the material:***

The choice of the material is very important. Different criteria were considered for this choice: low cost, easy manufacture, low weight, and good resistance to rust, good rigidity, recyclable material. The best option is to use aluminum to avoid rusting in salty water.

2. ***Geometry of turbine:***

The two circular end plates are used for better hydrodynamic performances. As a result no central shaft is necessary to reinforce the total rigidity of the turbine.

3. ***Selection of Bearings:***

The prototypes need to be mounted so the bearings are selected based on the following factors:

a) It can run continuously for years

b) It can support mechanical stresses due to the weight of rotor, centrifugal forces and the drag of rotor

c) The bearings should be resistant to corrosion . Teflon bearing were used during the lab testing.

4.4 Prototypes Descriptions

A. First Prototype

Figure 4.5 shows the geometry of conventional single stage Savonius rotor that has been built considering the factors that can give maximum efficiency as water turbine. In order to mount the rotor a rectangular frame has been designed. The rotor is held in vertical position using teflon bushing and bearing at the bottom and top of the frame respectively. The dimension of the rectangular frame is 35cm×35cm×50cm to maintain free flow of water. The material chosen for the frame is aluminum in order to avoid rusting.

Figure 4.5 Single Stage Savonius Rotor

B. Second Prototype

The second prototype built was also a single stage Savonius rotor in order to have the same geometrical shape as shown in Figure 4.2. New prototype was built 87% of the first prototype. The model is sized so that the output power is half of the first prototype. The two circular end plates are used for better hydrodynamic performances. As a result no central shaft is necessary to reinforce the total rigidity of the turbine.

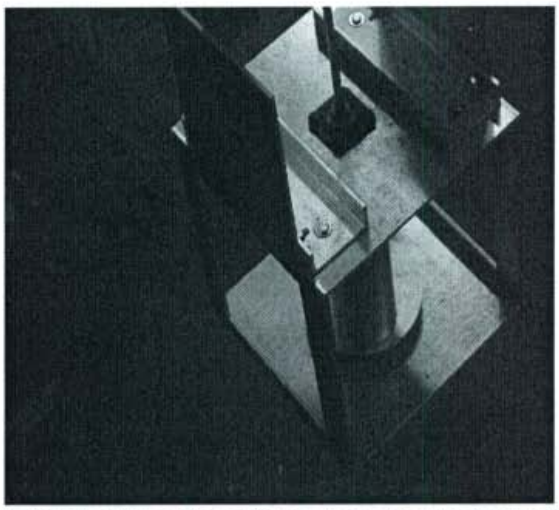

Figure 4.6 Single Stage Savonius Rotor with modified dimension

C. Third Prototype

The single stage Savonius shown in Figure 4.5 can be regarded as optimum Savonius rotor as it gives maximum value of power coefficient. It was found that for few directions of water current the starting torque would be so low that the rotor could not start alone. For this reason a double step Savonius rotor has been built as shown in Figure 4.7 where the upper and the lower paddles pairs are set at 90° to each other. It's been assumed that the torque variation decreases with a double step. The frame is open from all sides so that the water can flow from all ends.

Figure 4.7 Double Step Savonius Rotor

D. Fourth Prototype

Many researchers worked to improve the torque characteristics of Savonius rotor. A Savonius rotor with twisted rotor blade was proposed [29]. Although the twisted rotor has very good starting characteristics but it has been avoided due to complexity of blade shape and manufacturing difficulty. A three stage type Savonius rotor with three phases has been constructed as shown in Figure 4.8. It has three stages and the bucket of each stage has 60° phase shift between the adjacent stages. By this arrangement it is expected that there will be torque averaging.

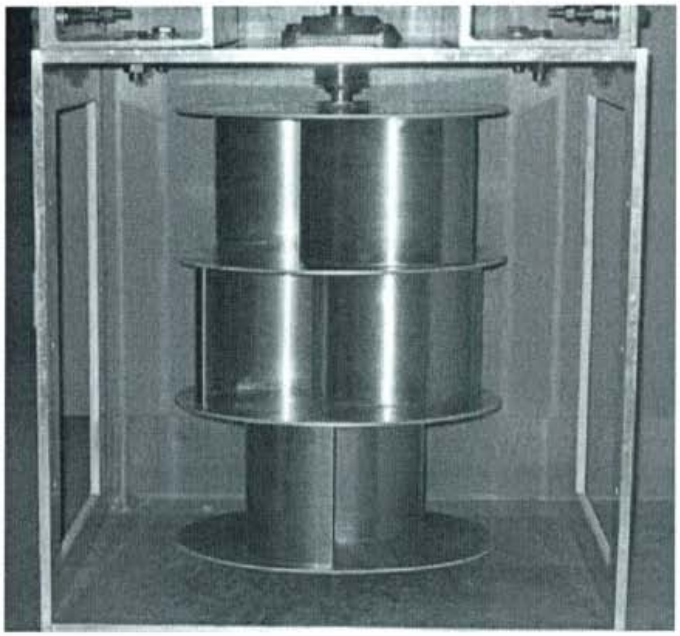

Figure 4.8 Three Stage Savonius Rotor

Sizing data for all three prototypes, and expected nominal characteristics is given in Table 4.1. The swept area of all three prototypes has been kept fixed for the comparison study of the performance.

Table 4.1 Prototypes Dimensions

Savonius Rotor Types			
Dimension	Single stage	Double stage	Three stage
Total height of the rotor (mm)	405	405	405
Height of each stage (mm)	405	202.5	135
Nominal diameter of the paddles (mm)	113	113	113
Diameter of the rotor (mm)	222	222	222
Swept area of the rotor (m^2)	0.088	0.088	0.088
Expected mechanical power (W) at 1m/s	2.25	2.25	2.25
Expected rotational speed (rev/min) at 1 m/s	120	120	120
Overlap ratio	0.207	0.207	0.207
Cut in speed (m/s)	0.38	0.38	0.40

4.5 Experimental Setup

The set up of the apparatus for the test of the prototypes in the Wave Tank and Wind Tunnel are illustrated below:

A. Wave Tank Test

The experiment was carried out in a wave tank at Memorial University of Newfoundland. At 54m x 5m x 3m, the tank is equipped with a towing carriage with a maximum speed of 5m/s and a wave maker capable of producing waves up to 0.5m in height. Figure 4.9 shows the diagram of experimental set up for measuring torque and RPM of the turbines.

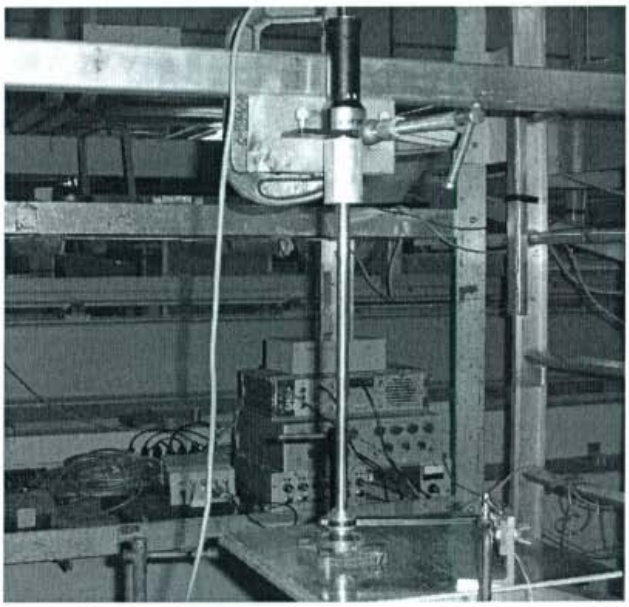

Figure 4.9 Set up of DAQ system with encoder and load cell in Wave Tank

The DAQ system was interfaced with a laptop using USB port and software DaqView 9.1. The rotational speed of the turbine is measured using rotary encoder. A calibrated load cell and a torque arm have been used to measure the torque of the rotor. The force exerted on the load cell by the torque arm times the length of arm is the torque of the

rotor. The sampling time of the data acquisition system is 0.2s. A number of wave tank tests were carried out for all three prototypes for making comparisons under different conditions. The tests included the study of constant torque, power coefficient and power output.

B. Wind Tunnel Test

Figure 4.10 shows the experimental setup in the wind tunnel. The test rotors was placed 1.5m downstream from the wind tunnel inlet and placed vertically in a center position of the cross section of wind tunnel. The torque and rpm of the rotors are measured in a similar way in the wave tank using calibrated load cell and encoder respectively. The torque arm is designed to compensate the very low friction in wind.

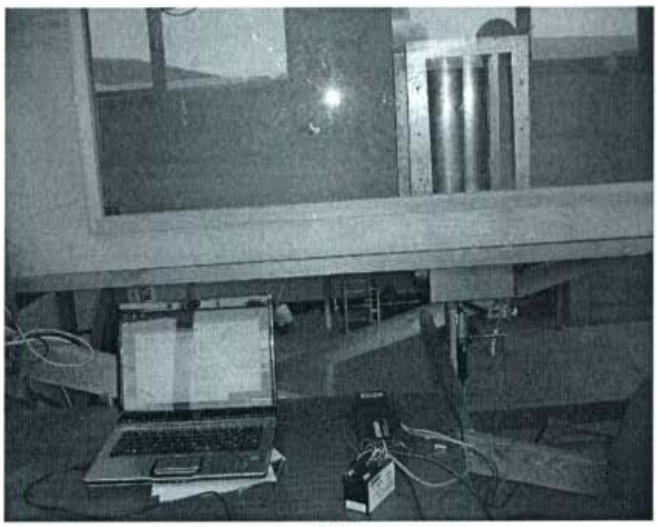

(a)

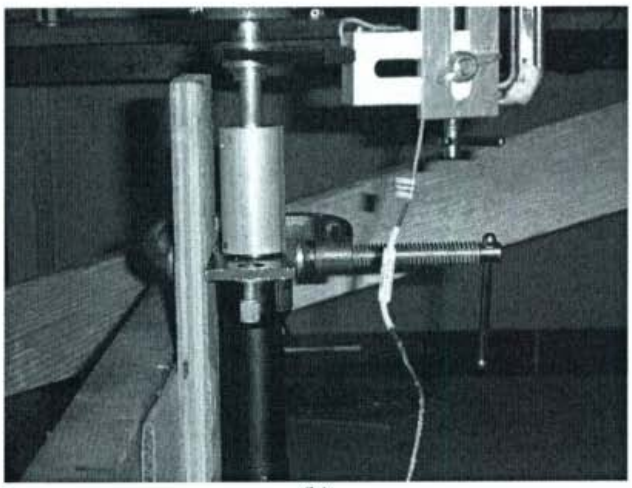

(b)

Fig. 4.10 Picture of lab setup (a) Wind Tunnel (b) Encoder & load cell

4.6 Experimental Results

MATLAB has been used to analyze the tests data and plot characteristics of the turbines (see Appendix A.1). Fig 4.11 (a) shows the output power of single step Savonius rotor. All the prototypes have been tested individually running at different speed in the wave tank. The carriage speed is maintained constant for different torque settings (i,e to maintain constant torque and constant speed) to measure steady output power. The water current speed is varied from 0.3m/s to 1.0 m/s. At a speed of 1 m/s the expected output power from the first prototype is 1.3W with the assumption that the efficiency of the turbine is 5%. From the experimental results the power obtained at 1 m/s is 1.3W which states that the efficiency of the single stage Savonius rotor is 3.8% . Figure 4.11(b) represents the power coefficient curve as a function of tip speed ratio.

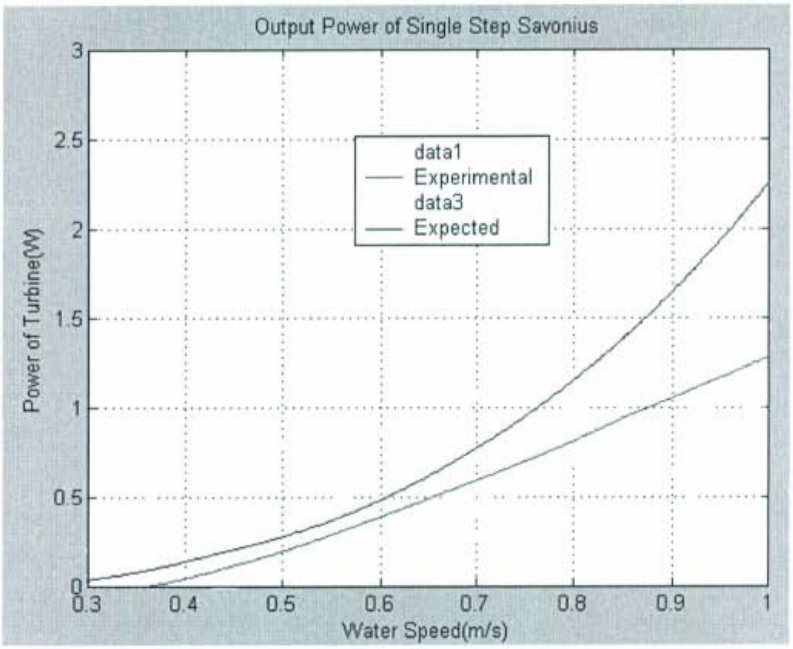

(a)

(b)

Figure 4.11 Single stage Savonius (a) Output power (b) Power coefficient

Figure 4.12 (a) shows the output power of double step Savonius rotor tested in the wave tank. The power measured at 1 m/s is 1.8W which is less than the single step Savonius

rotor. Also the efficiency of the turbine dropped below 6%.Figure 4.12(b) represents the power coefficient curve of double step Savonius rotor.

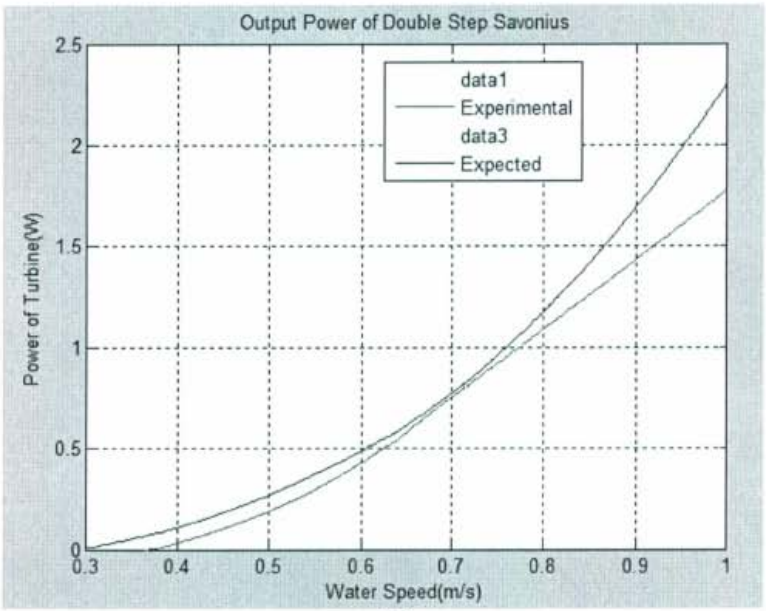

(a)

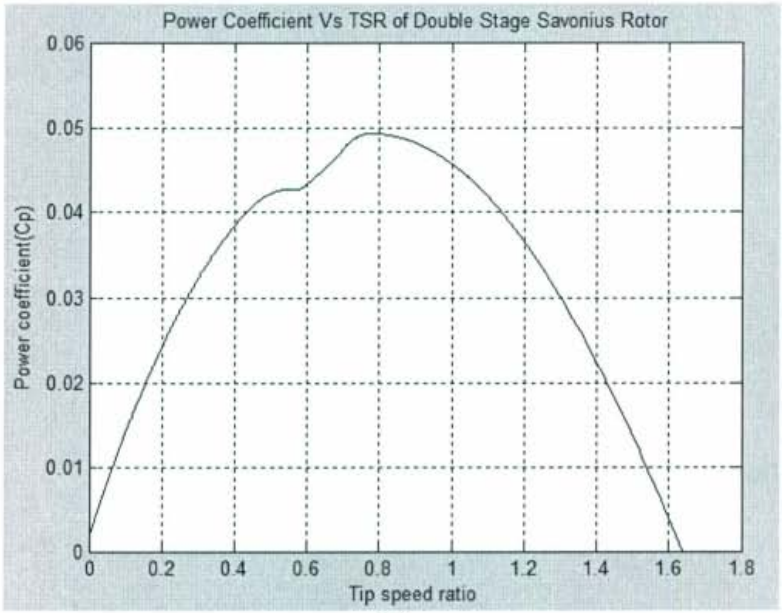

(b)

Figure 4.12 Double step Savonius (a) Output power (b) Power coefficient

The output power of the three stage Savonius rotor is shown in Figure 4.13 (a).The power obtained from three stage Savonius rotor is 1.7 W at 1 m/s and is less compared to single stage Savonius rotor. The small bump in the power curve may be also attributed to the overlap of each stage of the three phase rotor by the similarity to the one stage rotor [28]. The efficiency of a three stage Savonius rotor is found to be less than 5%. The power coefficient curve of the three stage Savonius rotor is shown in Figure 4.13(b).

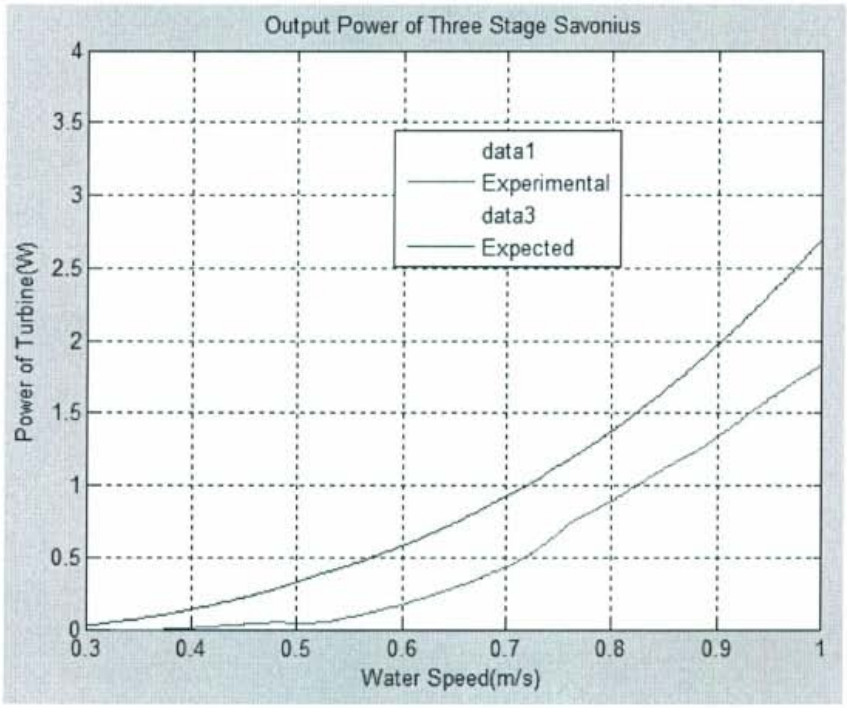

(a)

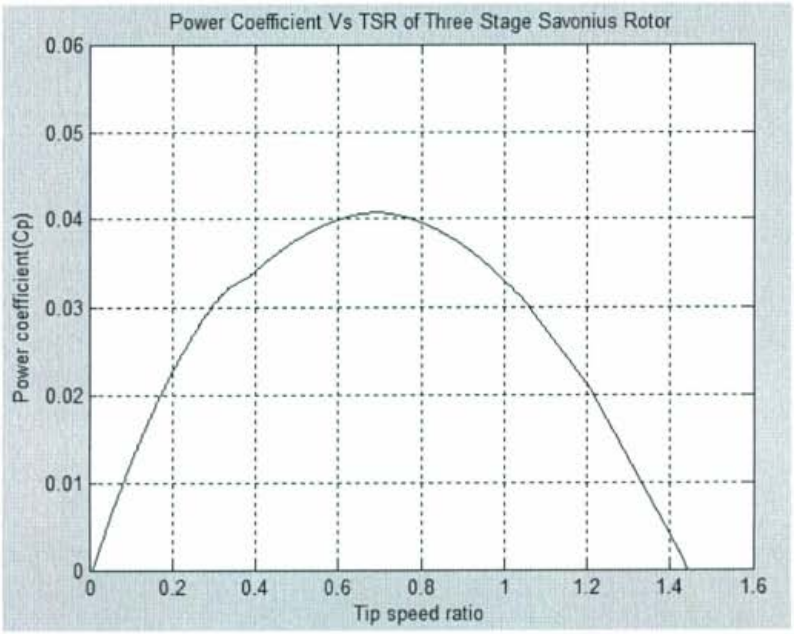

(b)

Figure 4.13 Three stage Savonius (a) Output power (b) Power coefficient

The RPM and torque characteristics of all three prototypes for water current of 0.8 m/s have been shown in Figure 4.14 and Figure 4.15 respectively. The RPM of the prototypes remains fairly steady throughout the time period. The torque peak variation is found to be less for a single phase Savonius rotor. Although the reasons for the torque variations with the progress in time is unclear. It can be considered that the effect of overlap might be an important factor [28]. Overlap might take different roles on the characteristics of rotors. Overlap might take different roles on the characteristics of rotors. Although it seems apparently that torque variation will be reduced with three stage rotor having 60° phase shift but no improvement has been found in the torque characteristics. Figure 4.16 shows the output power obtained for three different prototypes at water current of 0.8 m/s. It can

be seen that the least variation of power is observed for single step Savonius rotor (see Appendix A.2).

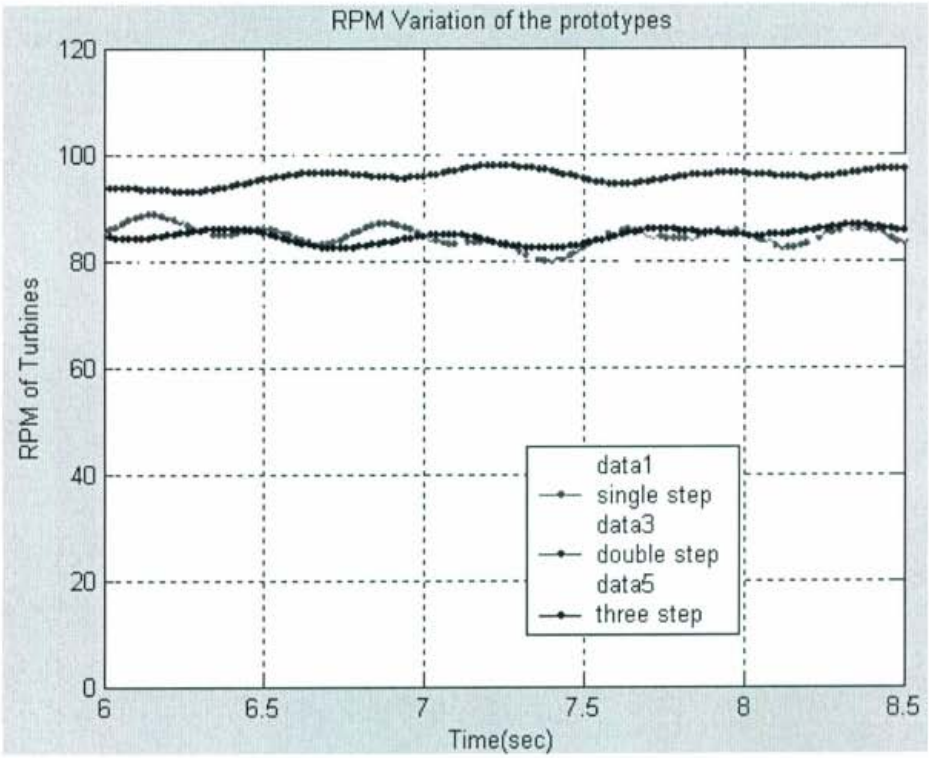

Figure 4.14 RPM variation of the prototypes

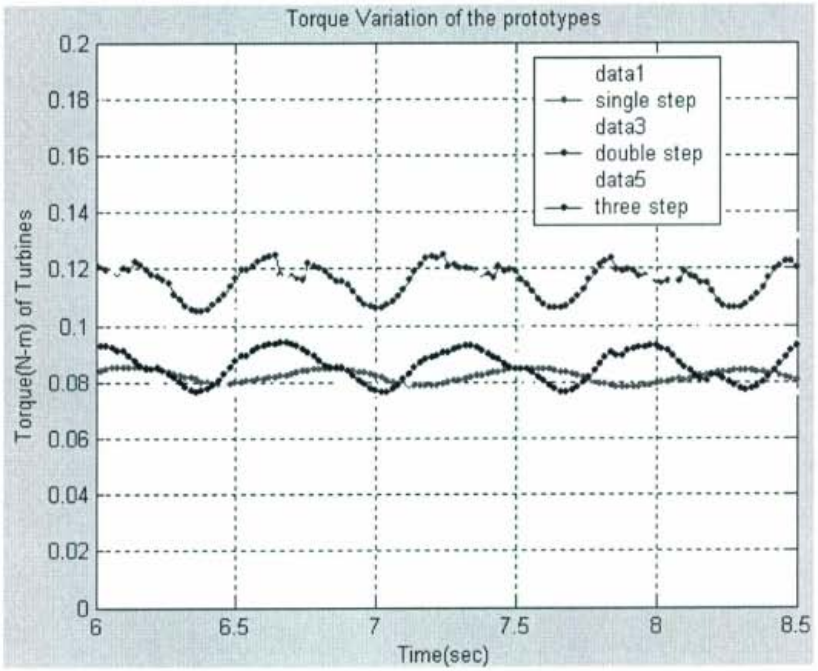

Figure 4.15 Torque variation of the prototypes

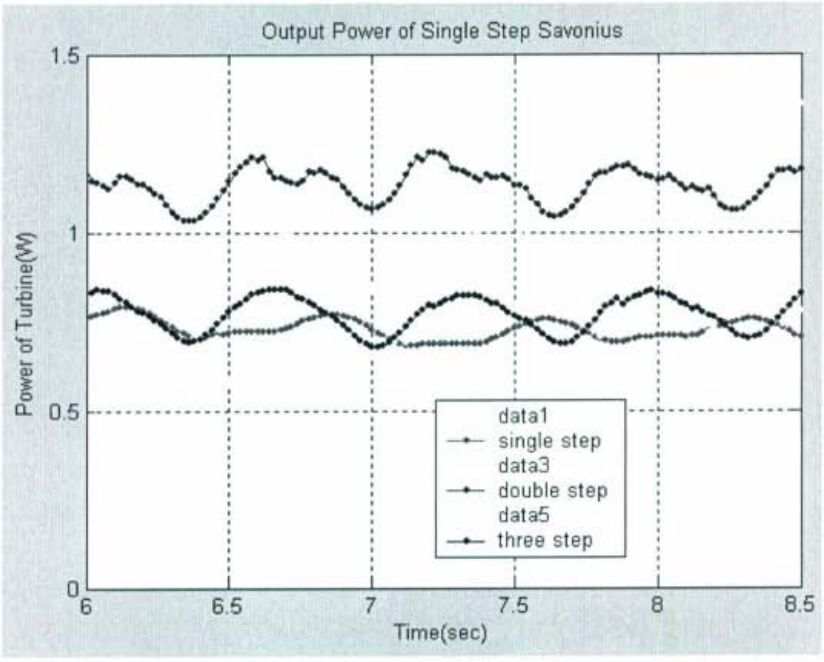

Figure 4.16 Output Power of the prototypes

Chapter 5

Power Electronic System

5.0 Introduction

The job for the power electronics in renewable energy systems is to convert the energy from one stage into another stage with the highest possible efficiency, the lowest cost and to keep a superior performance. The block diagram of the energy conversion system is shown in Figure 5.1 .Usually the power converter interfacing a dc source to the load consists of dc boost converter. This power electronic system can be used with many different loads and generators. In this case focus will be on water turbines.

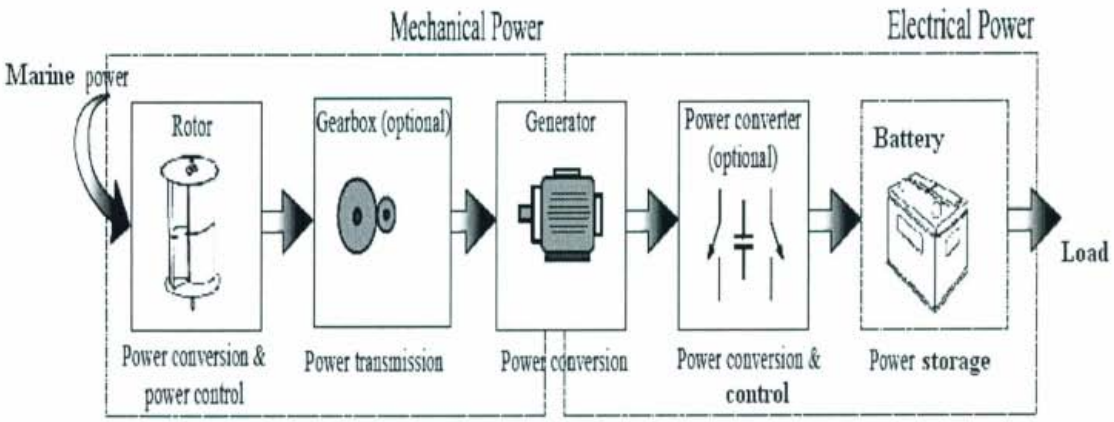

Figure 5.1 Conversion from Marine current power to Electrical power

4.7 Comparison of Prototypes

This thesis aims is to design, fabricate and test an autonomous, lightweight, low-cost, pressure-resistant energy generation system that can do power 'harvesting' from ocean current sources and deliver electric power to the 'Seaformatics' pod. Three different types of Savonius rotors have been tested to determine a suitable rotor for seafloor power generation system. The results of the experiment can be summarized as follows:

- The double and three stage Savonius rotor produced considerable amount of power.
- The maximum value of power coefficient (5%) has been found for double stage Savonius rotor. The output of the prototypes can be improved by enlarging the aspect ratio of each stage.
- The peak to peak dynamic torque variation of the single stage Savonius has been found to be smaller than the other two prototypes.
- Cut-in speed of single and double stage Savonius rotor is lowest as compared to three stage rotor.
- The small bumps were observed in the experimental result for all three prototypes and which is due to overlap.

The two stages and three stages Savonius were built to improve the torque characteristics of the rotors. From the experimental result the double stage and three stage Savonius rotor has the better performance among all three prototypes although it has high torque ripple.

Two single step Savonius rotor of same geometrical shape and different dimensions are made to justify the scaling laws of turbines.

Table 4.2 Single Step Savonius Rotor Dimensions

Dimension	First Prototype	Second prototype
Total height of the rotor(mm)	405	352.35
Nominal diameter of the paddles(mm)	113	98.31
Diameter of the rotor(mm)	222	193.14
Swept area of the rotor(m^2)	0.088	0.076
Mechanical power (W) at 10m/s in wind speed	1.8	0.9
Expected rotational speed (rev/min)at 10 m/s in wind speed	700	800
Mechanical output Power (W) at 1m/s in water current	2.25	1.13
Expected rotational speed (rev/min)at 1 m/s in water current	120	180
Overlap ratio	0.207	0.207

4.8 Wind Tunnel and Wave Tank Test Results

Matlab has been used to analyze the data obtained from the two prototypes. Figure 4.17 represents the output power of the two prototypes (see Appendix B.1). The powers measured of the first and second prototype are 1.3 W and 0.65 W respectively at 1m/s because the Savonius rotor has less efficiency. The output power of second prototype is approximately half of the first prototype at different water current (0.6m/s, 0.7m/s,0.8m/s and 0.9 m/s). Figure 4.4 also shows that the power measured of the second prototype at different water current speed is half of the first prototype. The power coefficient of the two prototypes have been plotted in using the standard technique (approach B) as shown

in Figure 4.18. The power coefficient of the two prototypes is found to coincide on each other. The friction in the bearings and the offset of the load cell can cause variation in the output power. It is recommended to use sensitive load cell with correct calibration. The offset needs to be adjusted to minimize error in readings.

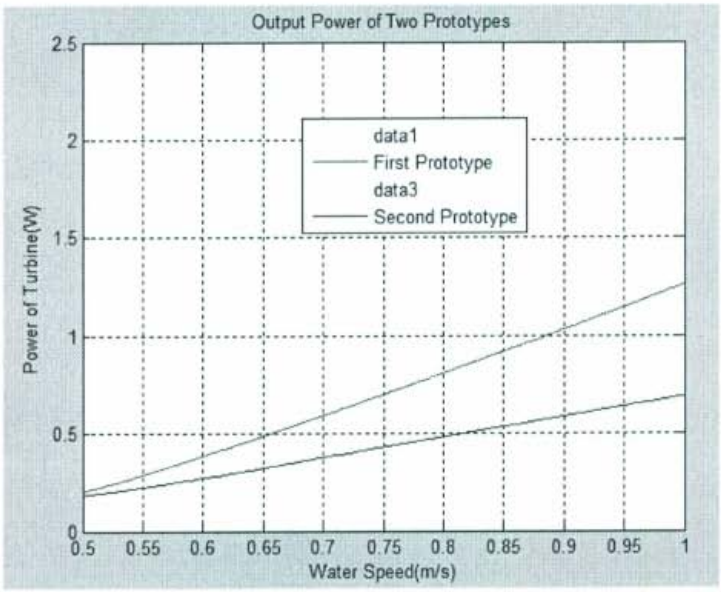

Figure 4.17 Output Power of both prototypes in the Wave Tank

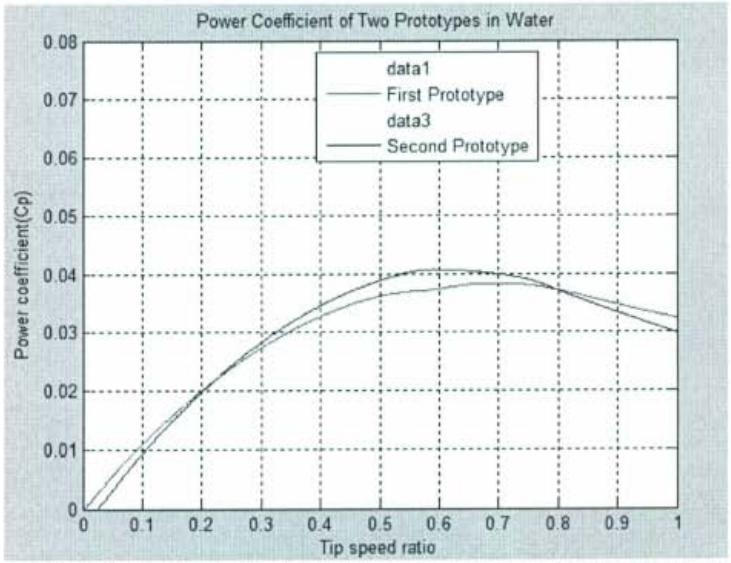

Figure 4.18 Power coefficients of both prototypes in the Wave Tank

Figure 4.19 represents the non dimensionalized power coefficient curve of both the prototypes tested in the wave tank using approach A (see Appendix B.4). Turbines of all sizes and shapes behave similarly when parameters are matched. If we restrict to turbines of the same geometry to hold the scaling law. It is advisable to adjust the offset of the load cell at the end of each run to minimize the error in measuring power.

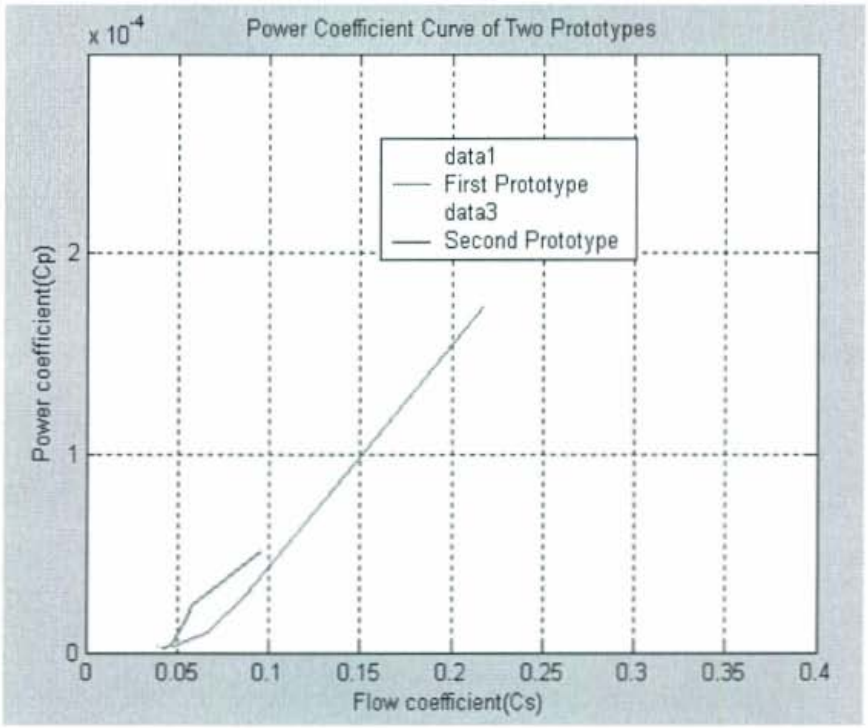

Figure 4.19 Non-dimensionalised power coefficient of both the prototypes in Wave Tank Using Approach A

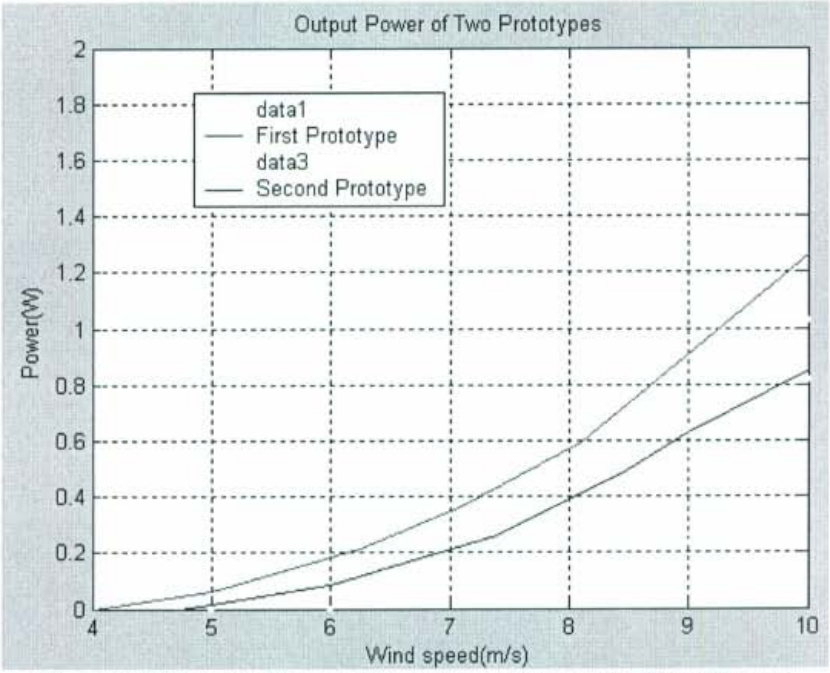

Figure 4.20 Output Power of both the prototypes in Wind Tunnel

Figure 4.20 shows the output power of the two prototypes in the wind tunnel. The power measured at 10 m/s of wind speed are 1.3W and 0.85W from the first and second prototype respectively (see Appendix B.2) .The power obtained for the second prototype at other wind speed (6m/s, 7m/s, 8 m/s, 9 m/s) is more or less half the power of the first prototype as shown in Fig 4.19.The power coefficient of both the prototypes is plotted using the approach B and A in Figure 4.21 and Figure 4.22 respectively.

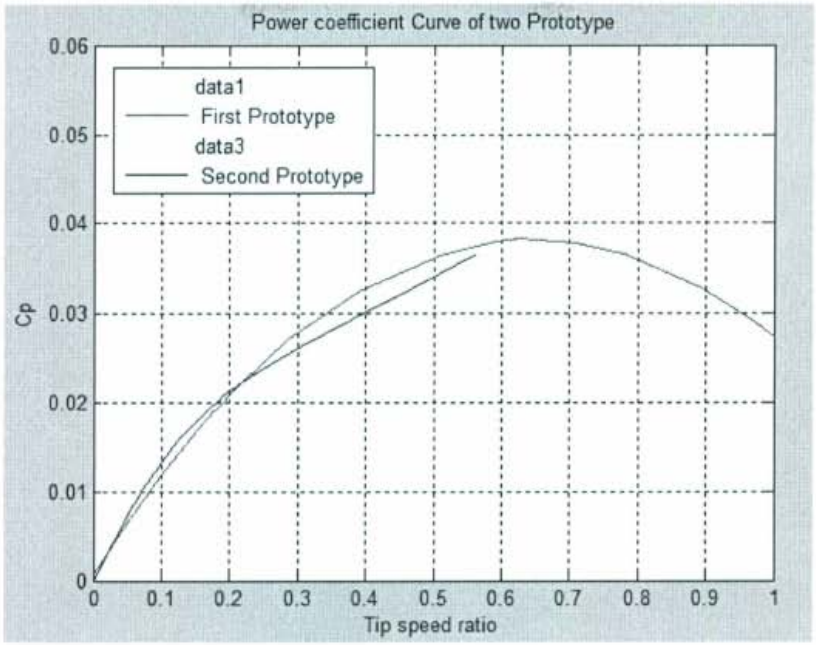

Figure 4.21 Power coefficients of both the prototypes in wind

It is being observed that the power measured at 1m/s of water current of the first prototype is 1.3W and which equal with the output power measured at 10 m/s of wind speed. Therefore the scaling laws have been justified by the Savonius rotor. Figure 4.21 shows the non dimensionalized power coefficient curve of both the prototypes tested in the wind tunnel (see Appendix B.4). In order to observe the similarity of the power coefficient curve in different types of medium, they are being plotted in Figure 4.23 and Figure 4.24 using approach B and A respectively (Appendix B.3 and B.4).The non dimensionalized power coefficient curves of two prototypes matches showing the validity of the scaling law.

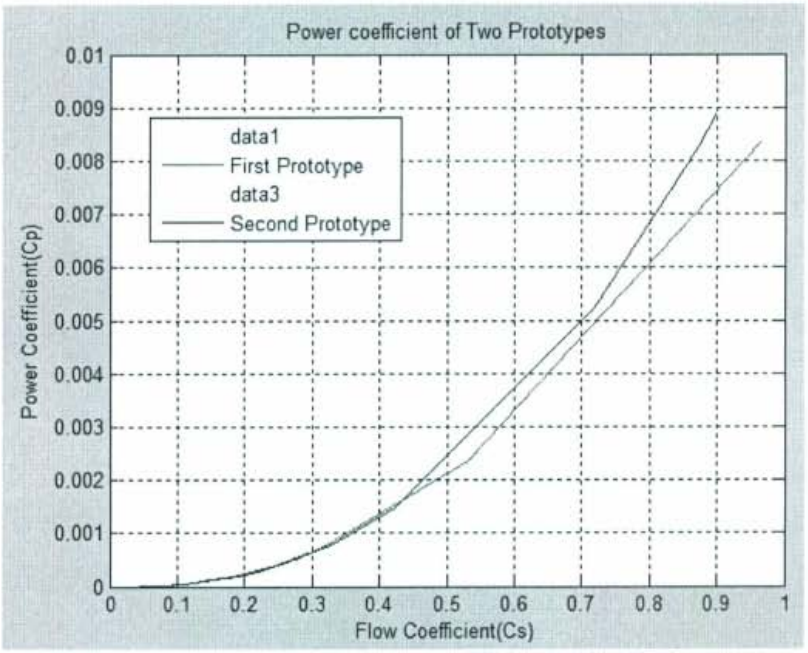

Figure 4.22 Non-dimensionalised power coefficients of both the prototypes in Wind

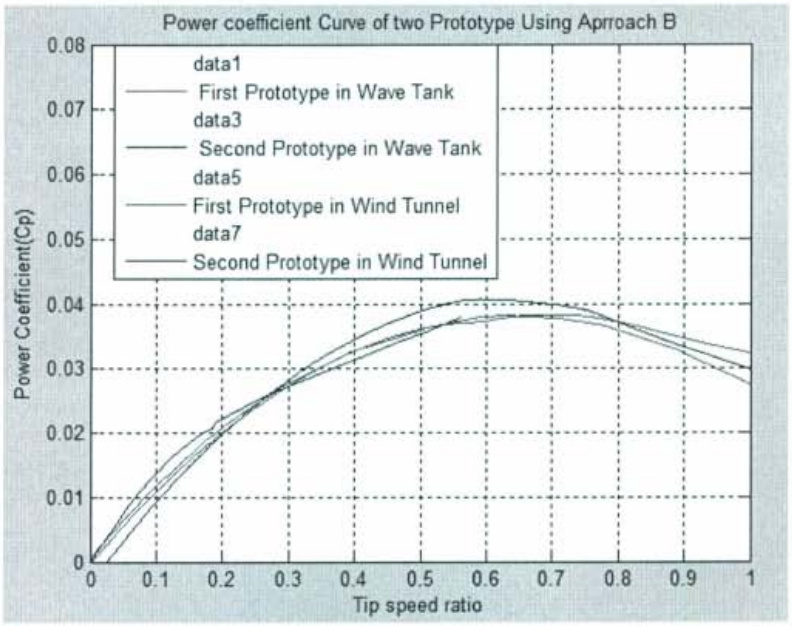

Figure 4.23 Power coefficients of both the prototypes in wind and water

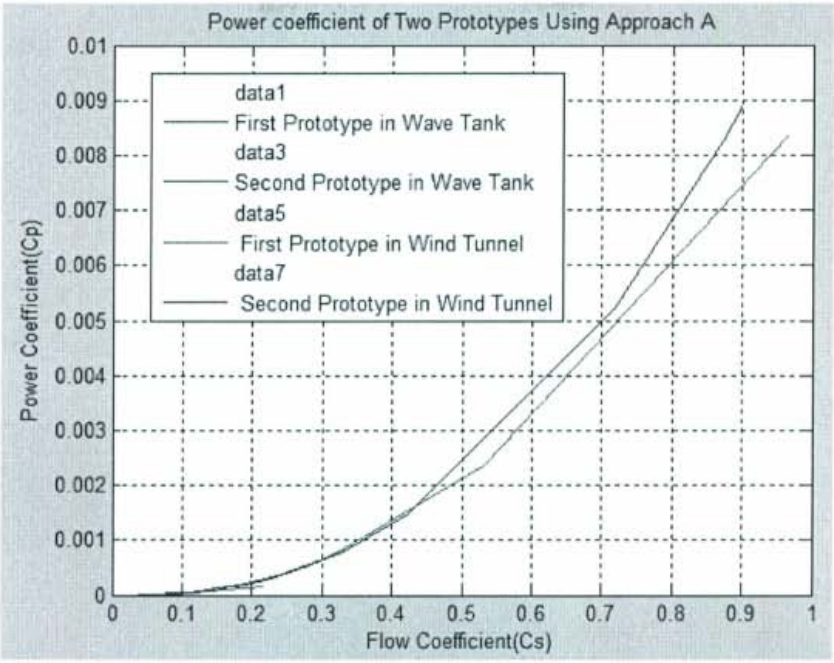

Figure 4.24 Power coefficient of both the prototypes in wind and water

4.9 Conclusions

The simplest method of dimensional analysis (a very powerful tool in experimental study of fluid mechanics) has been illustrated in this chapter. Performance parameters such as the flow, the power coefficient and the power output of turbine can be made dimensionless and form a basis for the performance prediction. Different sizes, turbines can be scaled up or down from a common design to give variations in performance characteristics. Turbine performance can also be varied by changing the operating speed. Dimensional analysis can be used to predict the effect of changes in the turbine speed, the size within a given housing on the performance of a turbine. The Savonius rotor follows the scaling law as discussed in this paper. This analysis assumes that the two turbines, model and actual, behave in a way that is captured by these laws. But the power lost due to particularly fluid friction, does not scale according to these laws and therefore cause

variation in the output of turbines. Actually, in general, smaller systems tend to have proportionately larger losses. However in Table 4.3 different size of Single step has been calculated using the scaling law.

Table 4.3Dimensions of Single Step Savonius Using Scaling Law

Scaling Power of 1st Prototype	**Height (m)**	**Diameter (m)**	**Area (m^2)**	**No. of turns (RPM)**	**Torque (N-m)**	**Power (W)**
10	0.642	0.352	0.226	98	1.267	13
20	0.737	0.404	0.298	85	2.92	26
30	0.800	0.438	0.350	78	4.77	39
40	0.847	0.464	0.393	75	6.62	52

It can be noted from the above Table 4.3 that a turbine of cross sectional area 0.298m^2 is suitable to extract few watts from marine current. This turbine is expected to generate a mechanical power of 26W at a water current of 1 m/s . If the turbine is placed in a place where there is a marine current of 0.5m/s then it will generate only a mechanical power of 4W. Since the RPM of the turbine is low, therefore either a gear box or a direct drive generator with multi-pole should be used.

Therefore the turbine needs to be placed where the current can be as high as 1 m/s to produce sufficient power. Also the single step Savonius rotor is being tested in Marine Institute Flume Tank with the side walls on to see the effect of any change in mechanical output power. The output power measured in Flume Tank is fairly same as the results found in the Wave Tank. Therefore the addition of side walls has no effect upon the change in power.

5.1 DC-DC Converters

There are many different types of dc-dc converter, each of which tends to be more suitable for some types of application than for others. For convenience they can be classified into various groups, however. For example some converters are only suitable for stepping down the voltage (buck type), while others are only suitable for stepping it up (boost type); a third group can be used for either (buck-boost). Efficiency, size, and cost are the primary advantages of switching power converters when compared to linear converters. Switching power converter efficiencies can run between 60-70%, whereas linear converters are usually 30% efficient. The basic element in power processing is the switching converter. An input voltage V_g is given to the switching converter and is controlled by a pulsed control signal to efficiently achieve the desired output voltage. The block diagram shown in Figure 5.2 depicts the fundamental components of a power converter:

- Input voltage
- Switching Converter block
- Control signal input

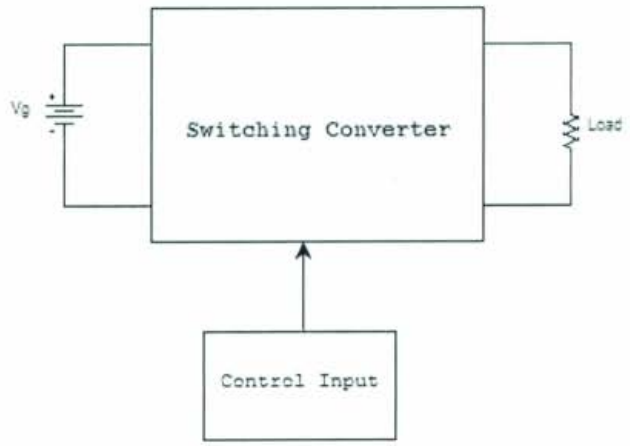

Figure 5.2 Switching Converter block diagram

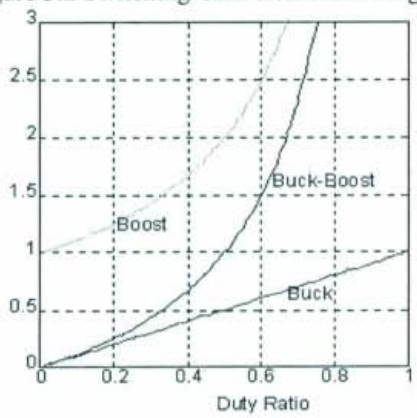

Figure 5.3 Gain Vs Duty Ratio of Different Converters

Fig 5.3 shows the voltage gain versus the duty ratio of different converters. The output voltage from the PMG is ac and its magnitude is low because of the low rpm for marine currents . It is converted into dc voltage by using a bridge rectifier converter. The dc-dc switching Boost Converter is designed to provide an efficient method of taking a given DC voltage supply and boosting it to a desired value. The dc-dc Switching Boost Converter will take a 5 Volt DC voltage supply with ±10 % tolerance and deliver 13 Volts across the load and also can charge the lead acid batteries. The basic building blocks of a boost converter circuit are shown in Fig. 5.4. The voltage source provides the

input DC voltage to the switch control, and to the magnetic field storage element. The switch control directs the action of the switching element, while the output rectifier and filter deliver an acceptable DC voltage to the output.

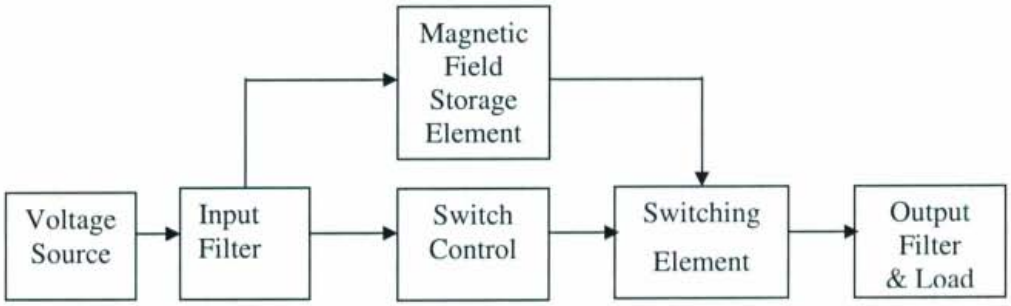

Figure 5.4 Boost converter block diagram

5.2 DC- DC Converter Operation

In many ways, a dc-dc converter can be treated as DC equivalent of a transformer . In dc-dc converters the dc energy is changed from one voltage level to another with minimum energy loss in the process. In other words, it can be described to perform the energy conversion with the highest possible efficiency. All dc-dc converters have one thing common that like a transformer, they essentially just change the input energy into a different impedance level. Inspite of any output voltage level, the output power all comes from the input and thus no energy is consumed inside the converter. Quite the contrary, in fact some energy is inevitably used up by the converter circuitry and components in the conversion process. We can therefore represent the basic power flow in a converter with the following equation:

$$P_{in} = P_{out} + P_{losses} \qquad (5.1)$$

where P_{in} is the power fed into the converter, P_{out} is the output power and P_{losses} is the power loss due to the components used inside the converter. In case of an ideal converter it would behave in the same way as a perfect transformer. There would be no losses, and Pout would be exactly the same as P_{in}. We could then say that:

$$V_{in} I_{in} = V_{out} I_{out} \tag{5.2}$$

It can be also written as:

$$\frac{V_{out}}{V_{in}} = \frac{I_{in}}{I_{out}} \tag{5.3}$$

In other words the voltage step up of a converter steps down the current, and vice-versa. As there is no perfect dc-dc converter just as there are no perfect transformers. Most converters achieve least 60-70%, which compares very well with the efficiency of most standard ac transformers. The efficiency of converter is expressed as:

$$\text{Efficiency } (\%) = \frac{P_{out}}{P_{in}} \times 100$$

5.3 Design of Boost Converter

In order for the circuit to function properly, the external components need to be calculated carefully. Assuming continuous conduction, the circuit has two topologies – switch closed, and switch open. Both of them are shown in Figures 5.5 and 5.6.

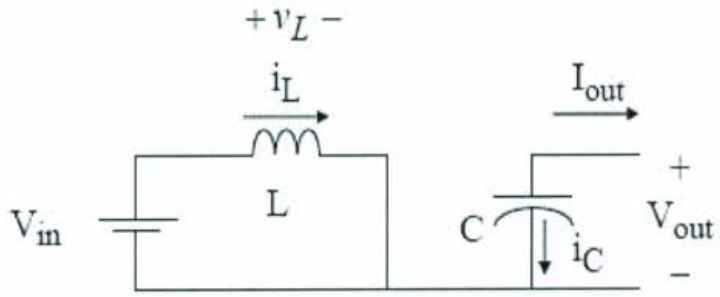

Figure 5.5 Switch Closed for DT Seconds

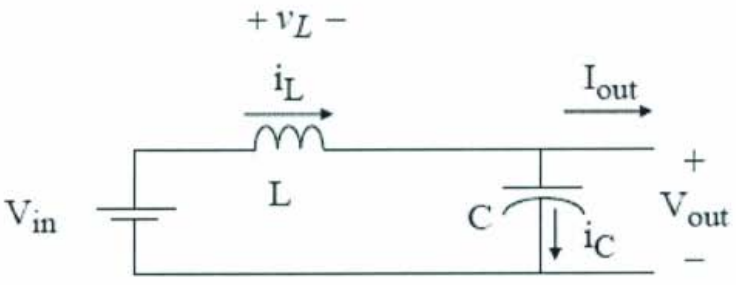

Figure 5.6 Switch Open for (1-D)T Seconds

The inductor current varies between its range of minimum and maximum values as a function of time[31]. When the inductor current is at its minimum and the switch S is closed at t = 0 then $V_{in}=V_S$. The differential equation for the inductor current, for $0 \le t \le T_{ON} = DT$ can be represented as:

$$v_L = L\frac{di_l(t)}{dt} = V_S \tag{5.4}$$

$$i_L(t) = \frac{V_S}{L}t + I_{L,\min} \tag{5.5}$$

where D is duty cycle of the converter

From (5.5) it can be seen that the inductor current increases linearly and attains its maximum value $I_{L,\max}$ as $t \rightarrow T_{ON} = DT$ such that

$$I_{L,\max} = \frac{V_S}{L} DT + I_{L,\min} \tag{5.6}$$

The change in the current from its minimum to maximum value as the peak-to-peak current ripple ΔI_L can be expressed as:

$$\Delta I_L = I_{L,\max} - I_{L,\min} = \frac{V_S}{L} DT \tag{5.7}$$

When the switch is closed the inductor current reaches its maximum value. The inductor current then supplies the load current and charge the capacitor. The corresponding differential equation for $T_{ON} \le t \le T$ is:

$$L \frac{di_l(t)}{dt} = V_S - V_o \tag{5.8}$$

The solution of (5.8) yields:

$$i_L(t) = \frac{V_S - V_O}{L}(t - DT) + I_{L,\max} \tag{5.9}$$

From (5.9) the inductor current decreases linearly form its maximum value at $t = T_{ON}$ to its minimum value as $t \rightarrow T$, such that

$$I_{L,\min} = \frac{V_S - V_O}{L}(1 - D)T + I_{L,\max} \tag{5.10}$$

Now the peak to peak ripple current is:

$$\Delta I_L = I_{L,\max} - I_{L,\min} = -\frac{V_S - V_O}{L}(1 - D)T \tag{5.11}$$

The current ripple in (5.7) and (5.11) should be same. Therefore we get

$$\frac{V_S}{L} DT = -\frac{V_S - V_O}{L}(1 - D)T \tag{5.12}$$

On simplification the equation we get

$$V_O = \frac{V_S}{1-D} \tag{5.13}$$

Equation (5.13) states that the output voltage of the boost converter is inversely proportional to (1-D) and directly proportional to the source voltage. The duty cycle is usually less than unity so the output voltage is greater than the applied voltage. Due to this reason a boost converter is commonly called the **step-up converter**.

When the switch, the inductor, and the capacitor are treated as ideal elements, the average power dissipated by these components is zero. Consequently, the average power supplied by the source must be equal to the average power delivered to the load.

$$V_S I_S = V_O I_O = \frac{V_S}{1-D} I_O \tag{5.14}$$

From (5.14) we can express the average source current in terms of the average load current as:

$$I_S = \frac{V_S}{1-D} I_O \tag{5.15}$$

The average current in the inductor for the boost converter [32] is not the same as the average load current. The source current is exactly the same as the inductor current, the average inductor current is:

$$I_{L,avg} = I_S = \frac{V_S}{1-D} I_O \tag{5.16}$$

The maximum and minimum currents through the inductor may now be written as:

$$I_{L,\max} = I_{L,avg} + \frac{\Delta I_L}{2} \tag{5.17}$$

$$= \frac{V_O}{R(1-D)} + \frac{V_O}{2Lf}(1-D)D \tag{5.18}$$

$$I_{L,\min} = I_{L,avg} - \frac{\Delta I_L}{2} \tag{5.19}$$

$$= \frac{V_O}{R(1-D)} - \frac{V_O}{2Lf}(1-D)D \tag{5.20}$$

Figure 5.7 shows the inductor current in continuous conduction mode.

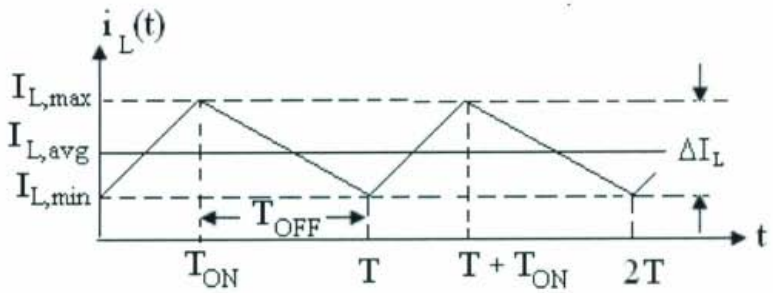

Figure 5.7 Inductor and the source currents

Now the peak to peak ripple current from (46) can be expressed as:

$$\Delta I_L = \frac{V_S}{L} DT = \frac{V_O}{Lf}(1-D)D \tag{5.21}$$

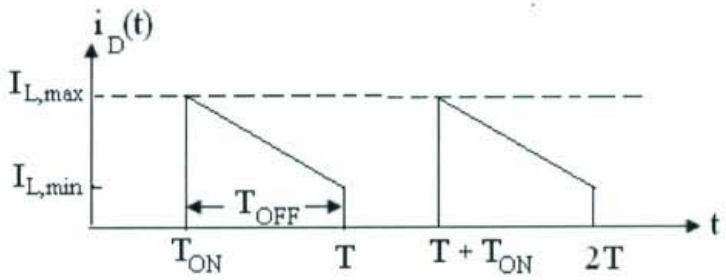

Figure 5.8 Waveform of Diode Current

The current i_D (t) through the diode is shown in Figure 5.8. Its average value is:

$$I_{D,avg} = \left(\frac{I_{L,\max} + I_{L,\min}}{2}\right)\frac{T_{off}}{T} = \frac{V_O}{R} \tag{5.22}$$

The average current in the diode is equal to the average current through the load resistor R. The average current in the capacitor should be zero. When the switch is in its closed position, the capacitor supplies the load current. Therefore for $0 \le t \le T_{ON} = DT$ the capacitor current must be:

$$i_C(t) = -I_O = \frac{V_0}{R} \tag{5.23}$$

Now when the switch is opened, the inductor current supplies both the capacitor current and the load current. Thus, during the time interval from $T_{ON} \le t_1 \le T$ the capacitor current is

$$i_C(t_1) = i_L(t) - I_O \tag{5.24}$$

When the switch is in open position the maximum and minimum values of the capacitor current are:

$$I_{C,\max} = I_{L,\max} - I_O \tag{5.25}$$

$$= \frac{V_O D}{R(1-D)} + \frac{V_O}{2Lf}(1-D)D \tag{5.26}$$

$$I_{C,\min} = I_{L,\min} - I_O \tag{5.27}$$

$$= \frac{V_O D}{R(1-D)} - \frac{V_O}{2Lf}(1-D)D \tag{5.28}$$

Figure 5.9 shows the current waveform of the capacitor in a boost converter.

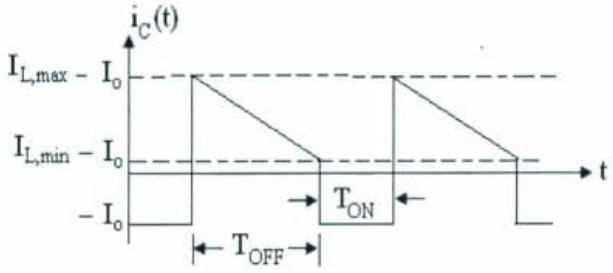

Figure 5.9 Waveform of current $i_c(t)$ through capacitor

The boost converter can operate both in continuous conduction mode or discontinuous conduction mode. When it operates in the continuous conduction mode, there will be always a current in the inductor. The minimum current in the continuous conduction mode can be zero at the time of switching. Therefore the minimum value of the inductor that ensures its continuous conduction mode is:

$$\frac{V_O}{R(1-D)} - \frac{V_O}{2L_{\min} f}(1-D)D = 0$$

$$\Rightarrow L_{\min} = \frac{R}{2f} D(1-D)^2 \tag{5.29}$$

From the peak-to-peak current ripple, we can also obtain an expression for the percent current ripple as

$$\%CR = \frac{\Delta I_L}{I_{L,avg}} \times 100 = \frac{100R}{Lf} D(1-D)^2 = 100\left(\frac{L_{\min}}{L}\right) \tag{5.30}$$

5.3.1 Boost Converter Characteristics

Figure 5.10 shows the schematic of the boost converter being made to increase the low input voltage. The circuit parameters are being extrapolated from the previous section 5.3. Matlab has been used to analyse the performance of the converter and to calculate

the circuit parameters (Appendix C.1). A load of 50 ohm is placed across the output of the converter.

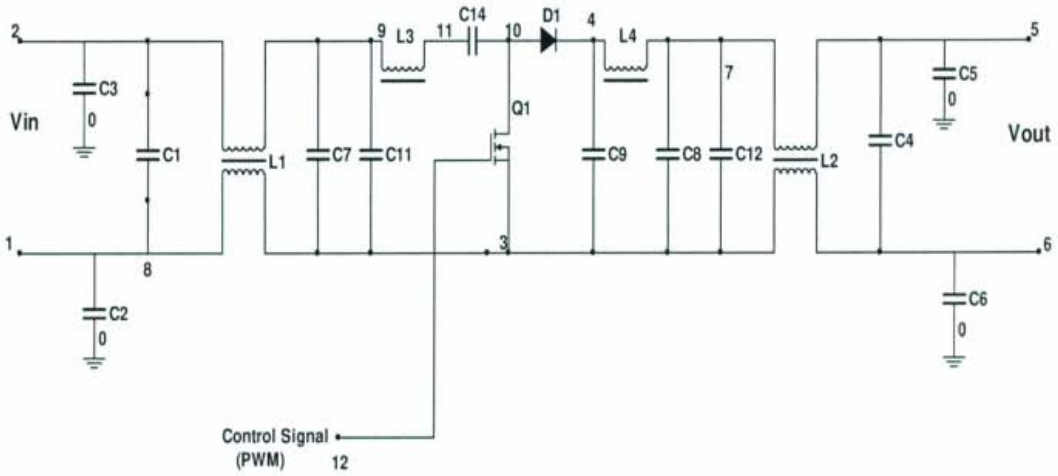

Fig.5.10 Schematic of Boost Converter

Generating the PWM signal is only one step in switching the MOSFETs. A microcontroller is only able to supply currents of 20mA and this is insufficient to do hard switching of the MOSFETs. Hard switching refers to turning a MOSFET on and off as fast as possible. This reduces losses in the converter as less time is spent in the triode region (or linear region), where high currents and voltages are experienced by the MOSFET. In order to avoid this a logic level MOSFET IRF630 has been chosen for low power application and needs V_{GS} less than 5V. Therefore, there is no need for a driver circuit for the switching of MOSFET.

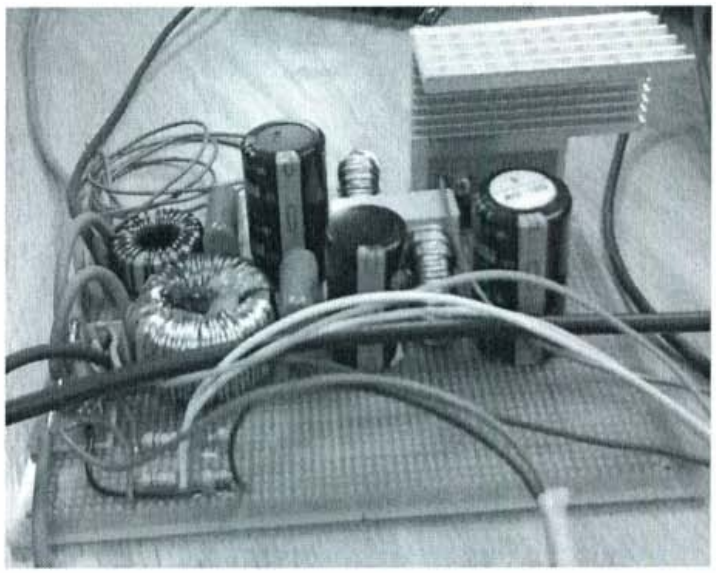

Fig.5.11 Picture of Boost Converter in Lab

Figure 5.11 shows the boost converter built and tested in the lab. The output voltage of the boost converter for varying input voltage are shown in Fig 5.12. For an input voltage of 5V the converter gives an output voltage of 13V.

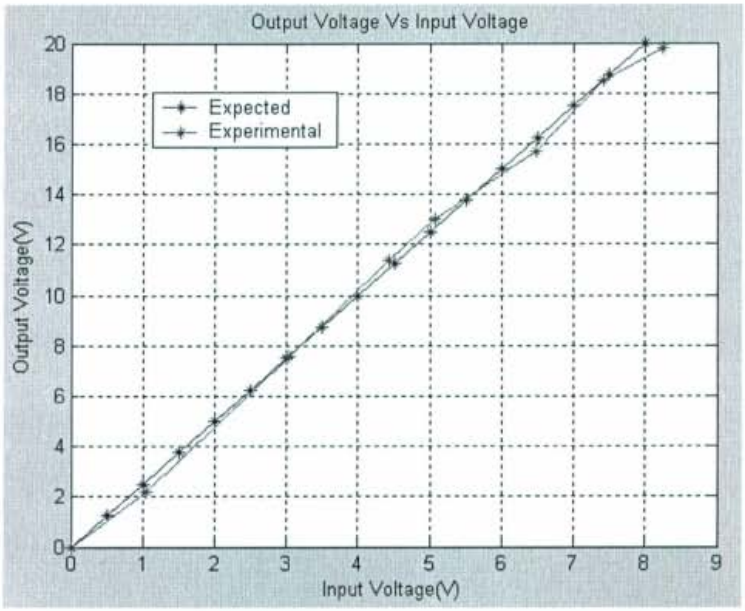

Figure 5.12 Output voltage of the Boost Converter

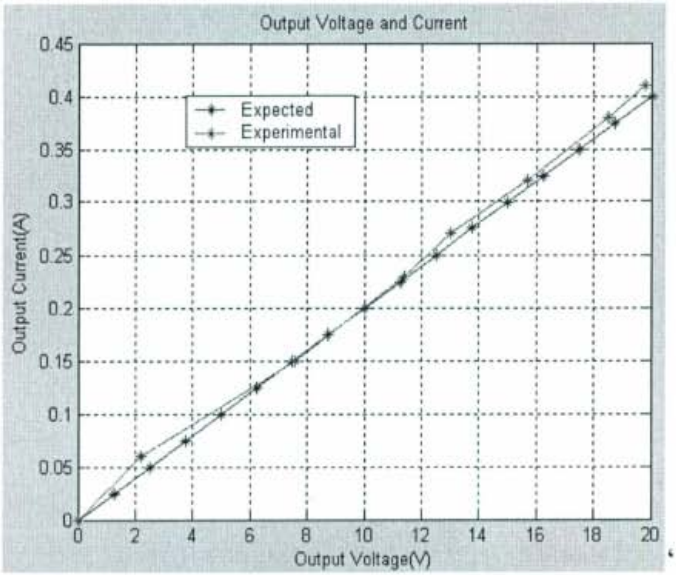

Figure 5.13 Output current of the Boost Converter

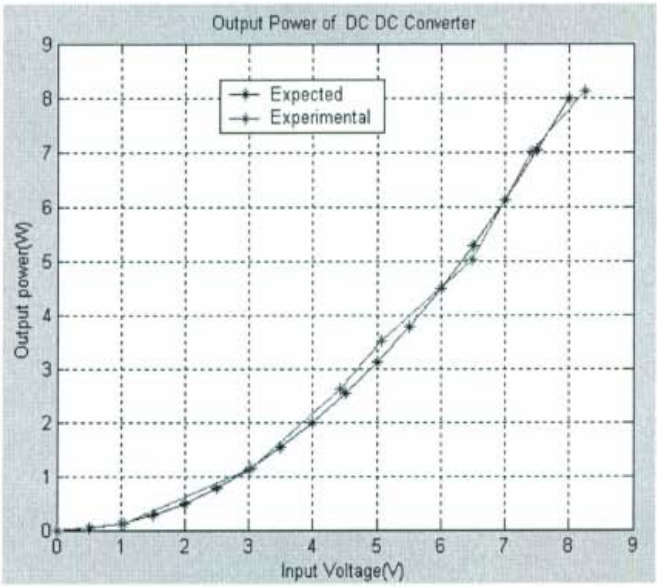

Figure 5.14 Output power of the Boost Converter

Figure 5.13 shows the output current of the converter when the load is 50 ohm. The load current obtained for an input voltage of 8.2V is 0.41A. The high percent of ripple voltage is always threatening for the battery charging. Two common mode filters (L1 and L2) are

used both in the input and output to reduce ripple in the output. In addition to this a pi filter is also used to remove the spikes from the output. Table 5.1 shows the list of components to make the boost converter.

Table 5.1 List of Components of Boost Converter

Label	Description	Quantity
C1,C2,C3,C4,C5,C6	0.01uf electrolytic capacitor	6
C7,C12	250uf electrolytic capacitor	2
C8	470uf electrolytic capacitor	1
C9,C11	680uf electrolytic capacitor	2
L1	150uh inductor	1
L3,L4	380uh inductor	2
L2	260uh inductor	1
Q1	IRF630	1
D1	MUR815 Diode	1

5.4 Pulse Width Modulation

Power-switching is the basis of operation of all dc-dc converters. For a certain switching frequency f_s, i.e. period Ts, the output voltage would be an equivalent intermittent form of the input voltage. The output voltage is given to be the average of the alternating waveform. Switching control is mostly done using Pulse Width Modulation switching or

PWM control. In PWM switching a saw tooth waveform carrier is compared to a reference voltage. Whenever the reference voltage is greater in amplitude than the saw tooth amplitude, the switch turns on, and it turns off when this voltage is lower.

There are various ways to generate pulse width modulation, PWM analogue circuitry, PWM chips, digital counters, and the timers on microcontrollers. As a microcontroller is required to design a maximum power point tracking system, using a microcontroller to generate the PWM represents a cheap solution and requires no additional hardware. Many of the microcontrollers allowed for their timers to be used for PWM and the control signal is generated using PIC 16F877.

Normal PWM uses a counter that counts up and down between the maximum counter and zero [33]. This repeats itself continuously with each increment or decrement occurring at the clock frequency or a prescaled division of the clock frequency. A compare register is used to generate the PWM output from the counter. When the compare value matches the counter value a pin was set high if the counter is counting down or low if the counter is counting up. This generated the PWM output as seen in Figure 5.15 and once started the PWM required no intervention from the microcontroller.

Figure 5.15 Normal PWM operations

The compare value sets the duty cycle of the PWM and the maximum frequency of the PWM can be derived as f_{max}. A reasonable frequency is 20 MHz and the counter range

for most microcontrollers is 10bits, 320. This creates a maximum frequency of 31.25 kHz.

$$f_{\max} = \frac{f_{clk}}{2 \times CounterRange} \tag{5.31}$$

5.5 Efficiency

The perfect dc-dc converter would be one where none of the incoming dc energy is wasted in the converter it would all end up converted and fed to the output. Needless to say this doesn't occur in the real world.

Inevitably practical converters have losses i,e voltage drops due to resistance in the inductor, 'on resistance' in the MOSFET's, forward voltage drop in the rectifier diodes, eddy current and hysteresis losses in the inductor . In this converter design all of these losses have been to the lowest possible level, to make the converter as efficient as possible. MOSFETs has been used as switches in most of the converter circuits because modern MOSFETs make the most efficient electronic switches of high dc currents. When 'off' it is virtually an open circuit, and when 'on' they are very close to a short circuit and possess typically only a few milliohms and thus waste very little power.

The diodes used in most modern dc-dc converters are of the Schottky or fast recovery. These have a significantly lower forward voltage drop than silicon diodes, and hence waste less power. Although using high frequency allows the use of smaller inductors and capacitors to handle the same power level. And this in turn allows a reduction in both the size and material cost of the converters. But moving to a higher operating frequency also increases some kinds of losses. The efficiency of the converter is 65%. Although increasing the input power results in an increased output power but the switching and

conduction losses of the converter do not increase at the same rate. The switching power loss remains constant.

5.6 System Instrumentation

5.6.1Voltage Sensor

The ADC input of microcontrollers varies between GND and V_{cc}. As microcontrollers generally operate with a V_{cc} of 5V, the analogue input voltages to the microcontroller vary between 0V to 5V for the current and voltage sensors. For the voltage sensor the expected range of its operation is 0V to 20V. This is as simple as a voltage divider, shown in Figure 5.16.

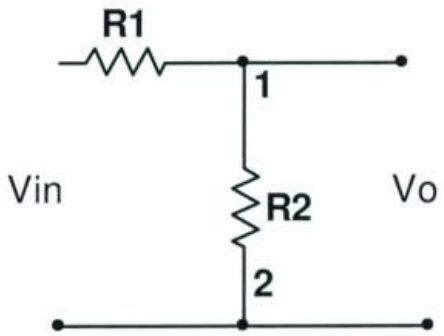

Figure 5.16 Voltage Divider Circuit

The input resistance of the microcontroller is in the Mega ohm range, and this resistance is placed in parallel to R2. To prevent this extra resistance from causing significant error the resistor R2 is smaller than 20k for a possible 1% error when MΩ is placed in parallel. Having R2 and R1 too small means the voltage sensor can cause too much of a power drain.

$$V_o = \left(\frac{R2}{R1+R2}\right)V_{in} \tag{5.32}$$

The value of R1 and R2 calculated are 3KΩ and 1KΩ respectively. Two voltage divider circuits have been used both at the input and output of the converter. In order to read the voltage properly a calibration factor has been used.

5.6.2 Current Sensor

The current sensor is not as simple. The ADC of the microcontroller only measures voltages so the current must be converted into a voltage reading. The Allegro ACS713 has been used to measure the DC current as shown in Fig 5.16.

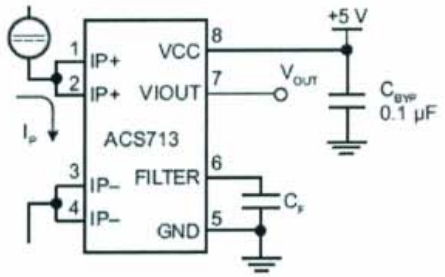

Figure 5.17 Connection diagram of ACS713

When current flowing through the primary copper conduction path increases (from pins 1 and 2, to pins 3 and 4) the output of the device has a positive slope and the path is used for current sensing. The internal resistance of this conductive path is very small 1.2 mΩ to provide low power losses. The thickness of the copper allows five times over current to flow through it. The ACS713 is provided in a small, surface mount SOIC8 package.

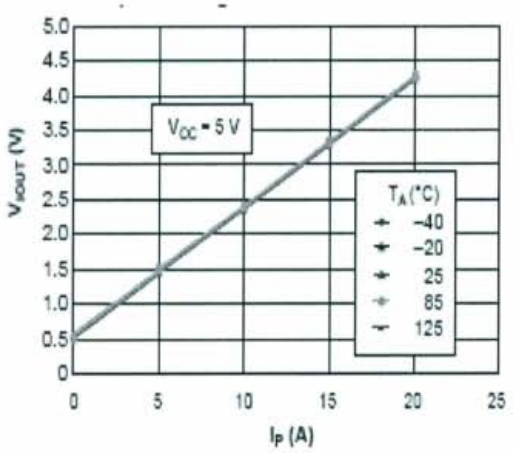

Fig 5.18 Output Voltage versus Sensed Current

In order to read the current properly a calibration equation is used. Figure 5.17 shows the variation of output voltage with current.

5.7 Energy Storage System

An energy storage mechanism has been built for an autonomous design. This energy storage system should meet power requirements and effectively store any excess power generated from the system. Energy storage in the form of a battery of electrochemical cells is considered. Five batteries chemical were considered for the storage: Lithium-ion (Li-Ion), Nickel-Metal-hydride (Ni-Mh), Nickel-Cadmium (Ni-Cd), Sealed Lead Acid (SLA), and Nickel-Zinc (Ni-Zn). Properties considered include cost, energy density, cycle life, memory effects, availability, self-discharge rate, and charging rate.

Sealed Lead Acid (SLA) or "gel cell" batteries are most available and inexpensive and known as the most rechargeable battery technology .They are also well known for it's reliability and low self-discharge rate. They are large in size providing 10-20 Whr/lb. It is free of memory effects and prefers shallow cycling. They have a short deep-cycle life (100-500 cycles), but this figure improves dramatically with more shallow cycling.

Nickel Cadmium (Ni-Cd) batteries have relatively a better energy density (20-30 Whr/lb), long cycle life and a high discharge rate. They are more prone to memory effects than any other battery and requires deep cycling to maintain optimal performance.

Nickel Metal Hydride (Ni-MH) has high energy density (25-35 Wh/lb) and medium-length cycle life (approximately 1000 cycles). They are the most popular rechargeable batteries and ideally suitable for personal use. They have a small memory effect and a high self-discharge rate and being used occasionally in renewable energy-based products, particularly where weight and size are a concern.

Lithium-Ion (Li-Ion) possesses a very long life cycle and are free of memory effects and the high energy density in the market. It's the most expensive battery considered. It is complicated to charge these batteries and do not handle trickle-charging very well. High-capacity Li-Ion's are very rare and typically used only in small-size/small power requirement applications.

Ni-Zn batteries is a new technology and very popular. It has a high energy density (25-30 Wh-lb) and an excellent life cycle (500-10,000 but varies exponentially with depth of discharge). The charging regime is very strict, requiring a sustained high-current source

Table 5.2 shows a short review of typical properties for different type of battery considered. The "Environmental Impact" is an important issue when focusing into "green" technology. This comparison is based upon perceived environmental stigmas associated particularly with using lead and cadmium. Sealed lead acid battery has been found to be a suitable choice for charging in seafloor.

Chapter 6

Experimental Energy Conversion System

6.0 Introduction

This chapter describes the setup and test results of a small marine current energy conversion in the laboratory. A block diagram of the system is shown in Figure 6.1. The power system developed consists of drag-type Savonius rotor, a multi-pole permanent magnet generator, energy storage, a controlled dc-dc converter, instrumentation and a microcontroller-based control system. The system will supply power to charge batteries and signal conditioning circuits of a seafloor instrumentation system. Microcontroller controls the dc-dc converter to extract the maximum power from the system. Such a control scheme is based on the voltage, current and speed measurement of the system. Maximum power algorithm based control scheme makes sure that the system is always extracting the maximum power from the water current.

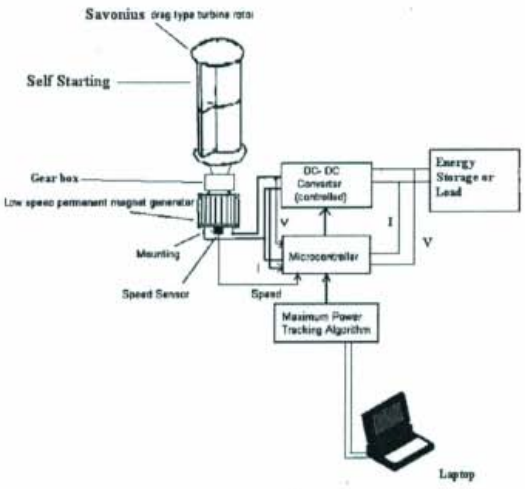

Figure 6.1 Block Diagram of the Energy Conversion System

Table 5.2 Comparison of Battery Properties

Battery Attributes	**Ni-Cd Nickel-Cadmium**	**Ni-MH Nickel-Metal Hydride**	**SLA Sealed Lead Acid**	**Li-Ion Lithium Ion**
Cycle Life (80% of Initial Capacity)	1500	300 to 1500	200 to 300	500 to 1000
Power Density (Whr/kg)	45 to 80	60 to 120	30 to 50	110 to 160
Operating Temperature Range (°C)	-40 to 60	-20 to 60	-20 to 60	-20 to 60
Charge Time (Hours)	1	2 to 4	8 to 16	2 to 4
Cost ($ US / Cycle)	0.04	0.12	0.10	0.14
Environmental Impact	Very High	Low	Moderate	Low

5.8 Battery Charger Circuit

Figure 5.18 shows the lead acid battery charger. The LM317 is an adjustable 3 terminal

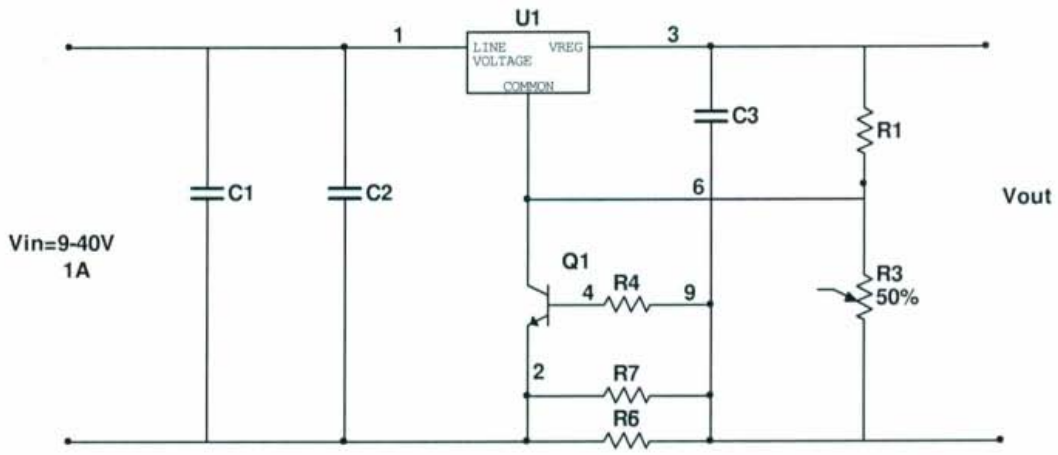

Figure 5.19 Lead –Acid Battery Charger

positive voltage regulator capable of supplying in excess of 1.5 amps over an output range of 1.25 to 37 volts. The output voltage can be adjusted by three resistors R1, R2

and R3 as shown in Fig 5.17. The voltage across R1 is a constant 1.25 volts [34] and the adjustment terminal current is less than 100uA. The output voltage can be approximated by the following relationship:

Table 5.3 Component List of Lead Acid Battery Charger

Label	Description	Quantity
C1	1000uf electrolytic capacitor	1
C2,C3	220nf electrolytic capacitor	2
R1	120 ohm	1
R3	5 kohm variable	1
R4	100ohm	1
R6	1ohm ,10W	1
R7	1 ohm,10W	1
Q1	2N3904 N-type transistor	1
U1	LM317 ,Adjustable Regulator	1
Heat Sink	Attached with LM317	1

$$V_{out} = 1.2 \times \left(1 + \frac{R3}{R1}\right) \tag{5.37}$$

For a 12 V battery the value for R3 is equal to 1250 ohm. As the battery charging circuit acts as a constant current model with current limit. The current limit is being set when it reaches $\frac{0.6}{(R6 \parallel R7)}$ .The excess current biases Q1 and drops output voltage. Table 5.3 shows the circuit parameters of lead acid battery charger circuit.

The output voltage of the converter is fed into the battery charger circuit to charge the batteries.

5.8 Conclusions

In this chapter the design and test result of the boost converter has been presented. A simple battery charger circuit used to charge the lead acid battery is also discussed. The next chapter will discuss the control of the dc-dc converter for a small marine energy conversion system.

6.1 Water Current Turbine Emulator

A water current turbine emulator (WCTE) is important equipment for developing marine current energy conversion systems. The emulator can be used to drive an electrical generator in a similar way as a water current turbine, by reproducing the torque developed by a water current turbine for a given marine current. It offers a controllable test environment that allows the evaluation and improvement of control schemes for electric generators and which is hard to achieve with an actual water turbine since it's not possible to test in the wave tank all the time. A dc motor is the usual choice to provide the variable output torque, because the torque it develops is proportional to the armature current. It is generally assumed that the proposed turbine will drive the generator at a constant tip speed ratio (TSR) and not exceeding the critical velocity for cavitation. Also a direct drive machine will experience variable generator rotor speed depending on the current velocities. In order to test the energy conversion system a laboratory prototype is built using a permanent magnet dc motor driven by manual controlled dc voltage as shown in Figure 6.4 . A variable dc supply is being used to vary the speed of the generator and to observe the output at different operating speed. It is being considered that the generator will be connected with the turbine of swept area of 0.35 m^2 and a gear box ratio 1:3 as described in Chapter 4 .The generator has been purchased from Aquair and known as UW submersible generator.

The expected rotational speed of the turbine is shown in Figure 6.2. The output voltage and current of the generator that can be used with this turbine is shown in Figure 6.3.

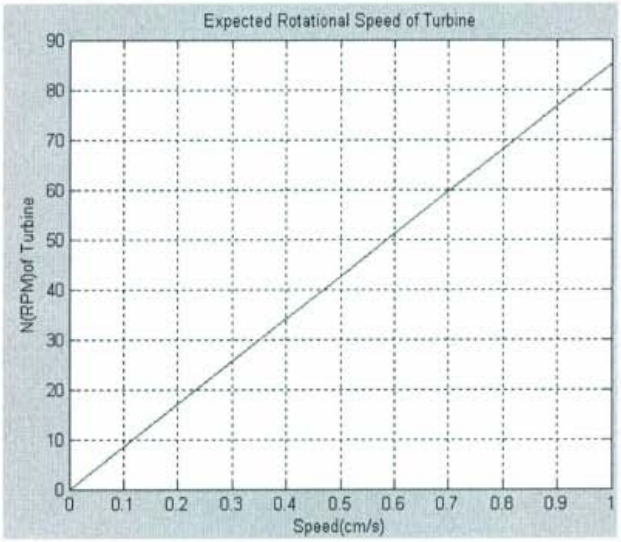

Fig 6.2 RPM of Turbine at different Marine Current

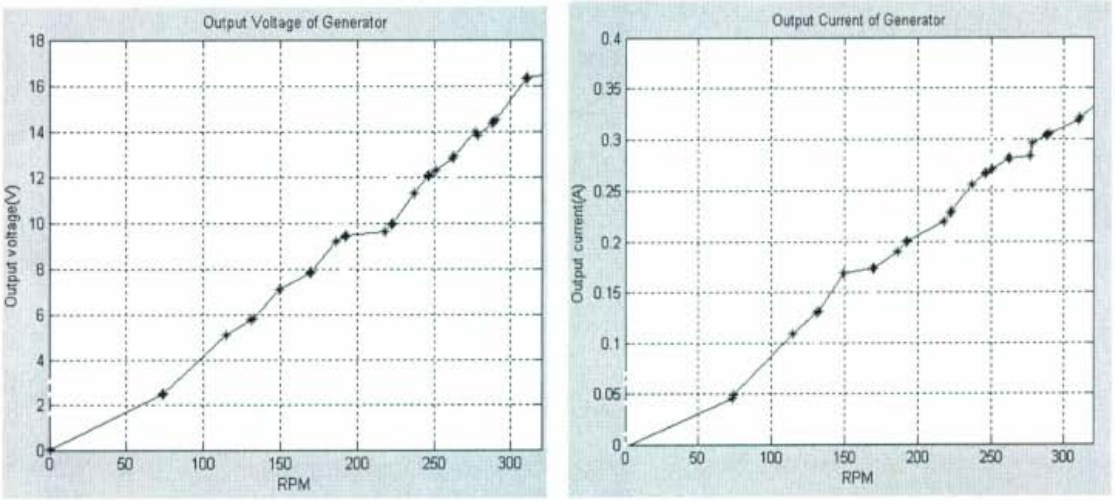

(a) (b)

Fig 6.3 Generator (a) Output Voltage (b) Output Current for a 50 ohm load

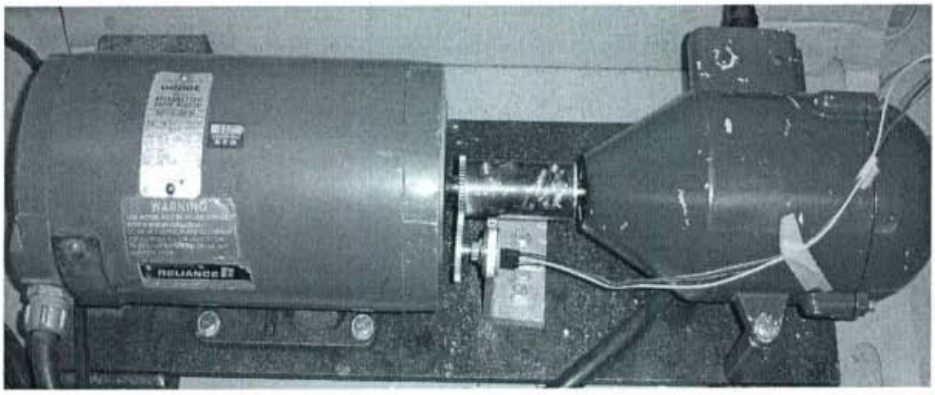

Fig 6.4 Water Current Turbine Emulator

6.2 Generator Selection

For marine current energy conversion systems there are two ways of selecting a generator

- a conventional and relatively high speed generator together with a gearbox
- a direct drive generator.

Study from the wind power energy conversion systems indicates that a system without a gearbox offers higher overall efficiency and reliability (low maintenance) [35-37].

According to Faradays law of induction a voltage E is induced due to rate of change of an alternating magnetic flux Φ in N number of coil turns.

$$E = -N\frac{d\phi}{dt} \tag{6.1}$$

The total induced voltage E in a generator is the sum of the voltages induced in each individual coil of the machine. In the magnetic circuit of a generator the magnetic flux Φ is the magnetic flux density B in the stator integrated over the loop area due to the coil sides of the stator winding.

The root mean square (rms) voltage for a generator can be derived from Faradays law of induction as follows:

$$E_i = 4.44 f N \varphi_{max} k_w \tag{6.2}$$

where N denotes number of turns per phase, k_w represents winding factor and Φ_{max} is the maximum magnetic flux per pole in the air gap. The frequency of the generated voltage is given by (6.3) where n is the rotor speed in revolutions per minute (RPM) and P is the number of poles.

$$f = \frac{p}{2} \cdot \frac{n}{60} \tag{6.3}$$

It is seen from above equations that the induced voltage largely depends on the rotational speed and the air gap flux. From (6.3) it can be seen that the low rotational speeds can be compensated by increasing the number of poles [38]. The result will be a generator with a very large diameter.

6.2.1 Cogging Torque in Low RPM Generators

It is important to reduce the cogging torque in a PM generator because it affects the starting ability and produces noise and mechanical vibration . Cogging is a phenomena occurring due to the non homogenous stator reluctance and therefore the magnets tends to cling to the stator teeth. Cogging torque is the torque produced by the shaft when the rotor of a PM generator is rotated with respect to the stator at no load condition. Cogging torque is an inherent characteristic of PM generators and is caused by the geometry of the generator. The following are two cogging torque conditions:

Turbine Start-up:

During start-up, when the rotor speed is very low the TSR is also low. At low TSR, the resulting Cp is very low, thus the hydrodynamic power is low. Hence it is desirable that during start-up the cogging torque of the PM generator is low enough that the hydrodynamic power can overcome it. Otherwise, with a large cogging torque, the turbine may not start.

Turbine Running Condition:

Small turbines typically have lower rotor inertia than large turbines because of their shorter blades and lower mass. Thus, the cogging torque excites the structure of the wind turbine and the smoothing effect of inertia is not very dominant. This is particularly apparent in a small wind turbine during low wind speeds when the rotor rotational speed is low. Noise and mechanical vibration may be excited by the cogging torque. This type of vibration may threaten the integrity of the mechanical structure of an improperly designed small wind turbine. In high wind speed, the amount of torque and the kinetic energy stored in the rotor is sufficiently large that the cogging torque is insignificant.

6.2.2 Elimination of Cogging Effect

Factors contributing to the cogging torque include the following:

- Pole shape: the non uniform (bread loaf) pole shape of the permanent magnet reduce cogging torque.
- Pole arc to pole pitch ratio: There is a minimum cogging torque as the pole arc to pole pitch ratio is varied.
- Skewing: A perfect skew can nearly eliminate cogging torque.

There are two types of windings commonly employed, distributed and concentric windings. The difference between the two is merely due to the different arrangement of the end connections. Fractional pitched windings are mainly used in synchronous generators with large number of poles, in order to reduce cogging and harmonics. A fractional winding reduces such effects since the stator slots are not consistently distributed across every pole. The symmetry is broken and cogging is reduced considerably [40]. When fractional windings are used the induced voltage is reduced with a winding factor, $k_w=k_d*k_p$ where k_p is the pitch factor and k_d is the distribution factor.

6.2.3 Generator Losses and Efficiency

The electromagnetic losses in a generator can be categorized as copper losses and iron losses. Copper losses occur due to the losses in the stator windings while the iron losses occur in the stator iron lamination. The iron losses in the machine can be divided into hystersis losses and eddy current losses. However, the eddy current part is small and can be neglected because stranded conductors and the low permeability of copper. The copper losses can be expressed as:

$$P_{cu} = I^2R \tag{6.4}$$

where R is the winding resistance and I is the current. The total iron losses are due to the varying magnetic field in the stator core and are given by sum of hysteresis, eddy current and excess losses respectively.

$$P_{Fe}=k_hB_{max}+k_{eddy}(B_{max}f)^2+k_e(B_{max}f)^{1.5} \tag{6.5}$$

From the above (6.5) right hand terms represent the hysteresis losses, eddy current losses and excess losses respectively where k_h, k_e and k_{eddy} are coefficients of hysteresis, excess and eddy current losses, B_{max} is the maximum magnetic field and f is the fundamental frequency. Hysteresis losses are due to the energy needed to reverse the magnetisation of the armature core. Eddy current losses are ohmic losses in the stator steel due to induced currents in the armature core. Excess losses (or anomalous losses) are due to changes in the magnetic domain structures when a variable magnetic field is applied to the magnetic material [42]. As the eddy current losses depend on the frequency therefore the generators operating at low frequencies compared to 60 Hz applications will have less influence on the total efficiency. Other non electrical losses such as ventilation losses and frictional losses in bearings, etc. also contribute to the lowering of the overall generator efficiency. Therefore system efficiency can be improved by reducing loss in the components of converter. In marine current applications when the generator is surrounded by the flowing water a cooling system is assumed to be unnecessary, since it is a large machine with low power, low frequency and with low surrounding temperatures.

6.2.4 Choice of Generator

The selection of a suitable generator for this thesis was very difficult due to very low rpm of the turbine. As the design of a suitable generator for low rpm is beyond the scope of this research so different types of generators available in market is being tried. Some of the factors being considered as described in Article 6.2 to select different types of generators for this research work.

6.2.4.1 Stepper Motor as Generator

The first type of motor being used as generator are stepper motors. Unlike small DC motors, steppers motors can generate power at very low rotation speed typically only about 200 rpm for a good output which is ten or fifteen times slower than the rate for a DC motor.

Steppers come with different resolutions. Virtually all steppers are either 1.8° or 7.5° per step (200 steps or 48 steps per revolution) the difference can be felt easily if you turn the spindle by hand. The 1.8° ones are good for generating at really low rpm. The coils in steppers have a relatively large inductance, and beyond a certain speed the output frequency gets so high that the impedance of the coils starts to become significant and limits the current. When making a stepper-based generator the motor speed needs to be around a couple of hundred revolution per minute.

Stepper motors are also a small multi-pole alternator, but being more modern they have four phases. As with a DC permanent magnet motor, turning the motor's shaft makes it work backwards, causing pulses of current to come out of the windings. However, the current is AC, going plus as a magnet pole approaches a coil and then minus as it goes away again. Usually there are four phases at 90-degree intervals so when one comes down to zero, the next one has reached maximum. This is a benefit as it means the output can be rectified to produce much smoother DC with hardly any gaps, but it means they have a large number of wires coming out.

Due to this features of stepper motors nowdays they have wide use in direct driven wind turbine generator. The same concept has been implemented to observe the performance of stepper motor as marine current generator.

In order to increase the voltage output from the stepper motor as generator a voltage doubler circuit is considered. A voltage doubler circuit doubles the voltage.The power generated by the stepper motor does not change but following ohm's law it can be seen that the output current must be halved if the voltage is to double. Using a voltage doubler enables a useful voltage to be ouput at low rotational speeds with the disadvantage that the current generated at high speeds is lower than it would be without the voltage doubler.

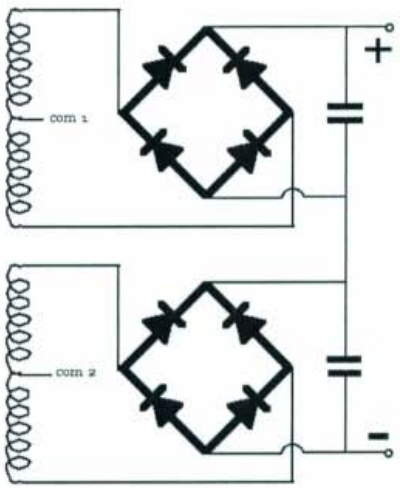

Figure 6.5 Voltage doubler circuit

Making a voltage doubler for a stepper motor is very simple because stepper motors generate four-phase alternating current ac electricity. Therefore a couple of suitably rated bridge rectifiers wired is required as per the circuit diagram shown in Figure 6.5. The ac voltage from each of the two pairs of stepper motor coils is rectified by a bridge rectifier into dc voltage and the two output voltages are then added together giving a total output of double the original voltage, but with a current equivalent to that generated by just one pair of coils. The two capacitors are used to give a smooth output dc voltage. Two different types of stepper motor were used as generator. One is LM 73008 and the other one is OS Series OS22BSNFLY.

The direct drive system is being built using the single step Savonius rotor described in Chapter 3 . The turbine is connected directly by means of a coupler with the two stepper motors. The experiment was carried out in flume channel. The flume tank comprises a rectangular section of channel with inlet and discharge tanks, which is supported by a pair of rigid pedestals. A service module incorporating a sump tank and submersible pump provides a source of water which is continuously re-circulated through the channel section making the unit self contained. The level in the working section of the flume may be controlled by an overshot weir arrangement at the exit consisting of stop logs in a slot. Stop logs are simply added or taken away to provide the required depth of water in the working section. Water exiting from the channel enters the discharge tank where it returns by gravity to the service module.

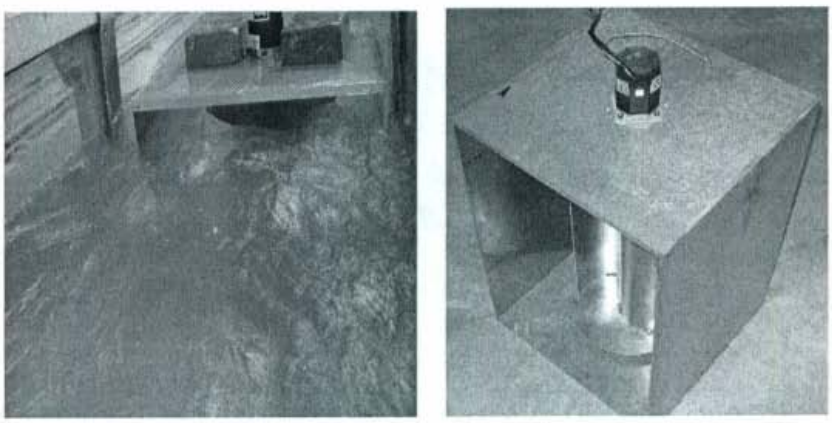

Figure 6.6 Turbine with generator fully immersed in Flume Tank

The flume channel in Memorial University of Newfoundland has got a dimension of 40 cm width and 50 cm height. The turbine is submerged fully under water in the channel, which is shown in Figure 6.6. The flow of water is varied by the control valve and four different flow rates can be maintained. The experiment is carried out for different loads starting from 1 to 10 ohm to record the maximum power.

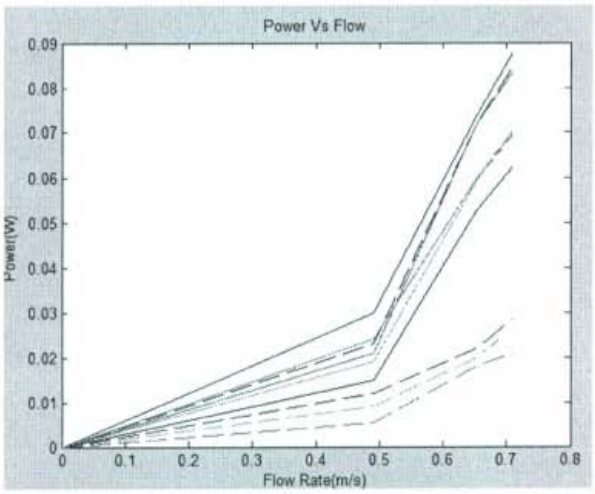

(a)

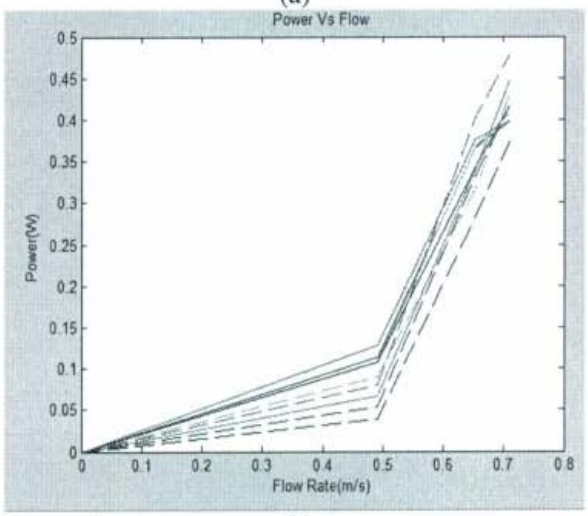

(b)

Figure 6.7 Power curve obtained from the turbine using (a) LM 73008 and (b) OS22BSNFLY

Figure 6.7 shows the output power of the generators for different loads at three different water flow. The maximum power that can be obtained is 0.45W at 0.71m/s for a load of 4 ohm from the stepper motor series OS22BSNFLY. The generators did not produce any satisfactory result which can be noticed from the expected power curve of the turbine. Therefore the use of stepper motor as a generator for marine energy is not a good choice.

6.2.4.2 Permanent Magnet Generator

Most small wind turbines nowdays use permanent magnet (PM) generators. The generators are usually direct-drive i.e., no gearbox is required. Direct-drive PM generators are characterized by low maintenance and high efficiency. Generally small turbines are self-starting and require very simple controls.The other generator that has been tested for a full scale turbine model proposed in Chapter 4 is Aquair UW . The UW is submersible water driven generator which can be used to charge batteries. The two phase alternator has two stator windings and two permanent magnet rotors on a common shaft running in two sealed and grease packed ball bearings. The rotors are staggered at 30° to each other to minimise starting torque due to magnetic cogging. The reason for selecting this particular generator is designed for low rpm application . A water turbine emulator is built as described in Article 6.1 to test the performance of the generator and design a maximum power point tracking (MPPT) based energy conversion system.

6.3 MPPT Techniques

For a change in marine current it is necessary to extract maximum power from the current. A general approach for the power feedback control is to measure and maximize the power at the load terminal, and it assumes that the power obtained from the marine current is equal to the maximum load power. However, this maximizes the power to the load but not the power from the water current.

To be able to extract the maximum power from the water current to track the changes due to change in flow a maximum power point tracking (MPPT) should be implemented. Devices that can perform this desired function are known as Maximum Power Point Trackers, also called MPPTs or trackers. A tracker basically consists of two components as shown in Figure 6.8, a switch-mode converter and a control with tracking capability. The

switch-mode converter is the core of the entire supply. The converter allows energy at one potential to be drawn stores as magnetic energy in an inductor, and then releases at a different potential. By setting up the switch-mode section in various topologies either high-to-low (buck converter) or low-to-high (boost) voltage converters can be constructed. The goal of a switch-mode power supply is to provide a constant output voltage or current.

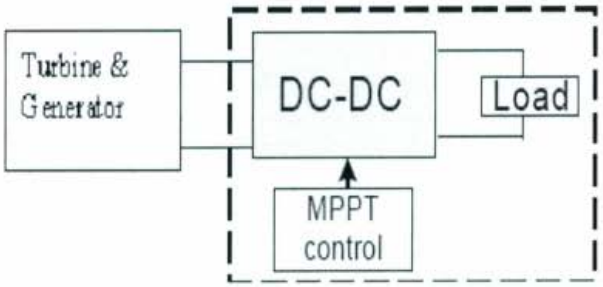

Figure 6.8 Basic components of a MPPT system

Many MPPT techniques are used nowdays but there are three main methods, which are the most widely used [44]:

- Perturb and Observe (P&O)
- Incremental Conductance (INC)
- Constant Voltage (CV)

The first two are so called 'hill-climbing' methods, and they are using the fact that on the V-P characteristic, on the left of the MPP [44] the variation of the power against voltage $dP/dV > 0$, while at the right, $dP/dV < 0$ (see Figure 6.9). The CV method is based on the fact that generally the ratio $V_{MPP}/V_{OC} \approx 0.76(\text{ PV })$. However all these methods are used to extract maximum power from PV system.

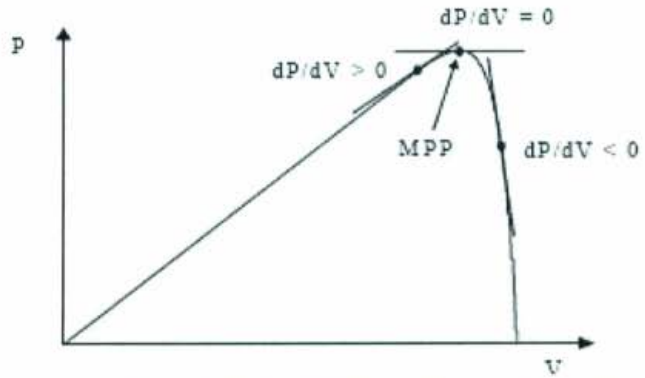

Figure 6.9 Sign of the dP/dV at different positions on the power characteristic

6.3.1 Constant Voltage and Current Method

The constant voltage algorithm is based on the observation from I–V curves that the ratio of the maximum power voltage V_{mp} to its open-circuit voltage V_{oc} is approximately constant:

$$V_{mp}/V_{OC} = K < 1 \tag{6.6}$$

The MPPT calculates the correct operating point using Eq.(6.6) and the preset value of K, and adjusts the input voltage until the calculated V_{mp} is reached. This operation is repeated periodically to track the position of the MPP. Although the method is simple but it is difficult to choose the optimal value of the constant K. The MPPT tracking efficiency is low relative to those of other algorithms. The flowchart of the algorithm is shown in Fig 6.10 .This method is only applicable for solar cells and cannot be applied for MPPT based marine current energy conversion system.

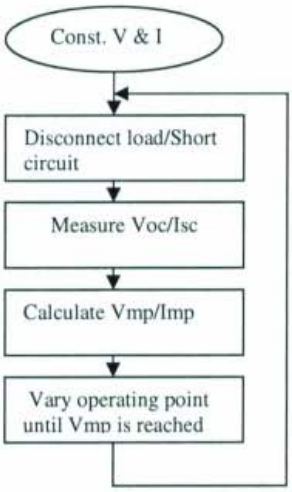

Figure 6.10 The flowchart of Constant Voltage and Current method

6.3.2 Perturb and Observe Method

Perturb and Observe (P&O) is the simplest method to implement [44]. In Fig. 6.9 if the operating voltage of the generator voltage is perturbed in a given direction and $dP/dV > 0$, it is known that the perturbation moved the operating point toward the MPP. The P&O algorithm would then continue to perturb the generator voltage in the same direction. If $dP/dV < 0$, then the change in operating point moved away from the MPP, and the P&O algorithm reverses the direction of the perturbation. In other words the system works by increasing or decreasing the operating voltage and observing its impact on the output power. The operating voltage is perturbed with every MPPT cycle. As soon as the MPP is reached, V will oscillate around the ideal operating voltage.

The flowchart of the algorithm is shown in Fig 6.11 .The advantage of the P&O method is that it is a very simple technique. However, it has some limitations like oscillations around the MPP in steady state operation, slow response speed, and even tracking in wrong way under any rapidly changing conditions [45-53].This approach can be applied for a MPPT based marine current energy conversion system.

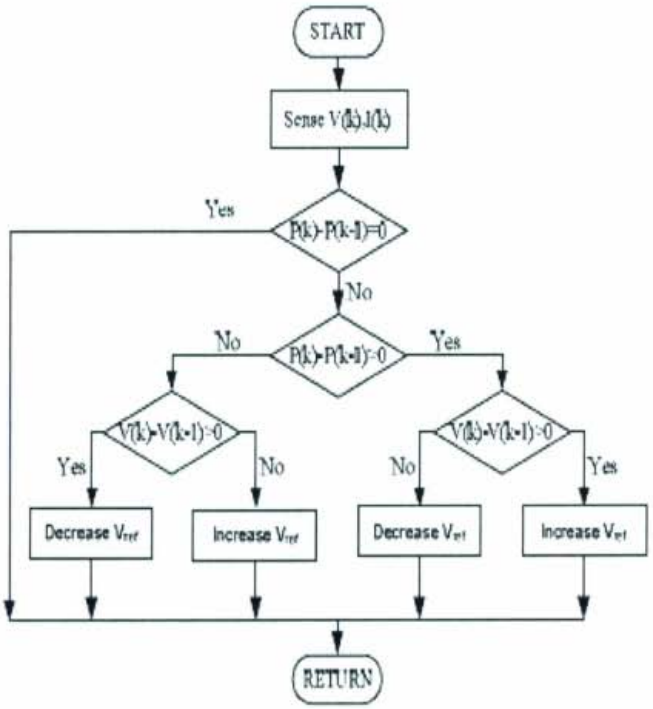

Figure 6.11 The flowchart of Perturb & Observe Method

6.3.3 Incremental Conductance Method

The incremental conductance (IncCond) method is based on comparing the instantaneous input conductance with the incremental conductance [54]. This method has a good performance under rapidly changing conditions. The algorithm uses the fact that the derivative of the output power P with respect to the voltage V is equal to zero at the maximum power point:

$$\frac{dP}{dV} = I\frac{dV}{dV} + V\frac{dI}{dV} = I + V\frac{dI}{dV} = 0 \tag{6.4}$$

The flowchart of the algorithm is shown in Fig 6.12 . One of the advantages of the IncCond algorithm is that it does not oscillate around the MPP. However, because of noise and errors

due to measurement and quantization this method can produce oscillations around the MPP and can be confused in rapidly changing conditions. Another disadvantage of this algorithm is the increased complexity when compared to perturb and observe which increases computational time.

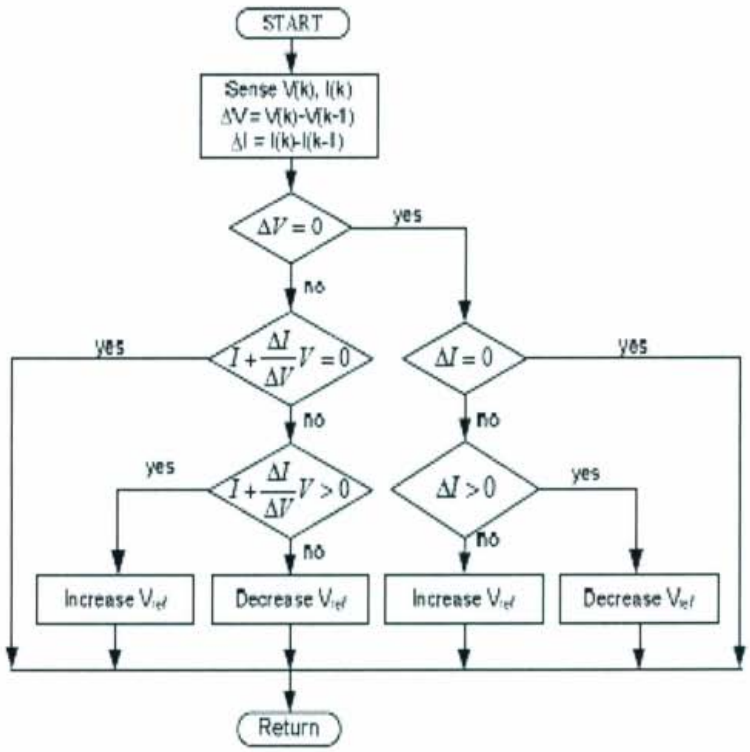

Figure 6.12 The flowchart of INC method

6.4 MPPT Algorithm

The most commonly used MPPT algorithm i,e Perturb and Observe (P&O) has been implemented to extract maximum power at every instant. Figure 6.13 summarized the control action of the P&O method. The flowchart of the implemented algorithm is shown in Fig. 6.14. The operating voltage is perturbed with every MPPT cycle. As soon as the MPP is reached, V

will oscillate around the set operating voltage. For example if the controller senses that the input power increases (dP > 0) and voltage decreases (dV < 0), it will decrease (-) V_{ref} to bring it closer to MPP. The addition of a 'waiting' function causes a momentary cessation of perturbations if the algebraic sign of the perturbation is reversed several times in a row, indicating that the MPP has been reached.

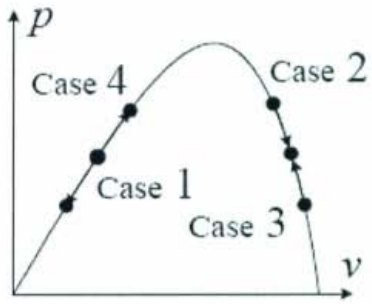

Case	dP	dV	Action
1	<0	<0	+
2	<0	>0	-
3	>0	<0	-
4	>0	>0	+

Figure 6.13 Perturb and Observe Control Action

It is much easier and quicker to write code in a higher level language like C . Therefore a compiler from customer computer service CCS has been used. The CCS C compiler has a lot of nice built in functions to access the PIC hardware which make it easy to quickly write useful programs. It is not however strictly ANSI C compatible. The program written in C has been given in Appendix D.1. The PIC has a built-in serial port that is used to output data from the MPPT so it can be logged externally. The serial port can also be used for simple control of the MPPT during debugging.

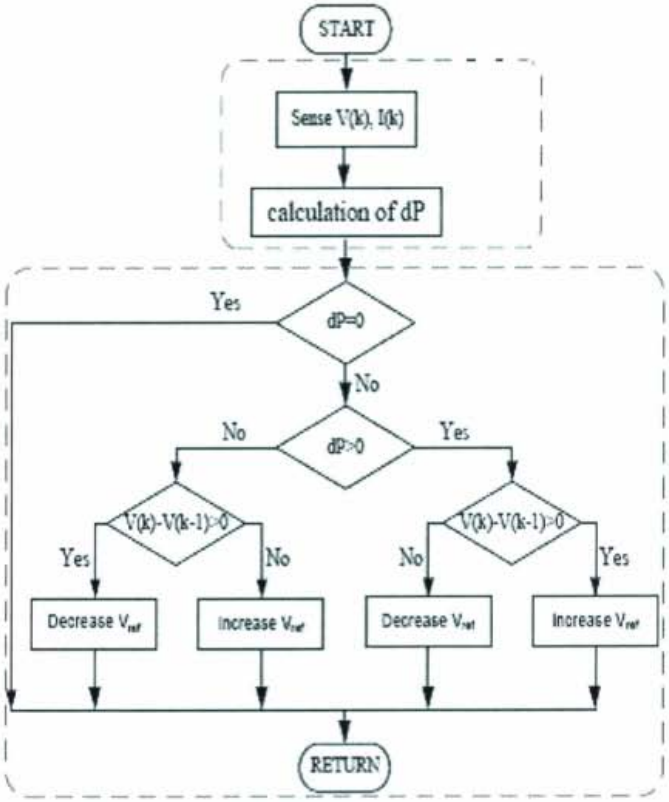

Figure 6.14 The flowchart of P & O method

6.5 Circuit Description

The schematic of the energy conversion system is shown in Figure 6.15. The proposed power generation system consist of a low rpm generator, batteries for energy storage, a controlled dc-dc converter, instrumentation and a micro controller based control system for the turbine. In order to measure the low rpm of the generator accurately a high resolution encoder (Grayhill) with 256 cycles/rev have been used .A laptop of model Dell 520(Pentium 4)1.66Ghz has been used to program the microcontroller. Two wattmeter method (Power Analyzer Pro) is used to measure the input and output power of the system.

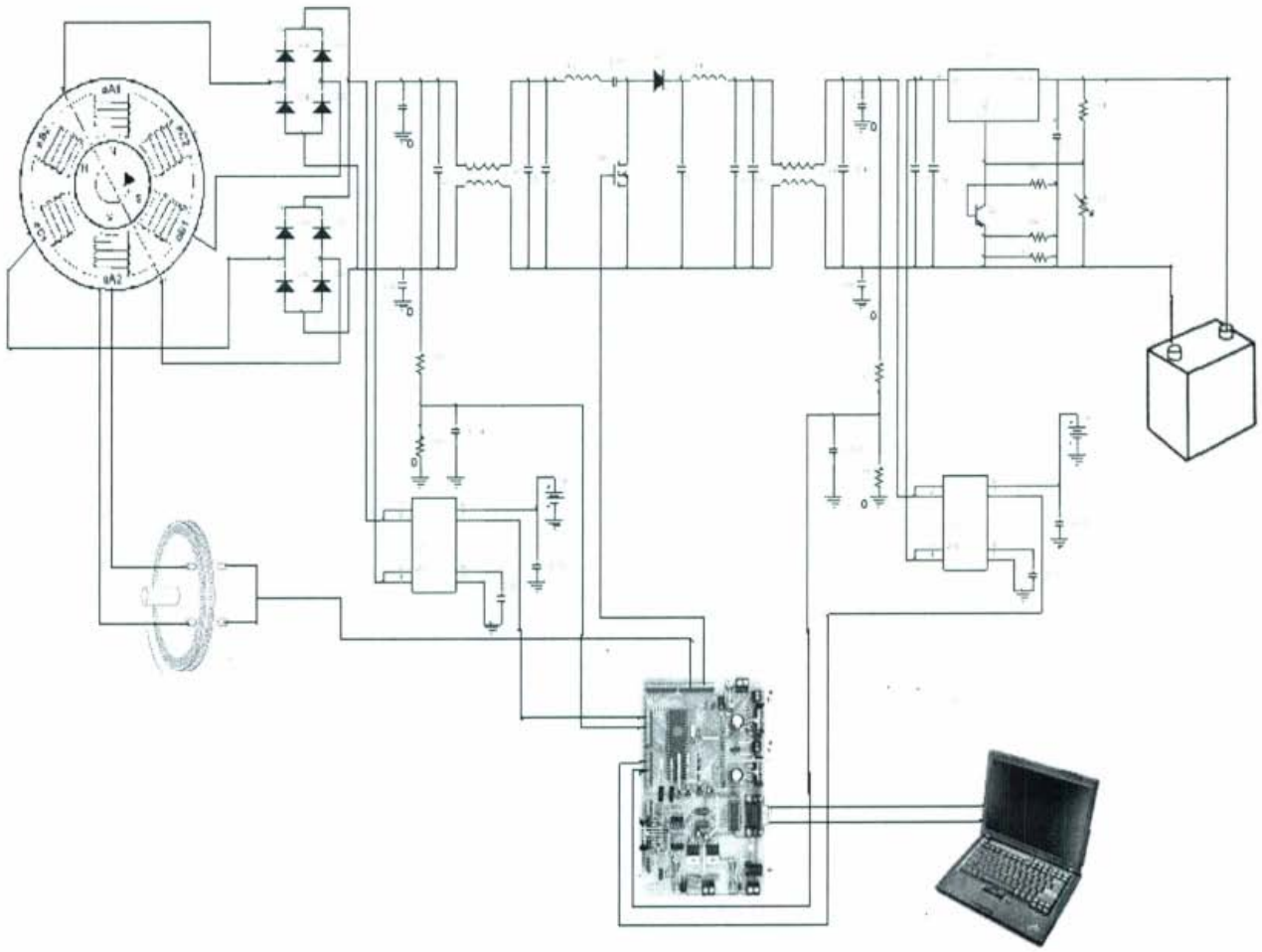

Figure 6.15 Schematic of Energy Conversion System

The system control unit also consists of:

a) PIC 16F877 low-power consumption, CMOS microcontroller.

b) interface circuits which comprise of sensors and signal conditioners connected to the microcontroller A/D converter;

The microcontroller unit 16F877 features a 16 bit, four channels, successive approximation A/D converter, used by the control program to measure the signals required for the power flow control. The 16 bit resolution is adequate for the present application. Also, it features two

PWM outputs with program controlled duty cycle and 39.2 kHz maximum frequency when driven by the 20-MHz clock of the unit. Each of the PWM outputs can be used to control a separate MPPT system. This type of microcontroller was chosen because it has the necessary features for the proposed system, such as an on-chip A/D converter , PWM outputs, 16-bit architecture, high clock rate, low-power consumption and low cost. Figure 6.16 shows the laboratory set up of the energy conversion system.

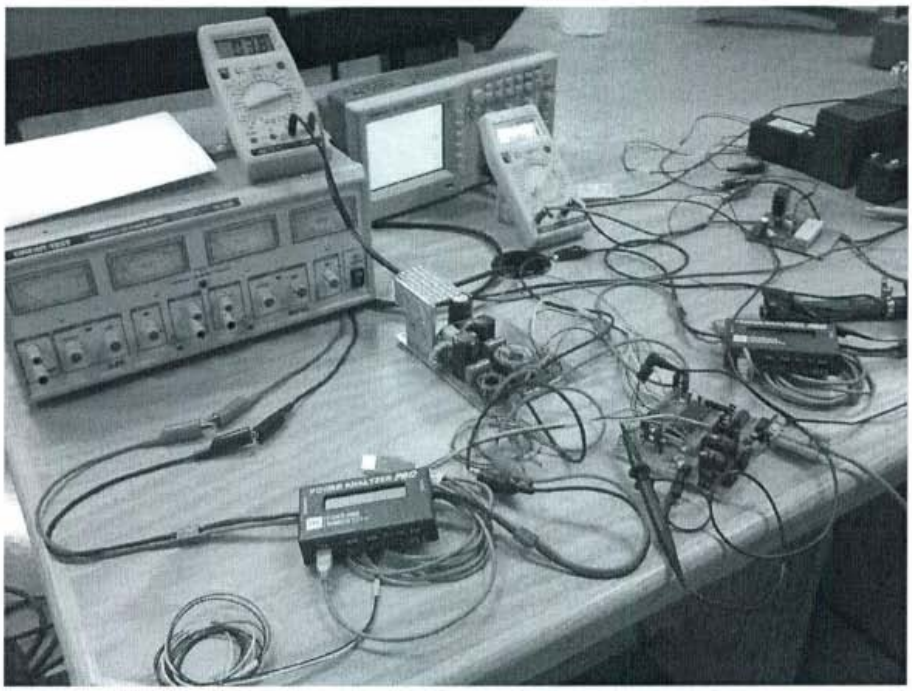

Fig. 6.16 Experimental Energy Conversion System

6.6 System Limits and Test Results

The speed of the dc motor is set to drive the generator at a water current speed of 1m/s when it attains a speed of 240 rpm . A 250 pulse per revolution from the encoder is fed to PIC to measure the rev/min of the generator. The generator does not produce a suitable power below

this speed so a gear box of 1:3 can be placed between generator and turbine. Fig 6.17 shows the rpm of the generator at a water current speed of 1m/s.

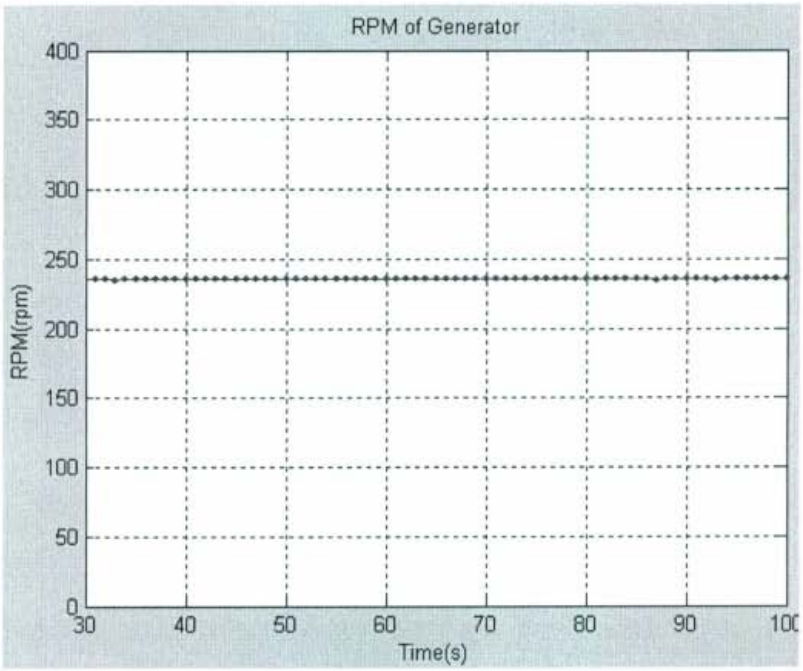

Fig. 6.17 RPM of AQUAIR UW Generator

The PIC16F877 controls the conversion ratio of the of the DC/DC converter. The frequency of the PWM is set to 5 KHz by the program. The PWM output of the PIC is used to control the duty cycle of the DC/DC converter which sets its voltage conversion ratio. The duty cycle of the PWM signal sets the ratio of the on time for the high side MOSFET switch versus the on time of the low side MOSFET switch. The action is performed by the iterative algorithm loaded in microcontroller. Fig 6.18(a&b) shows the variation of the PWM signal fed to MOSFET with the change in input power.

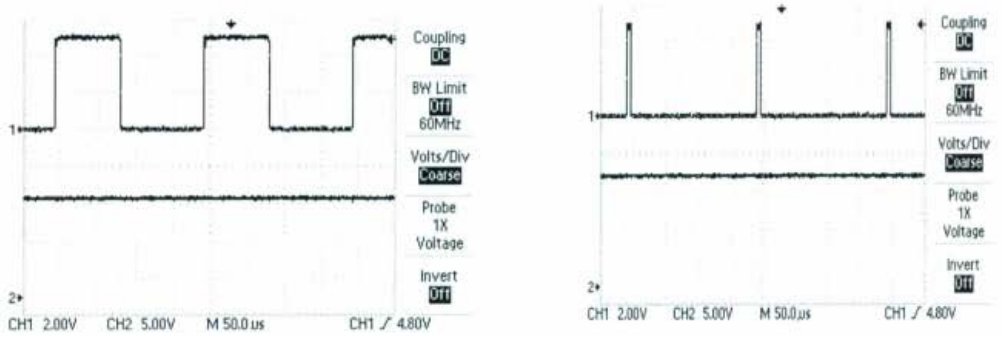

(a) (b)

Fig. 6.18 PWM signal generated from PIC 16F877

The microprocessor transmits out the serial port all the values it has measured and calculated (volts, amps and watts) once a second to be logged by an external computer. The input and output power for a 50 ohm load is then plotted using Matlab shown in Figure 6.19.The average power measured at 240 rpm without implementing the MPPT is 6.2W.The average output power measured from the system is 7.4W with MPPT on at same rpm.Thus an increase in output power is achieved by the implementation of MPPT.

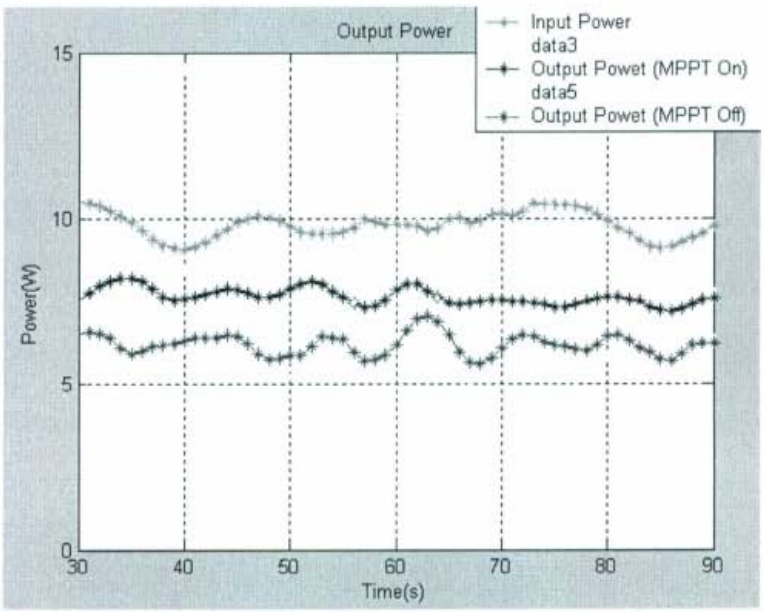

Figure 6.19 System Output power at MPPT and without MPPT

An increase of 20% of output power is observed by the implementation of MPPT.It has been also seen that the efficiency of the system increases with the MPPT on as shown in Figure 6.20.The two filters in the input and output reduces the voltage ripple on both ends. The measured input and output voltage ripple factors are less than 1% in both cases when loaded.

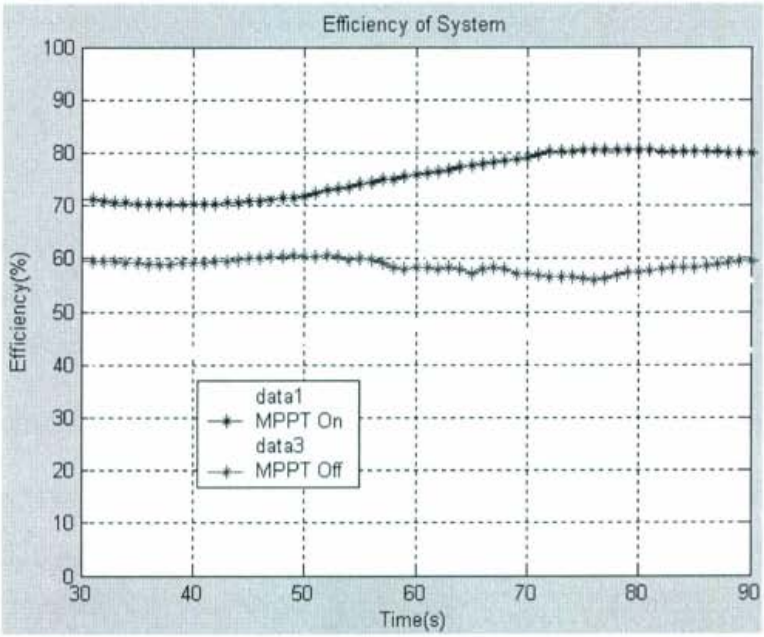

Figure 6.20 System Efficiency with MPPT and without MPPT

The oscillation around a maximum power point causes a power loss that depends on the step width of a single perturbation. The value for the ideal step width is system dependent and needs to be determined experimentally to pursue the tradeoff of increased losses under stable or slowly changing conditions. In fact, since the AC component of the output power signal is much smaller than the dc component and will contain a high noise level due to the switching dc-dc converter.

6.7 Conclusion

There are many other MPPT methods and most of them are based on the combination of the three methods discussed . The execution time of the control algorithm loop has been calculated to be less than half a minute. Since the ocean current is steady throughout, therefore the system is expected to track effectively the maximum power at every instant. A very simple MPPT control algorithm has been used that only looks at limiting the maximum voltage of the battery. The efficiency of the system can be improved by more robust and sophisticated control algorithm. A direct drive system has a better efficiency than with a gear box. In order to have a direct drive system a generator needs to be designed by considering the characteristics of the turbine depending upon site, required power output and water current. The optimum rotor configuration, rotor electromagnetic and mechanical design, and the stator electromagnetic design must be matched to achieve a higher efficient machine of the desired load characteristics, high power factor, and high efficiency and performance.

Chapter 7

Conclusion

7.0 Research Conclusion

A micro sea-floor power generation system being designed and developed at Electrical Energy System Lab, Memorial University of Newfoundland. Marine Current Energy is a promising alternative energy source capable of producing electricity with minimal environmental impact.

In this thesis three different types of drag type Savonius rotor has been built and tested to select a suitable water current turbine .The characteristics of the turbine is analyzed by studying the mechanical output power, torque and power coefficient. Experimental results show that Savonius rotor can be used as an underwater turbine.

The marine power delivered to a load can be maximized using MPPT control systems, which consist of a power conditioner to interface the marine output to the load, and a control unit, which drives the power conditioner such that it extracts the maximum power from marine current. In this thesis a low-cost, low-power consumption MPPT system for battery charging and supplying power to signal conditioning circuits has been developed and tested. The system consists of a high-efficiency, Boost dc/dc converter and a microcontroller-based unit which controls the dc/dc converter directly by power measurements. Experimental results show that the use of the proposed MPPT control increases the marine output power by as much as 20% .The proposed control unit can be implemented also with analog circuits, but the microcontroller-based alternative was chosen since it permits easy system modifications. The proposed system can be also used

in a hybrid system where the microcontroller performs simultaneously the MPPT control of more than one renewable energy source.

7.1 Thesis Contribution

The overall research objective is to enhance the ocean energy sector in through developing novel, environmentally-neutral platform ocean technology. This thesis concentrates to develop, integrate, test and commercialize a low cost device to harvest energy from ocean floor currents to power marine technologies. The contributions of this research work are listed as below:

- An autonomous, lightweight, low-cost, pressure-resistant energy generation system that can extract power from ocean current source has been designed in this research work.
- The ocean current data around Newfoundland is collected and analysed . It shows a significantly low non-tidal ocean current speed (in the range of 0.11-0.15m/s) at various depths. Therefore a site needs to be selected where the marine current is high (>0.5 m/s).
- Three different types of lightweight, drag-type Savonius turbine were designed that is responsive to low marine current. Three prototypes of same cross section area being tested to compare the performance of water current turbine. A three stage type Savonius rotor with three phases has been constructed. It has three stages and the bucket of each stage has 60° phase shift between the adjacent stages. This type of arrangement will make the rotor omni directional. All three prototypes have been found to produce decent amount of power.

- An established dimensional analysis method is applied to water current turbines. Dimensional analysis and scaling laws for a single rotor turbine are derived. Two rotor prototypes are built and tested in the lab to prove the validity of scaling laws.
- A very simple microcontroller based micro energy conversion system is being developed and tested in the Energy lab of Memorial University of Newfoundland. The MPPT based control strategy ensures that the system is extracting maximum power at every instant.

7.2 Future Work

The work presented in this thesis is only a part of the research project on marine current energy conversion system that is being studied at Memorial University of Newfoundland. The results and conclusions presented within this thesis is a step ahead into a better understanding of the marine current power generation systems presented in this thesis. It is also acknowledged that much more theoretical and experimental investigations are still needed so as to develop an efficient and cost effective electrical energy conversion from marine currents especially for very low speeds. Some of the future work that could be studied or continued with reference to the present work is the following:

- It is necessary to collect more information as possible about the ocean currents off the Grand Banks from: the Canadian Hydrographic Service, Canadian Tide and Current Tables, the Department of Fisheries and Oceans; and oil companies operating offshore. To analyze and synthesize the available information into a theoretical model to estimate ocean current velocities and velocity profiles near

the seafloor. This will guide the proper placement of turbine in areas where ocean currents are sufficiently strong (>0.5m/s).

- A next-generation, lightweight, drag-type turbine of double-helix can be designed which can generate considerable amount of torque in order to make it highly-responsive to low-current velocities. The turbine will be omni-directional so that an ocean current will produce the same amount of power for any flow direction. Testing of turbine both on site and in the laboratory, although of great importance, cannot give complete information on their own, not to mention the high costs involved. Numerical simulation combined with measurements is therefore most likely to constitute the basis for the analysis and design of marine current devices.
- Computational Fluid Dynamics (CFD) can be used in the analysis of systems involving fluid flow by means of computer-based simulation and which enables the creation of a 'virtual prototype' of the turbine to analyze the effects of different current.
- An energy conversion system with a gear box reduces the efficiency of the system. A slow-rotating, permanent magnet, multiple-pole electrical power generator to work in low-current, deep-sea marine environments should be designed. A numerical simulation based on various generator designs in an underwater environment can be done to compare the results in terms of the power conversion efficiency, mechanical complexities and cost. Finally it is necessary to verify the functionality of both the turbine and the generator to integrate them into a single device which will be evaluated for any corrosion that might occur in a marine environment.

- A more robust and sophisticated algorithm can be developed for tracking the maximum power point (MPP) of marine current. It should confirm excellent tracking effectiveness and rapid dynamic response. To develop a power management system to efficiently coordinate the power-using resources and direct the activity sequences in real time.

Bibliography

[1] "The Kyoto Protocol, available at the United Nations Framework on Climate Change: http://unfccc.int/resource/docs/convkp/kpeng.pdf accessed 2005-08-17."

[2] "Status and research and development priorities," IEA/DTI report number FES-R-132 2003.

[3] J. A. Clarke, G. Connor, A. D. Grant, and C. M. Johnstone, "Regulating the output characteristics of tidal current power stations to facilitate better base load matching over the lunar cycle," *Renewable Energy*, vol. 31, pp. 173-180, 2006.

[4] M. Leijon, H. Bernhoff, M. Berg, and O. Ågren, "Economical considerations of renewable electric energy production - especially development of wave energy," *Renewable Energy* vol. 28, pp. 1201-1209, 2003.

[5] M. Leijon, A. Rehn, and A. Skoglund, "On the Physics, Engineering and Economics of Renewable Electric Energy Sources," *Submitted to Energy Policy* 2007.

[6] "Non Nuclear Energy - JOULE II, Wave energy project results, The Exploitation of Tidal Marine Currents," EU JOULE contract JOU2-CT94- 0355, 1996.

[7] I. G. Bryden, S. Naik, P. Fraenkel, and C. R. Bullen, "Matching tidal plants to local flow conditions," *Energy*, vol. 23, pp. 699-709 1998.

[8] M. D. Zaidman, V. Keller, A. R. Young, and D. Cadman, "Flow duration frequency behaviour of British rivers based on annual minima data," *Journal of hydrology*, pp. 195-213, 2003.

[9] A. S. Bahaj and L. E. Myers, "Fundamentals applicable to the utilization of marine current turbines for energy production," *Renewable Energy*, vol. 28,pp. 2205-2211, 2003

[10] Y. C. Chen and C. L. Chiu, "An efficient method of discharge measurement in tidal streams," *Journal of hydrology*, vol. 256, pp. 212-224, 2002.

[11] P. L. Fraenkel, "New development in tidal and wave power technologies,"presented at towards a renewable future: silver jubilee conference, Brighton, UK, 1999.

[12] "Tidal stream energy review," ETSU-T/05/00155/REP, 1993.

[13] M. Chaffey, E. Mellinger, and W. Paul,"Communication and power to the seafloor: MBARI's ocean Observing system mooring concept", MTS/IEEE Oceans 2001 Conference Proceedings, November 2001.

[14] D. Pugh, Changing sea levels, effects of tides weather and climate: Cambridge University Press, 2004.

[15] P. B. S. Lissaman and R. L. Radkey, "Coriolis Program - A review of the status of the ocean turbine energy system," presented at Oceans79, San Diego, USA, 1979.

[16] W. D. Liang, T. Y. Tang, Y. J. Yang, M. T. Ko, and W. S. Chuang, "Upper- ocean currents around Taiwan," Deep Sea Research Part II: Topical Studies in Oceanography, vol. 50, pp. 1085-1105, 2003.

[17] A. Kaneko, S. Mizuno, W. Koterayama, and R. L. Gordon, "Cross-stream velocity structures and their downstream variation of the Kuroshio around Japan," Deep Sea Research Part A. Oceanographic Research Papers, vol.39, pp. 1583-1594, 1992.

[18] M. H. Nielsen, "Baroclinic surface currents in the Kattegat," Journal of Marine Systems, pp. 97-121, 2005.

[19] J. Jachlewski, Wind solar project: Hybrid powered outdoor area lighting, Proceedings KGCOE 2005 of Multi disciplinary Engineering Design conference.

[20] T. Hayashi, Wind tunnel test on a different three phase Savonius rotor, vol 48, page 9-16, JSME 2005.

[21] S. J. Savonius, The S-Rotor and its Applications, Mechanical Engineering, Vol. 53, No. 5, May 1931, pp. 333-338.

[22] V.J Modi, N.J Roth. A prototype designand performance of the Savonius rotor based irrigation system.M.A.Sc Thesis,University of British Columbia,March 1985.

[23] J-L Menet, L-C Valde`s, B Me´nart. A comparative calculation of the wind turbines capacities on the basis of the L-r criterion. Renewable Energy Vol. 22 pp 491–506, 2001.

[24] J-L Menet, B Me´nart. Une proce´dure de comparaison de quelques e´oliennes classiques base´e surl'utilisation du crite`re L-sigma. In Proceedings of 15th French Mechanical Symposium, Nancy, France, September 3–7, 2001.

[25] J. L. Menet, A double-step Savonius rotor for local production of electricity: a design study, Renewable Energy vol.19 September 2004, page 1843-1862.

[26] I. Ushiyama , H. Nagai, Optimum design configurations and performances of Savonius rotors. Wind Engineering 1988;12(1):59–75.

[27] N. Fujisawa On the torque mechanism of Savonius rotors. Journal of Wind Engineering Industrial Aerodynamics 1992; 40:277–92.

[28] Tsutomo Hayashi, Wind tunnel tests on a different phase three stage Savonius rotor. JSME International Journal, Series B, Vol 48, No.1, 2005: pp 9-16.

[29] A. S.Grinspan, P. Suresh Kumar, U. K. Saha and P.Mahanta. Performance of Savonius wind turbine rotor with twisted bamboo blades. Proceedings of 19th Canadian congress of applied mechanics, Calgary, Alberta,Canada,Vol- 2, pp. 412 - 413, 2003.

[30] C. Merle Potter and C. David Wiggert, "Mechanics of Fluids," 2ed, 1997

[31] Ned Mohan ,"Power electronics : converters, applications, and design," 3ed,2003.

[32] M. H.Rashid,"Power electronics: circuits, devices, and applications," 3ed,2004.

[33] Atmel (November 2001), AT90S/LS8535,http://www.atmel.com/atmel/acrobat/doc1041.pdf

[34] Lead Acid Battery Charger :http://www.uoguelph.ca/%7Eantoon/circ/labc3.html.

[35] L. Söderlund, J. T. Eriksson, J. Salonen, H. Vihriälä, and R. Perälä, "A permanent magnet generator for wind power applications," IEEE Transaction on Magnetics, vol. 32, pp. 2389-2392, 1996.

[36] P. Lampola and J. Perho, "Electromagnetic analysis of a low speed permanent magnetized wind generator," presented at Opportunities and advances in international power generation, 1996.

[37] E. Spooner and A. C. Williamson, "Direct coupled permanent magnet generator for wind turbine applications," presented at Electr. Power Appl.,1996.

[38] K. E. Hallenius, Elektriska maskiner, Malmö: Liber läromedel, 1972.

[39] R. H. Park, "Two Reaction Theory of synchronous machines," AIEE Transactions, pp. 716-730, 1929.

[40] A. Grauers, "Design of direct drive PM generators for wind turbines," PhD, thesis Göteborg, Sweden: Chalmers University of Technology, 1996.

[41] A. E. Fitzgerald, C. Kingsley, and S. D. Umans, Electric machinery, Fifth edition ed: McGraw-Hill Inc, 1990.

[42] G. Bertotti, "General Properties of Power losses in soft ferromagnetic materials,"IEEE Transactions on Magnetics, vol. 24, 1988.

[43] K.Y. Khouzam, Optimum load matching in direct-coupled photovoltaic power systems-application to resistive loads, IEEE Transactions on Energy Conversion, vol. 5, no. 2, June 1990, pp.265 – 271.

[44] D.P. Hohm, M.E. Ropp: "Comparative Study of Maximum Power Point Tracking Algorithms Using an Experimental, Programmable, Maximum Power Point Tracking Test Bed". Conference Record of the Twenty-Eighth IEEE 15-22 Photovoltaic Specialists Conference Sept. 2000 Pages:1699 – 1702.

[44] Weidong Xiao, W.G Dunford: "A modified adaptive hill climbing MPPT method for photovoltaic power systems" Power Electronics Specialists Conference, 2004. PESC 04. 2004 IEEE 35th Annual Volume 3, 20-25 June 2004 Pages: 1957 - 1963 Vol.3

[45] N. Femia, G. Petrone, G. Spagnuolo, M. Vitelli: "Optimizing sampling rate of P&O MPPT technique" Power Electronics Specialists Conference, *2004.* PESC 04. 2004 IEEE 35th Annual Volume 3, 20-25 June 2004 Pages: 1945 - 1949 Vol.3

[46] N. Femia, G. Petrone, G. Spagnuolo, M. Vitelli: "Optimizing duty-cycle perturbation of P&O MPPT technique" Power Electronics Specialists Conference, 2004. PESC 04. 2004 IEEE 35th Annual Volume 3,20-25 June 2004 Pages: 1939 - 1944 Vol.3

[47] A. Brambilla, M. Gambarara, A. Garutti, F.Ronchi: "New approach to photovoltaic arrays maximum power point tracking".Power Electronics Specialists Conference, 1999. PESC 99. 30th Annual IEEE Volume 2, 27 June-1 July 1999 Pages: 632 – 637 vol.2

[48] Yeong-Chau Kuo, Tsorng-Juu Liang, Jiann-Fuh Chen: "Novel maximum-power-point-tracking controller for photovoltaic energy conversion system" Industrial Electronics, IEEE Transactions on Volume 48, Issue 3, June 2001 .

[49] M. Veerachary, T. Senjyu and K. Uezato, "Maximum power point tracking control of IDB converter supplied PV system", IEEE Proceedings Electric Power Applications, vol. 148, no.6, p. 494-502, 2001.

[50] Liu X., Lopes L.A.C.: "An improved perturbation and observation maximum power point tracking algorithm for PV arrays" *Power Electronics Specialists Conference, 2004. PESC 04. 2004* IEEE35th Annual Volume 3, 20-25 June 2004 Pages: 2005 - 2010 Vol.3

[51] Weidong Xiao, W.G. Dunford: "A modified adaptive hill climbing MPPT method for photovoltaic power systems" *Power Electronics Specialists Conference, 2004. PESC 04. 2004* IEEE35th Annual Volume 3, 20-25 June 2004 Pages: 1957 - 1963 Vol.3.

[52] X. Liu, L.A.C. Lopes: "An improved perturbation and observation maximum power point tracking algorithm for PV arrays" Power Electronics Specialists Conference, 2004. PESC 04. 2004 IEEE 35th Annual Volume 3, 20-25 June 2004 Pages: 2005 - 2010 Vol.3.

[53] K.H. Hussein, I. Muta, T. Hoshino, M. Osakada: "Maximum photovoltaic power tracking: an algorithm for rapidly changing atmospheric conditions". Generation, Transmission and Distribution, IEEE Proceedings-Volume 142 Issue 1, Jan. 1995 Pages: 59 – 64.

[54] G.J. Yu, Y.S. Jung, J.Y. Choi, I. Choy, J.H. Song, G.S. Kim: "A novel two-mode MPPT control algorithm based on comparative study of existing algorithms" Photovoltaic Specialists Conference,2002. Conference Record of the Twenty-Ninth IEEE 19-24 May 2002 Pages: 1531 – 1534

Appendix A

A.1 Measurement of Power and Coefficient of Power of Turbine

```
%Dimension of Turbine

H=0.405;      % H is height of rotor(m)
D=0.222;      % D is diameter of rotor(m)
d=0.14;       % d  is diameter of each bucket(m)
a=4 ;         % a  is aspect ratio of rotor
H1=D*a;       % H1 is height of double step rotor(H=H1/2 is for single step)
A=H*D;        % A is swept area of rotor in square meter
e=0.04 ;      % e is overlap between two bucket(m)
b=e/d;        % b is overlap ratio


% Processing Data for Measurement

offset=0;                                   % Load cell offset to measure torque

Ya=load('runttt0.4.txt');                   % Load Torque at different Speed
tora=abs(Ya( :,1).*0.001.*0.15.*9.8)+offset; % Calculating Torque
rpma=abs(Ya( :,2));
spa=abs(Ya(:,3));
wa=2*pi.*rpma/60;
tsra=(wa.*D)./(2*spa);
Pa=abs(tora.*wa);

Y0=load('runttt0.5.txt');
tor0=abs(Y0( :,1).*0.001.*0.15.*9.8)+offset;
rpm0=abs(Y0( :,2));
sp0=abs(Y0(:,3));
w0=2*pi.*rpm0/60;
tsr0=(w0.*D)./(2*sp0);
P0=abs(tor0.*w0);

Y1=load('runttt0.6.txt');
tor1=abs(Y1( :,1).*0.001.*0.15.*9.8)+offset;
rpm1=abs(Y1( :,2));
sp1=abs(Y1(:,3));
w1=2*pi.*rpm1/60;
tsr1=(w1.*D)./(2*sp1);
P1=abs(tor1.*w1);

Y2=load('runttt0.7.txt');
tor2=abs(Y2( :,1).*0.001.*0.15.*9.8)+offset;
```

```
rpm2=abs(Y2( :,2));
sp2=abs(Y2(:,3));
w2=2*pi.*rpm2/60;
tsr2=(w2.*D)./(2*sp2);
P2=abs(tor2.*w2);

Y3=load('runttt0.8.txt');
tor3=abs(Y3( :,1).*0.001.*0.15.*9.8)+offset;
rpm3=abs(Y3( :,2));
sp3=abs(Y3(:,3));
w3=2*pi.*rpm3/60;
tsr3=(w3.*D)./(2*sp3);
P3=abs(tor3.*w3);

Y4=load('runttt0.9.txt');
tor4=abs(Y4( :,1).*0.001.*0.15.*9.8)+offset;
rpm4=abs(Y4( :,2));
sp4=abs(Y4(:,3));
w4=2*pi.*rpm4/60;
tsr4=(w4.*D)./(2*sp4);
P4=abs(tor4.*w4);

Y5=load('runttt1.0.txt');
tor5=abs(Y5( :,1).*0.001.*0.15.*9.8)+offset;
rpm5=abs(Y5( :,2));
sp5=abs(Y5(:,3));
w5=2*pi.*rpm5/60;
tsr5=(w5.*D)./(2*sp5);
P5=abs(tor5.*w5);

sp=[spa;sp0;sp1 ;sp2 ;sp3 ;sp4 ;sp5];
rpm=[rpma;rpm0;rpm1;rpm2;rpm3;rpm4;rpm5];
w=[wa;w0;w1; w2 ;w3; w4 ;w5];
P=[Pa;P0;P1 ;P2 ;P3 ;P4 ;P5];
tsr=[tsra;tsr0;tsr1; tsr2; tsr3 ;tsr4; tsr5];

% Comparing thereotical and Measured Power

P1=0.5*1000*A*0.06*(sp.^3);
figure
yy1 = smooth(sp,P,0.1,'rloess');
[xx,ind] = sort(sp);
plot(xx,P(ind),'w.',xx,yy1(ind),'r.-')
hold on
yy1 = smooth(sp,P1,0.1,'rloess');
[xx,ind] = sort(sp);
```

```
plot(xx,P1(ind),'w.',xx,yy1(ind),'b.-')
set(gca,'XLim',[0.3 1])
set(gca,'YLim',[0  4])
xlabel('Water Speed(m/s)')
ylabel('Power of Turbine(W)')
title('Output Power of Three Stage Savonius')
grid

% Measuring coefficient of  Power of turbine

k=0.5*A*1000;
s1=sp.^3;
cp=P./(k.*s1);
Cp=smooth(cp);
figure
yy1 = smooth(tsr,Cp,0.1,'rloess');
[xx,ind] = sort(tsr);
plot(xx,Cp(ind),'w.',xx,yy1(ind),'k.-')
set(gca,'XLim',[0 1.6])
set(gca,'YLim',[0 0.05])
xlabel('Tip speed ratio')
ylabel('Power coefficient(Cp)')
title('Power Coefficient Vs TSR of Three Stage Savonius Rotor')
grid
```

A.2 Comaparison of Power,torque and RPM of Three Prototypes at constant speed

```
Y1=load('singlestep0.8.txt');
Y2=load('doublestep0.8.txt');
Y3=load('threestep0.8.txt');

% Calculating torque of turbines

tor1=Y1( :,1).*0.001.*0.15.*9.8;
tor2=Y2( :,1).*0.001.*0.15.*9.8;
tor3=Y3( :,1).*0.001.*0.15.*9.8;

% Calculating RPM of turbines

rpm1=abs(Y1( :,2));
rpm2=abs(Y2( :,2));
rpm3=abs(Y3( :,2));

% Measuring length of data

N1 =length(tor1);
```

```
N2 =length(tor2);
N3 =length(tor3);

%Measuring time span of operation

t1=(N1-1)/50;
t2=(N2-1)/50;
t3=(N3-1)/50;
sam=50;                    % sampling time

% Comparing torque of three prototypes at constant speed

ts=0:(1/sam):t1;
figure
yy1 = smooth(ts,tor1,0.1,'rloess');
[xx,ind] = sort(ts);
plot(xx,tor1(ind),'w.',xx,yy1(ind),'r.-')
hold on
td=0:(1/sam):t2;
yy1 = smooth(td,tor2,0.1,'rloess');
[xx,ind] = sort(td);
plot(xx,tor2(ind),'w.',xx,yy1(ind),'b.-')
hold on
tt=0:(1/sam):t3;
yy1 = smooth(tt,tor3,0.1,'rloess');
[xx,ind] = sort(tt);
plot(xx,tor3(ind),'w.',xx,yy1(ind),'k.-')
set(gca,'XLim',[6 8.5])
set(gca,'YLim',[0.05 0.15])
xlabel('Time(sec)')
ylabel('Torque(N-m) of Turbines')
title('Torque Variation of the prototypes')
grid

N1 =length(rpm1);
N2 =length(rpm2);
N3 =length(rpm3);
t1=(N1-1)/50;
t2=(N2-1)/50;
t3=(N3-1)/50;
sam=50;

% Comparing RPM of three prototypes at constant speed

figure
yy1 = smooth(ts,rpm1,0.1,'rloess');
```

```
[xx,ind] = sort(ts);
plot(xx,rpm1(ind),'w.',xx,yy1(ind),'r.-')
hold on
yy1 = smooth(td,rpm2,0.1,'rloess');
[xx,ind] = sort(td);
plot(xx,rpm2(ind),'w.',xx,yy1(ind),'b.-')
hold on
yy1 = smooth(tt,rpm3,0.1,'rloess');
[xx,ind] = sort(tt);
plot(xx,rpm3(ind),'w.',xx,yy1(ind),'k.-')
set(gca,'XLim',[6 8.5])
set(gca,'YLim',[50 110])
xlabel('Time(sec)')
ylabel('RPM of Turbines')
title('RPM Variation of the prototypes')
grid

% Comparing Power of three prototypes at constant speed

s1=Y1(:,3)
w1=(2*pi*rpm1)/60
P1=tor1.*w1
s2=Y2(:,3)
w2=(2*pi*rpm2)/60
P2=tor2.*w2;
s3=Y3(:,3);
w3=(2*pi*rpm3)/60;
P3=tor3.*w3;
figure
yy1 = smooth(ts,P1,0.1,'rloess');
[xx,ind] = sort(ts);
plot(xx,P1(ind),'w.',xx,yy1(ind),'r.-')
hold on
yy1 = smooth(td,P2,0.1,'rloess');
[xx,ind] = sort(td);
plot(xx,P2(ind),'w.',xx,yy1(ind),'b.-')
hold on
yy1 = smooth(tt,P3,0.1,'rloess');
[xx,ind] = sort(tt);
plot(xx,P3(ind),'w.',xx,yy1(ind),'k.-')
set(gca,'XLim',[6 8.5])
set(gca,'YLim',[0.5 1.5])
xlabel('Time(sec)')
ylabel('Power of Turbine(W)')
title('Output Power of Single Step Savonius')
grid
```

Appendix B

B.1 Comparison of two different size prototypes in Wave Tank

```
%   First Prototype Dimension

   H=0.405;   % H is height of rotor(m)
   D=0.222;   % D is diameter of rotor(m)
   d=0.14;    % d  is diameter of each bucket(m)
   A=H*D;     % A is swept area of rotor in square meter

%   Second  Prototype Dimension

   H1=0.87*H;
   D1=0.87*D;
   d1=0.87*d;
   A1=H1*D1;

% First Prototype Data Manipulation

offset=-0.008;

Ya=load('runtt0.4.txt');
tora=abs(Ya( :,1).*0.001.*0.15.*9.8)+offset;
rpma=abs(Ya( :,2));
spa=abs(Ya(:,3));
wa=2*pi.*rpma/60;
tsra=(wa.*D)./(2*spa);
Pa=abs(tora.*wa);

Y0=load('runtt0.5.txt');
tor0=abs(Y0( :,1).*0.001.*0.15.*9.8)+offset;
rpm0=abs(Y0( :,2));
sp0=abs(Y0(:,3));
w0=2*pi.*rpm0/60;
tsr0=(w0.*D)./(2*sp0);
P0=abs(tor0.*w0);

Y1=load('runtt0.6.txt');
tor1=abs(Y1( :,1).*0.001.*0.15.*9.8)+offset;
rpm1=abs(Y1( :,2));
sp1=abs(Y1(:,3));
w1=2*pi.*rpm1/60;
tsr1=(w1.*D)./(2*sp1);
```

```
P1=abs(tor1.*w1);

Y2=load('runtt0.7.txt');
tor2=abs(Y2( :,1).*0.001.*0.15.*9.8)+offset;
rpm2=abs(Y2( :,2));
sp2=abs(Y2(:,3));
w2=2*pi.*rpm2/60;
tsr2=(w2.*D)./(2*sp2);
P2=abs(tor2.*w2);

Y3=load('runtt0.8.txt');
tor3=abs(Y3( :,1).*0.001.*0.15.*9.8)+offset;
rpm3=abs(Y3( :,2));
sp3=abs(Y3(:,3));
w3=2*pi.*rpm3/60;
tsr3=(w3.*D)./(2*sp3);
P3=abs(tor3.*w3);

Y4=load('runtt0.9.txt');
tor4=abs(Y4( :,1).*0.001.*0.15.*9.8)+offset;
rpm4=abs(Y4( :,2));
sp4=abs(Y4(:,3));
w4=2*pi.*rpm4/60;
tsr4=(w4.*D)./(2*sp4);
P4=abs(tor4.*w4);

Y5=load('runtt1.0.txt');
tor5=abs(Y5( :,1).*0.001.*0.15.*9.8)+offset;
rpm5=abs(Y5( :,2));
sp5=abs(Y5(:,3));
w5=2*pi.*rpm5/60;
tsr5=(w5.*D)./(2*sp5);
P5=abs(tor5.*w5);

sp=[spa;sp0;sp1 ;sp2 ;sp3 ;sp4 ;sp5];
rpm=[rpma;rpm0;rpm1;rpm2;rpm3;rpm4;rpm5];
w=[wa;w0;w1; w2 ;w3; w4 ;w5];
P=[Pa;P0;P1 ;P2 ;P3 ;P4 ;P5];
tsr=[tsra;tsr0;tsr1; tsr2; tsr3 ;tsr4; tsr5];


% Second Prototype Data  Manipulation

offset1=0.004;

Y87a=load('run87tt0.4.txt');
```

```
tor87a=abs(Y87a( :,1).*0.001.*0.15.*9.8)+offset1;
rpm87a=abs(Y87a( :,2));
sp87a=abs(Y87a(:,3));
w87a=2*pi.*rpm87a/60;
tsr87a=(w87a.*D1)./(2*sp87a);
P87a=abs(tor87a.*w87a);

Y870=load('run87tt0.5.txt');
tor870=abs(Y870( :,1).*0.001.*0.15.*9.8)+offset1;
rpm870=abs(Y870( :,2));
sp870=abs(Y870(:,3));
w870=2*pi.*rpm870/60;
tsr870=(w870.*D1)./(2*sp870);
P870=abs(tor870.*w870);

Y871=load('run87tt0.6.txt');
tor871=abs(Y871( :,1).*0.001.*0.15.*9.8)+offset1;
rpm871=abs(Y871( :,2));
sp871=abs(Y871(:,3));
w871=2*pi.*rpm871/60;
tsr871=(w871.*D1)./(2*sp871);
P871=abs(tor871.*w871);

Y872=load('run87tt0.7.txt');
tor872=abs(Y872( :,1).*0.001.*0.15.*9.8)+offset1;
rpm872=abs(Y872( :,2));
sp872=abs(Y872(:,3));
w872=2*pi.*rpm872/60;
tsr872=(w872.*D1)./(2*sp872);
P872=abs(tor872.*w872);

Y873=load('run87tt0.8.txt');
tor873=abs(Y873( :,1).*0.001.*0.15.*9.8)+offset1;
rpm873=abs(Y873( :,2));
sp873=abs(Y873(:,3));
w873=2*pi.*rpm873/60;
tsr873=(w873.*D1)./(2*sp873);
P873=abs(tor873.*w873);

Y874=load('run87tt0.9.txt');
tor874=abs(Y874( :,1).*0.001.*0.15.*9.8)+offset1;
rpm874=abs(Y874( :,2));
sp874=abs(Y874(:,3));
w874=2*pi.*rpm874/60;
tsr874=(w874.*D1)./(2*sp874);
P874=abs(tor874.*w874);
```

```
Y875=load('run87tt1.0.txt');
tor875=abs(Y875( :,1).*0.001.*0.15.*9.8)+offset1;
rpm875=abs(Y875( :,2));
sp875=abs(Y875(:,3));
w875=2*pi.*rpm875/60;
tsr875=(w875.*D1)./(2*sp875);
P875=abs(tor875.*w875);

sp87=[0;sp87a;sp870; sp871 ;sp872 ;sp873 ;sp874 ;sp875];
rpm87=[0;rpm87a;rpm870;rpm871;rpm872;rpm873;rpm874;rpm875];
w87=[0;w87a;w870; w871; w872 ;w873; w874 ;w875];
P87=[0;P87a;P870; P871 ;P872 ;P873 ;P874 ;P875];
tsr87=[0;tsr87a;tsr870; tsr871; tsr872; tsr873 ;tsr874; tsr875];

% Plotting Power curve of Two Prototypes

figure
yy1 = smooth(sp,P,0.1,'rloess');
[xx,ind] = sort(sp);
plot(xx,P(ind),'w.',xx,yy1(ind),'r')
hold on
yy1 = smooth(sp87,P87,0.8,'rloess');
[xx,ind] = sort(sp87);
plot(xx,P87(ind),'w.',xx,yy1(ind),'b')
set(gca,'XLim',[0.3 1.0])
set(gca,'YLim',[0 2.5])
xlabel('Water Speed(m/s)')
ylabel('Power of Turbine(W)')
title('Output Power of Two Prototypes')
grid

% Plotting Power coefficient of Two Prototypes


  k=0.5*A*1000;
  s1=sp.^3;
  k1=0.5*A1*1000;
  s87=(sp87).^3;
  cp=P./(k.*s1);
  cp87=P87./(k1.*s87);
  Cp=smooth(cp);
  Cp87=smooth(cp87);
  figure
  yy1 = smooth(tsr,Cp,0.1,'rloess');
  [xx,ind] = sort(tsr);
```

```
plot(xx,Cp(ind),'w.',xx,yy1(ind),'r')
hold on
yy1 = smooth(tsr87,Cp87,0.8,'rloess');
[xx,ind] = sort(tsr87);
plot(xx,Cp87(ind),'w.',xx,yy1(ind),'b')
set(gca,'XLim',[0 1.0])
set(gca,'YLim',[0 0.08])
xlabel('Tip speed ratio')
ylabel('Power coefficient(Cp)')
title('Power Coefficient of Two Prototypes in Water ')
grid
```

B.2 Comparison of two different size prototypes in Wind Tunnel

```
%   First Prototype Dimension

   H=0.405;   % H is height of rotor(m)
   D=0.222;   % D is diameter of rotor(m)
   d=0.14;    % d  is diameter of each bucket(m)
   A=H*D;     % A is swept area of rotor in square meter

%   Second  Prototype Dimension

   H1=0.87*H;
   D1=0.87*D;
   d1=0.87*d;
   A1=H1*D1;

% First Prototype Data Manipulation

offset=0.023;

Y1=load('runt1.txt');
avgtor1=mean(Y1(:,1)).*0.001.*9.8.*0.15+offset;
avgrpm1=mean(Y1(:,2));

Y2=load('runt2.txt');
avgtor2=mean(Y2(:,1)).*0.001.*9.8.*0.15+offset;
avgrpm2=mean(Y2(:,2));

Y3=load('runt3.txt');
avgtor3=mean(Y3(:,1)).*0.001.*9.8.*0.15+offset;
avgrpm3=mean(Y3(:,2));
```

```
Y4=load('runt4.txt');
avgtor4=mean(Y4(:,1)).*0.001.*9.8.*0.15+offset;
avgrpm4=mean(Y4(:,2));


Y5=load('runt5.txt');
avgtor5=mean(Y5(:,1)).*0.001.*9.8.*0.15+offset;
avgrpm5=mean(Y5(:,2));


Y6=load('runt6.txt');
avgtor6=mean(Y6(:,1)).*0.001.*9.8.*0.15+offset;
avgrpm6=mean(Y6(:,2));

Y7=load('runt7.txt');
avgtor7=mean(Y7(:,1)).*0.001.*9.8.*0.15+offset;
avgrpm7=mean(Y7(:,2));

Y8=load('runt8.txt');
avgtor8=mean(Y8(:,1)).*0.001.*9.8.*0.15+offset;
avgrpm8=mean(Y8(:,2));

Y9=load('runt9.txt');
avgtor9=mean(Y1(:,1)).*0.001.*9.8.*0.15+offset;
avgrpm9=mean(Y1(:,2));

Y10=load('runt10.txt');
avgtor10=mean(Y10(:,1)).*0.001.*9.8.*0.15+offset;
avgrpm10=mean(Y10(:,2));

Y11=load('runt11.txt');
avgtor11=mean(Y11(:,1)).*0.001.*9.8.*0.15+offset;
avgrpm11=mean(Y11(:,2));

Y12=load('runt12.txt');
avgtor12=mean(Y12(:,1)).*0.001.*9.8.*0.15+offset;
avgrpm12=mean(Y12(:,2));

Y13=load('runt13.txt');
avgtor13=mean(Y13(:,1)).*0.001.*9.8.*0.15+offset;
avgrpm13=mean(Y13(:,2));


Y14=load('runt14.txt');
avgtor14=mean(Y14(:,1)).*0.001.*9.8.*0.15-offset;
avgrpm14=mean(Y14(:,2));
```

```
Y15=load('runt15.txt');
avgtor15=mean(Y15(:,1)).*0.001.*9.8.*0.15-offset;
avgrpm15=mean(Y15(:,2));

Y16=load('runt16.txt');
avgtor16=mean(Y16(:,1)).*0.001.*9.8.*0.15-offset;
avgrpm16=mean(Y16(:,2));

Y17=load('runt17.txt');
avgtor17=mean(Y17(:,1)).*0.001.*9.8.*0.15-offset;
avgrpm17=mean(Y17(:,2));

Y18=load('runt18.txt');
avgtor18=mean(Y18(:,1)).*0.001.*9.8.*0.15-offset;
avgrpm18=mean(Y18(:,2));

Y19=load('runt19.txt');
avgtor19=mean(Y19(:,1)).*0.001.*9.8.*0.15-offset;
avgrpm19=mean(Y19(:,2));

Y20=load('runt20.txt');
avgtor20=mean(Y20(:,1)).*0.001.*9.8.*0.15-offset;
avgrpm20=mean(Y20(:,2));


Y21=load('runt21.txt');
avgtor21=mean(Y21(:,1)).*0.001.*9.8.*0.15-offset;
avgrpm21=mean(Y21(:,2));

Y22=load('runt22.txt');
avgtor22=mean(Y22(:,1)).*0.001.*9.8.*0.15-offset;
avgrpm22=mean(Y22(:,2));

Y23=load('runt23.txt');
avgtor23=mean(Y23(:,1)).*0.001.*9.8.*0.15-offset;
avgrpm23=mean(Y23(:,2));

Y24=load('runt24.txt');
avgtor24=mean(Y24(:,1)).*0.001.*9.8.*0.15-offset;
avgrpm24=mean(Y24(:,2));

Y25=load('runt25.txt');
avgtor25=mean(Y25(:,1)).*0.001.*9.8.*0.15-offset;
avgrpm25=mean(Y25(:,2));
```

```
Y26=load('runt26.txt');
avgtor26=mean(Y26(:,1)).*0.001.*9.8.*0.15-offset;
avgrpm26=mean(Y26(:,2));

Y27=load('runt27.txt');
avgtor27=mean(Y27(:,1)).*0.001.*9.8.*0.15-offset;
avgrpm27=mean(Y27(:,2));

Y28=load('runt28.txt');
avgtor28=mean(Y28(:,1)).*0.001.*9.8.*0.15-offset;
avgrpm28=mean(Y28(:,2));

Y29=load('runt29.txt');
avgtor29=mean(Y29(:,1)).*0.001.*9.8.*0.15-offset;
avgrpm29=mean(Y29(:,2));

Y30=load('runt30.txt');
avgtor30=mean(Y30(:,1)).*0.001.*9.8.*0.15+offset;
avgrpm30=mean(Y30(:,2));

Y30=load('runt30.txt');
avgtor30=mean(Y30(:,1)).*0.001.*9.8.*0.15+offset;
avgrpm30=mean(Y30(:,2));

Y30=load('runt30.txt');
avgtor30=mean(Y30(:,1)).*0.001.*9.8.*0.15+offset;
avgrpm30=mean(Y30(:,2));

Y31=load('runt31.txt');
avgtor31=mean(Y31(:,1)).*0.001.*9.8.*0.15+offset;
avgrpm31=mean(Y31(:,2));

Y32=load('runt32.txt');
avgtor32=mean(Y32(:,1)).*0.001.*9.8.*0.15+offset;
avgrpm32=mean(Y32(:,2));

Y33=load('runt33.txt');
avgtor33=mean(Y33(:,1)).*0.001.*9.8.*0.15+offset;
avgrpm33=mean(Y33(:,2));

Y34=load('runt34.txt');
avgtor34=mean(Y34(:,1)).*0.001.*9.8.*0.15+offset;
avgrpm34=mean(Y34(:,2));
```

```
sp=[0 1 2 3 4 5 6.25 6.25 7.1 7.1 8.1 8.1 8.1  10.1 10.1 10.1 10.1 10.1 10.1 10.1 11.0 11.0
11.0 11.0 11.0 12 12 12 12 12 12 12 13.6 13.6 13.6 13.6 ]
tor=[0 0 0 0 0 0 avgtor1 avgtor2 avgtor3 avgtor4 avgtor5 avgtor6 avgtor7  avgtor12
avgtor13 avgtor14  avgtor15 avgtor16 avgtor17 avgtor18 avgtor19 avgtor20 avgtor21
avgtor22 avgtor23 avgtor24 avgtor25 avgtor26 avgtor27 avgtor28 avgtor29 avgtor30
avgtor31 avgtor32 avgtor33 avgtor34 ]
rpm=[0 0 0 0 0 0 avgrpm1 avgrpm2  avgrpm3 avgrpm4 avgrpm5 avgrpm6 avgrpm7
avgrpm12 avgrpm13 avgrpm14 avgrpm15 avgrpm16 avgrpm17 avgrpm18 avgrpm19
avgrpm20 avgrpm21 avgrpm22 avgrpm23 avgrpm24 avgrpm25 avgrpm26 avgrpm27
avgrpm28 avgrpm29 avgrpm30 avgrpm31 avgrpm32 avgrpm33 avgrpm34 ]


% Second Prototype Data  Manipulation

offset1=0.038;

Y1=load('runtt1.txt');
avgtor1=mean(Y1(:,1)).*0.001.*9.8.*0.15+offset1;
avgrpm1=mean(Y1(:,2));

Y2=load('runtt2.txt');
avgtor2=mean(Y2(:,1)).*0.001.*9.8.*0.15+offset1;
avgrpm2=mean(Y2(:,2));

Y3=load('runtt3.txt');
avgtor3=mean(Y3(:,1)).*0.001.*9.8.*0.15+offset1;
avgrpm3=mean(Y3(:,2));

Y4=load('runtt4.txt');
avgtor4=mean(Y4(:,1)).*0.001.*9.8.*0.15+offset1;
avgrpm4=mean(Y4(:,2));


Y5=load('runtt5.txt');
avgtor5=mean(Y5(:,1)).*0.001.*9.8.*0.15+offset1;
avgrpm5=mean(Y5(:,2));


Y6=load('runtt6.txt');
avgtor6=mean(Y6(:,1)).*0.001.*9.8.*0.15+offset1;
avgrpm6=mean(Y6(:,2));

Y7=load('runtt7.txt');
avgtor7=mean(Y7(:,1)).*0.001.*9.8.*0.15+offset1;
```

```
avgrpm7=mean(Y7(:,2));

Y8=load('runtt8.txt');
avgtor8=mean(Y8(:,1)).*0.001.*9.8.*0.15+offset1;
avgrpm8=mean(Y8(:,2));

Y9=load('runtt9.txt');
avgtor9=mean(Y1(:,1)).*0.001.*9.8.*0.15+offset1;
avgrpm9=mean(Y1(:,2));

Y10=load('runtt10.txt');
avgtor10=mean(Y10(:,1)).*0.001.*9.8.*0.15+offset1;
avgrpm10=mean(Y10(:,2));

Y11=load('runtt11.txt');
avgtor11=mean(Y11(:,1)).*0.001.*9.8.*0.15+offset1;
avgrpm11=mean(Y11(:,2));

Y12=load('runtt12.txt');
avgtor12=mean(Y12(:,1)).*0.001.*9.8.*0.15+offset1;
avgrpm12=mean(Y12(:,2));

Y13=load('runtt13.txt');
avgtor13=mean(Y13(:,1)).*0.001.*9.8.*0.15+offset1;
avgrpm13=mean(Y13(:,2));


Y14=load('runtt14.txt');
avgtor14=mean(Y14(:,1)).*0.001.*9.8.*0.15+offset1;
avgrpm14=mean(Y14(:,2));

Y15=load('runtt15.txt');
avgtor15=mean(Y15(:,1)).*0.001.*9.8.*0.15+offset1;
avgrpm15=mean(Y15(:,2));

Y16=load('runtt16.txt');
avgtor16=mean(Y16(:,1)).*0.001.*9.8.*0.15+offset1;
avgrpm16=mean(Y16(:,2));

Y17=load('runtt17.txt');
avgtor17=mean(Y17(:,1)).*0.001.*9.8.*0.15+offset1;
avgrpm17=mean(Y17(:,2));

Y18=load('runtt18.txt');
avgtor18=mean(Y18(:,1)).*0.001.*9.8.*0.15+offset1;
avgrpm18=mean(Y18(:,2));
```

```
Y19=load('runtt19.txt');
avgtor19=mean(Y19(:,1)).*0.001.*9.8.*0.15+offset1;
avgrpm19=mean(Y19(:,2));

Y20=load('runtt20.txt');
avgtor20=mean(Y20(:,1)).*0.001.*9.8.*0.15+offset1;
avgrpm20=mean(Y20(:,2));


Y21=load('runtt21.txt');
avgtor21=mean(Y21(:,1)).*0.001.*9.8.*0.15+offset1;
avgrpm21=mean(Y21(:,2));

Y22=load('runtt22.txt');
avgtor22=mean(Y22(:,1)).*0.001.*9.8.*0.15+offset1;
avgrpm22=mean(Y22(:,2));

sp1=[ 0 1 2 3 4 5 6 7.4 8.45 8.45 8.45 8.45 8.45 9 9 9 10 10 11 11 12 12 12 12 13.6 13.6
13.6 13.6 13.6]
tor1=[0 0 0 0 0 0 0 avgtor1 avgtor2 avgtor3 avgtor4 avgtor5 avgtor6 avgtor7 avgtor8
avgtor9  avgtor10  avgtor11 avgtor12  avgtor13 avgtor14  avgtor15 avgtor16 avgtor17
avgtor18 avgtor19 avgtor20 avgtor21 avgtor22 ]
rpm1=[0 0 0 0 0 0 0 avgrpm1 avgrpm2  avgrpm3 avgrpm4 avgrpm5 avgrpm6 avgrpm7
avgrpm8 avgrpm9 avgrpm10  avgrpm11 avgrpm12 avgrpm13 avgrpm14 avgrpm15
avgrpm16 avgrpm17 avgrpm18 avgrpm19 avgrpm20 avgrpm21 avgrpm22 ]


% Plotting Power curve of  Prototypes in Wind


w=abs((2*pi.*rpm)/60);
Pm=abs(tor.*w);
figure
yy1 = smooth(sp,Pm,0.3,'rloess');
[xx,ind] = sort(sp);
plot(xx,Pm(ind),'w.',xx,yy1(ind),'r')
hold on
w1=abs((2*pi.*rpm1)/60);
Pm1=abs(tor1.*w1);
yy1 = smooth(sp1,Pm1,0.5,'rloess');
[xx,ind] = sort(sp1);
plot(xx,Pm1(ind),'w.',xx,yy1(ind),'b')
set(gca,'XLim',[4 10])
set(gca,'YLim',[0  1.5])
xlabel('Wind speed(m/s)')
```

```
ylabel('Power(W)')
title('Output Power of Two Prototypes')
grid

% Plotting Power coefficient curves of  Prototypes in Wind

  k=0.5*A*1.29;
  tsr=(w.*D)./(2*sp);
  s1=sp.^3;
  Cp=Pm./(k.*s1);
  figure
  yy1 = smooth(tsr,Cp,0.1,'rloess');
  [xx,ind] = sort(tsr);
  plot(xx,Cp(ind),'w.',xx,yy1(ind),'r.-')
  hold on
  k1=0.5*A1*1.29;
  tsr1=(w1.*D1)./(2*sp1);
  s2=sp1.^3;
  Cp1=Pm1./(k1.*s2);
  yy1 = smooth(tsr1,Cp1,0.1,'rloess');
  [xx,ind] = sort(tsr1);
  plot(xx,Cp1(ind),'w.',xx,yy1(ind),'b.-')
  set(gca,'XLim',[0 1])
  set(gca,'YLim',[0 0.05])
  xlabel('Tip speed ratio')
  ylabel('Cp')
  title('Power coefficient Curve of two Prototypes')
  grid
```

B.3 Plotting the Power coefficient curve of two prototypes in water and wind Using Approach A

```
% First Prototype Dimension

  H=0.405;   % H is height of rotor(m)
  D=0.222;   % D is diameter of rotor(m)
  d=0.14;    % d  is diameter of each bucket(m)
  A=H*D;     % A is swept area of rotor in square meter

%   Second  Prototype Dimension

  H1=0.87*H;
  D1=0.87*D;
  d1=0.87*d;
  A1=H1*D1;
```

```
% First Prototype Data Manipulation in Wave Tank

offset=-0.008;

Ya=load('runtt0.4.txt');
tora=abs(Ya( :,1).*0.001.*0.15.*9.8)+offset;
rpma=abs(Ya( :,2));
spa=abs(Ya(:,3));
wa=2*pi.*rpma/60;
tsra=(wa.*D)./(2*spa);
Pa=abs(tora.*wa);

Y0=load('runtt0.5.txt');
tor0=abs(Y0( :,1).*0.001.*0.15.*9.8)+offset;
rpm0=abs(Y0( :,2));
sp0=abs(Y0(:,3));
w0=2*pi.*rpm0/60;
tsr0=(w0.*D)./(2*sp0);
P0=abs(tor0.*w0);

Y1=load('runtt0.6.txt');
tor1=abs(Y1( :,1).*0.001.*0.15.*9.8)+offset;
rpm1=abs(Y1( :,2));
sp1=abs(Y1(:,3));
w1=2*pi.*rpm1/60;
tsr1=(w1.*D)./(2*sp1);
P1=abs(tor1.*w1);

Y2=load('runtt0.7.txt');
tor2=abs(Y2( :,1).*0.001.*0.15.*9.8)+offset;
rpm2=abs(Y2( :,2));
sp2=abs(Y2(:,3));
w2=2*pi.*rpm2/60;
tsr2=(w2.*D)./(2*sp2);
P2=abs(tor2.*w2);

Y3=load('runtt0.8.txt');
tor3=abs(Y3( :,1).*0.001.*0.15.*9.8)+offset;
rpm3=abs(Y3( :,2));
sp3=abs(Y3(:,3));
w3=2*pi.*rpm3/60;
tsr3=(w3.*D)./(2*sp3);
P3=abs(tor3.*w3);

Y4=load('runtt0.9.txt');
```

```
tor4=abs(Y4( :,1).*0.001.*0.15.*9.8)+offset;
rpm4=abs(Y4( :,2));
sp4=abs(Y4(:,3));
w4=2*pi.*rpm4/60;
tsr4=(w4.*D)./(2*sp4);
P4=abs(tor4.*w4);

Y5=load('runtt1.0.txt');
tor5=abs(Y5( :,1).*0.001.*0.15.*9.8)+offset;
rpm5=abs(Y5( :,2));
sp5=abs(Y5(:,3));
w5=2*pi.*rpm5/60;
tsr5=(w5.*D)./(2*sp5);
P5=abs(tor5.*w5);

sp=[spa;sp0;sp1 ;sp2 ;sp3 ;sp4 ;sp5];
rpm=[rpma;rpm0;rpm1;rpm2;rpm3;rpm4;rpm5];
w=[wa;w0;w1; w2 ;w3; w4 ;w5];
P=[Pa;P0;P1 ;P2 ;P3 ;P4 ;P5];
tsr=[tsra;tsr0;tsr1; tsr2; tsr3 ;tsr4; tsr5];


% Second Prototype Data Manipulation in Wave Tank

offset1=0.004;

Y87a=load('run87tt0.4.txt');
tor87a=abs(Y87a( :,1).*0.001.*0.15.*9.8)+offset1;
rpm87a=abs(Y87a( :,2));
sp87a=abs(Y87a(:,3));
w87a=2*pi.*rpm87a/60;
tsr87a=(w87a.*D1)./(2*sp87a);
P87a=abs(tor87a.*w87a);

Y870=load('run87tt0.5.txt');
tor870=abs(Y870( :,1).*0.001.*0.15.*9.8)+offset1;
rpm870=abs(Y870( :,2));
sp870=abs(Y870(:,3));
w870=2*pi.*rpm870/60;
tsr870=(w870.*D1)./(2*sp870);
P870=abs(tor870.*w870);

Y871=load('run87tt0.6.txt');
tor871=abs(Y871( :,1).*0.001.*0.15.*9.8)+offset1;
rpm871=abs(Y871( :,2));
sp871=abs(Y871(:,3));
```

```
w871=2*pi.*rpm871/60;
tsr871=(w871.*D1)./(2*sp871);
P871=abs(tor871.*w871);

Y872=load('run87tt0.7.txt');
tor872=abs(Y872( :,1).*0.001.*0.15.*9.8)+offset1;
rpm872=abs(Y872( :,2));
sp872=abs(Y872(:,3));
w872=2*pi.*rpm872/60;
tsr872=(w872.*D1)./(2*sp872);
P872=abs(tor872.*w872);

Y873=load('run87tt0.8.txt');
tor873=abs(Y873( :,1).*0.001.*0.15.*9.8)+offset1;
rpm873=abs(Y873( :,2));
sp873=abs(Y873(:,3));
w873=2*pi.*rpm873/60;
tsr873=(w873.*D1)./(2*sp873);
P873=abs(tor873.*w873);

Y874=load('run87tt0.9.txt');
tor874=abs(Y874( :,1).*0.001.*0.15.*9.8)+offset1;
rpm874=abs(Y874( :,2));
sp874=abs(Y874(:,3));
w874=2*pi.*rpm874/60;
tsr874=(w874.*D1)./(2*sp874);
P874=abs(tor874.*w874);

Y875=load('run87tt1.0.txt');
tor875=abs(Y875( :,1).*0.001.*0.15.*9.8)+offset1;
rpm875=abs(Y875( :,2));
sp875=abs(Y875(:,3));
w875=2*pi.*rpm875/60;
tsr875=(w875.*D1)./(2*sp875);
P875=abs(tor875.*w875);

sp87=[0;sp87a;sp870; sp871 ;sp872 ;sp873 ;sp874 ;sp875];
rpm87=[0;rpm87a;rpm870;rpm871;rpm872;rpm873;rpm874;rpm875];
w87=[0;w87a;w870; w871; w872 ;w873; w874 ;w875];
P87=[0;P87a;P870; P871 ;P872 ;P873 ;P874 ;P875];
tsr87=[0;tsr87a;tsr870; tsr871; tsr872; tsr873 ;tsr874; tsr875];


 % Analysis of power coefficient curve in Water

  k=0.5*A*1000;
```

```
s1=sp.^3;
k1=0.5*A1*1000;
s87=(sp87).^3;
cp=P./(k.*s1);
cp87=P87./(k1.*s87);
Cp=smooth(cp);
Cp87=smooth(cp87);
figure
yy1 = smooth(tsr,Cp,0.1,'rloess');
[xx,ind] = sort(tsr);
plot(xx,Cp(ind),'w.',xx,yy1(ind),'r')
hold on
yy1 = smooth(tsr87,Cp87,0.1,'rloess');
[xx,ind] = sort(tsr87);
plot(xx,Cp87(ind),'w.',xx,yy1(ind),'b')
hold on

% First Prototype Data Manipulation in Wind Tunnel

offset=0.023;

Y1=load('runt1.txt');
avgtor1=mean(Y1(:,1)).*0.001.*9.8.*0.15+offset;
avgrpm1=mean(Y1(:,2));

Y2=load('runt2.txt');
avgtor2=mean(Y2(:,1)).*0.001.*9.8.*0.15+offset;
avgrpm2=mean(Y2(:,2));

Y3=load('runt3.txt');
avgtor3=mean(Y3(:,1)).*0.001.*9.8.*0.15+offset;
avgrpm3=mean(Y3(:,2));

Y4=load('runt4.txt');
avgtor4=mean(Y4(:,1)).*0.001.*9.8.*0.15+offset;
avgrpm4=mean(Y4(:,2));


Y5=load('runt5.txt');
avgtor5=mean(Y5(:,1)).*0.001.*9.8.*0.15+offset;
avgrpm5=mean(Y5(:,2));


Y6=load('runt6.txt');
avgtor6=mean(Y6(:,1)).*0.001.*9.8.*0.15+offset;
avgrpm6=mean(Y6(:,2));
```

```
Y7=load('runt7.txt');
avgtor7=mean(Y7(:,1)).*0.001.*9.8.*0.15+offset;
avgrpm7=mean(Y7(:,2));

Y8=load('runt8.txt');
avgtor8=mean(Y8(:,1)).*0.001.*9.8.*0.15+offset;
avgrpm8=mean(Y8(:,2));

Y9=load('runt9.txt');
avgtor9=mean(Y1(:,1)).*0.001.*9.8.*0.15+offset;
avgrpm9=mean(Y1(:,2));

Y10=load('runt10.txt');
avgtor10=mean(Y10(:,1)).*0.001.*9.8.*0.15+offset;
avgrpm10=mean(Y10(:,2));

Y11=load('runt11.txt');
avgtor11=mean(Y11(:,1)).*0.001.*9.8.*0.15+offset;
avgrpm11=mean(Y11(:,2));

Y12=load('runt12.txt');
avgtor12=mean(Y12(:,1)).*0.001.*9.8.*0.15+offset;
avgrpm12=mean(Y12(:,2));

Y13=load('runt13.txt');
avgtor13=mean(Y13(:,1)).*0.001.*9.8.*0.15+offset;
avgrpm13=mean(Y13(:,2));


Y14=load('runt14.txt');
avgtor14=mean(Y14(:,1)).*0.001.*9.8.*0.15-offset;
avgrpm14=mean(Y14(:,2));

Y15=load('runt15.txt');
avgtor15=mean(Y15(:,1)).*0.001.*9.8.*0.15-offset;
avgrpm15=mean(Y15(:,2));

Y16=load('runt16.txt');
avgtor16=mean(Y16(:,1)).*0.001.*9.8.*0.15-offset;
avgrpm16=mean(Y16(:,2));

Y17=load('runt17.txt');
avgtor17=mean(Y17(:,1)).*0.001.*9.8.*0.15-offset;
avgrpm17=mean(Y17(:,2));
```

```
Y18=load('runt18.txt');
avgtor18=mean(Y18(:,1)).*0.001.*9.8.*0.15-offset;
avgrpm18=mean(Y18(:,2));

Y19=load('runt19.txt');
avgtor19=mean(Y19(:,1)).*0.001.*9.8.*0.15-offset;
avgrpm19=mean(Y19(:,2));

Y20=load('runt20.txt');
avgtor20=mean(Y20(:,1)).*0.001.*9.8.*0.15-offset;
avgrpm20=mean(Y20(:,2));


Y21=load('runt21.txt');
avgtor21=mean(Y21(:,1)).*0.001.*9.8.*0.15-offset;
avgrpm21=mean(Y21(:,2));

Y22=load('runt22.txt');
avgtor22=mean(Y22(:,1)).*0.001.*9.8.*0.15-offset;
avgrpm22=mean(Y22(:,2));

Y23=load('runt23.txt');
avgtor23=mean(Y23(:,1)).*0.001.*9.8.*0.15-offset;
avgrpm23=mean(Y23(:,2));

Y24=load('runt24.txt');
avgtor24=mean(Y24(:,1)).*0.001.*9.8.*0.15-offset;
avgrpm24=mean(Y24(:,2));

Y25=load('runt25.txt');
avgtor25=mean(Y25(:,1)).*0.001.*9.8.*0.15-offset;
avgrpm25=mean(Y25(:,2));

Y26=load('runt26.txt');
avgtor26=mean(Y26(:,1)).*0.001.*9.8.*0.15-offset;
avgrpm26=mean(Y26(:,2));

Y27=load('runt27.txt');
avgtor27=mean(Y27(:,1)).*0.001.*9.8.*0.15-offset;
avgrpm27=mean(Y27(:,2));

Y28=load('runt28.txt');
avgtor28=mean(Y28(:,1)).*0.001.*9.8.*0.15-offset;
avgrpm28=mean(Y28(:,2));

Y29=load('runt29.txt');
```

```
avgtor29=mean(Y29(:,1)).*0.001.*9.8.*0.15-offset;
avgrpm29=mean(Y29(:,2));

Y30=load('runt30.txt');
avgtor30=mean(Y30(:,1)).*0.001.*9.8.*0.15-offset;
avgrpm30=mean(Y30(:,2));

Y30=load('runt30.txt');
avgtor30=mean(Y30(:,1)).*0.001.*9.8.*0.15-offset;
avgrpm30=mean(Y30(:,2));

Y30=load('runt30.txt');
avgtor30=mean(Y30(:,1)).*0.001.*9.8.*0.15-offset;
avgrpm30=mean(Y30(:,2));

Y31=load('runt31.txt');
avgtor31=mean(Y31(:,1)).*0.001.*9.8.*0.15-offset;
avgrpm31=mean(Y31(:,2));

Y32=load('runt32.txt');
avgtor32=mean(Y32(:,1)).*0.001.*9.8.*0.15-offset;
avgrpm32=mean(Y32(:,2));

Y33=load('runt33.txt');
avgtor33=mean(Y33(:,1)).*0.001.*9.8.*0.15-offset;
avgrpm33=mean(Y33(:,2));

Y34=load('runt34.txt');
avgtor34=mean(Y34(:,1)).*0.001.*9.8.*0.15-offset;
avgrpm34=mean(Y34(:,2));

sp=[0 1 2 3 4 5 6.25 6.25 7.1 7.1 8.1 8.1 8.1  10.1 10.1 10.1 10.1 10.1 10.1 10.1 10.1 11.0 11.0
11.0 11.0 11.0 12 12 12 12 12 12 12 13.6 13.6 13.6 13.6 ]
tor=[0 0 0 0 0 0 avgtor1 avgtor2 avgtor3 avgtor4 avgtor5 avgtor6 avgtor7  avgtor12
avgtor13 avgtor14  avgtor15 avgtor16 avgtor17 avgtor18 avgtor19 avgtor20 avgtor21
avgtor22 avgtor23 avgtor24 avgtor25 avgtor26 avgtor27 avgtor28 avgtor29 avgtor30
avgtor31 avgtor32 avgtor33 avgtor34 ]
rpm=[0 0 0 0 0 0 avgrpm1 avgrpm2  avgrpm3 avgrpm4 avgrpm5 avgrpm6 avgrpm7
avgrpm12 avgrpm13 avgrpm14 avgrpm15 avgrpm16 avgrpm17 avgrpm18 avgrpm19
avgrpm20 avgrpm21 avgrpm22 avgrpm23 avgrpm24 avgrpm25 avgrpm26 avgrpm27
avgrpm28 avgrpm29 avgrpm30 avgrpm31 avgrpm32 avgrpm33 avgrpm34 ]


% Plotting Power coefficient curve of First Prototype in Wind

  w=abs((2*pi.*rpm)/60);
```

```
Pm=abs(tor.*w);
k=0.5*A*1.29;
tsr=(w.*D)./(2*sp);
s1=sp.^3;
Cp=Pm./(k.*s1);
yy1 = smooth(tsr,Cp,0.1,'rloess');
[xx,ind] = sort(tsr);
plot(xx,Cp(ind),'w.',xx,yy1(ind),'r')
hold on


% Second Prototype Data Manipulation in Wind Tunnel

offset1=0.04;

Y1=load('runtt1.txt');
avgtor1=mean(Y1(:,1)).*0.001.*9.8.*0.15+offset1;
avgrpm1=mean(Y1(:,2));

Y2=load('runtt2.txt');
avgtor2=mean(Y2(:,1)).*0.001.*9.8.*0.15+offset1;
avgrpm2=mean(Y2(:,2));

Y3=load('runtt3.txt');
avgtor3=mean(Y3(:,1)).*0.001.*9.8.*0.15+offset1;
avgrpm3=mean(Y3(:,2));

Y4=load('runtt4.txt');
avgtor4=mean(Y4(:,1)).*0.001.*9.8.*0.15+offset1;
avgrpm4=mean(Y4(:,2));


Y5=load('runtt5.txt');
avgtor5=mean(Y5(:,1)).*0.001.*9.8.*0.15+offset1;
avgrpm5=mean(Y5(:,2));


Y6=load('runtt6.txt');
avgtor6=mean(Y6(:,1)).*0.001.*9.8.*0.15+offset1;
avgrpm6=mean(Y6(:,2));

Y7=load('runtt7.txt');
avgtor7=mean(Y7(:,1)).*0.001.*9.8.*0.15+offset1;
avgrpm7=mean(Y7(:,2));

Y8=load('runtt8.txt');
```

```
avgtor8=mean(Y8(:,1)).*0.001.*9.8.*0.15+offset1;
avgrpm8=mean(Y8(:,2));

Y9=load('runtt9.txt');
avgtor9=mean(Y1(:,1)).*0.001.*9.8.*0.15+offset1;
avgrpm9=mean(Y1(:,2));

Y10=load('runtt10.txt');
avgtor10=mean(Y10(:,1)).*0.001.*9.8.*0.15+offset1;
avgrpm10=mean(Y10(:,2));

Y11=load('runtt11.txt');
avgtor11=mean(Y11(:,1)).*0.001.*9.8.*0.15+offset1;
avgrpm11=mean(Y11(:,2));

Y12=load('runtt12.txt');
avgtor12=mean(Y12(:,1)).*0.001.*9.8.*0.15+offset1;
avgrpm12=mean(Y12(:,2));

Y13=load('runtt13.txt');
avgtor13=mean(Y13(:,1)).*0.001.*9.8.*0.15+offset1;
avgrpm13=mean(Y13(:,2));


Y14=load('runtt14.txt');
avgtor14=mean(Y14(:,1)).*0.001.*9.8.*0.15+offset1;
avgrpm14=mean(Y14(:,2));

Y15=load('runtt15.txt');
avgtor15=mean(Y15(:,1)).*0.001.*9.8.*0.15+offset1;
avgrpm15=mean(Y15(:,2));

Y16=load('runtt16.txt');
avgtor16=mean(Y16(:,1)).*0.001.*9.8.*0.15+offset1;
avgrpm16=mean(Y16(:,2));

Y17=load('runtt17.txt');
avgtor17=mean(Y17(:,1)).*0.001.*9.8.*0.15+offset1;
avgrpm17=mean(Y17(:,2));

Y18=load('runtt18.txt');
avgtor18=mean(Y18(:,1)).*0.001.*9.8.*0.15+offset1;
avgrpm18=mean(Y18(:,2));

Y19=load('runtt19.txt');
avgtor19=mean(Y19(:,1)).*0.001.*9.8.*0.15+offset1;
```

```
avgrpm19=mean(Y19(:,2));

Y20=load('runtt20.txt');
avgtor20=mean(Y20(:,1)).*0.001.*9.8.*0.15+offset1;
avgrpm20=mean(Y20(:,2));


Y21=load('runtt21.txt');
avgtor21=mean(Y21(:,1)).*0.001.*9.8.*0.15+offset1;
avgrpm21=mean(Y21(:,2));

Y22=load('runtt22.txt');
avgtor22=mean(Y22(:,1)).*0.001.*9.8.*0.15+offset1;
avgrpm22=mean(Y22(:,2));

sp=[ 0 1 2 3 4 5 6 7.4 8.45 8.45 8.45 8.45 8.45 9 9 9 10 10 11 11 12 12 12 12 13.6 13.6
13.6 13.6 13.6]
tor=[0 0 0 0 0 0 0 0 avgtor1 avgtor2 avgtor3 avgtor4 avgtor5 avgtor6 avgtor7 avgtor8
avgtor9  avgtor10  avgtor11 avgtor12  avgtor13 avgtor14  avgtor15 avgtor16 avgtor17
avgtor18 avgtor19 avgtor20 avgtor21 avgtor22 ]
rpm=[0 0 0 0 0 0 0 0 avgrpm1 avgrpm2  avgrpm3 avgrpm4 avgrpm5 avgrpm6 avgrpm7
avgrpm8 avgrpm9 avgrpm10  avgrpm11 avgrpm12 avgrpm13 avgrpm14 avgrpm15
avgrpm16 avgrpm17 avgrpm18 avgrpm19 avgrpm20 avgrpm21 avgrpm22 ]



% Plotting Power coefficient curve of Second Prototype in Wind

  k=0.5*A1*1.29;
  w=abs((2*pi.*rpm)/60);
  Pm=abs(tor.*w);
  tsr=(w.*D1)./(2*sp);
  s1=sp.^3;
  Cp=Pm./(k.*s1);
  yy1 = smooth(tsr,Cp,0.1,'rloess');
  [xx,ind] = sort(tsr);
  plot(xx,Cp(ind),'w.',xx,yy1(ind),'b')
  set(gca,'XLim',[0 1.0])
  set(gca,'YLim',[0 0.08])
  xlabel('Tip speed ratio')
  ylabel('Power Coefficient(Cp)')
  title('Power coefficient Curve of two Prototype Using Aprroach B')
  grid
```

B.4 Plotting the Power coefficient curve of two prototypes in water and wind Using Approach B

```
%  First Prototype Dimension

   H=0.405;   % H is height of rotor(m)
   D=0.222;   % D is diameter of rotor(m)
   d=0.14;    % d  is diameter of each bucket(m)
   A=H*D;     % A is swept area of rotor in square meter

%  Second  Prototype Dimension

   H1=0.87*H;
   D1=0.87*D;
   d1=0.87*d;
   A1=H1*D1;

% First Prototype Data Manipulation in Wave Tank

offset=-0.008
Y1=load('runtt0.4.txt');
avgspeed1=mean(Y1(:,3));
avgtor1=mean(Y1( :,1).*0.001.*0.15.*9.8)+offset;
avgrpm1=mean(Y1(:,2));

Y2=load('runtt0.5.txt');
avgspeed2=mean(Y2(:,3));
avgtor2=mean(Y2( :,1).*0.001.*0.15.*9.8)+offset;
avgrpm2=mean(Y2(:,2));

Y3=load('runtt0.6.txt');
avgspeed3=mean(Y3(:,3));
avgtor3=mean(Y3( :,1).*0.001.*0.15.*9.8)+offset;
avgrpm3=mean(Y3(:,2))+offset;

Y4=load('runtt0.7.txt');
avgspeed4=mean(Y4(:,3));
avgtor4=mean(Y4( :,1).*0.001.*0.15.*9.8)+offset;
avgrpm4=mean(Y4(:,2));

Y5=load('runtt0.8.txt');
avgspeed5=mean(Y5(:,3));
avgtor5=mean(Y5( :,1).*0.001.*0.15.*9.8)+offset;
avgrpm5=mean(Y5(:,2));
```

```
Y6=load('runtt0.9.txt');
avgspeed6=mean(Y6(:,3));
avgtor6=mean(Y6( :,1).*0.001.*0.15.*9.8)+offset;
avgrpm6=mean(Y6(:,2))

Ya0=load('runttttttt0.9.txt');
avgspeeda0=mean(Ya0(:,3));
avgtora0=mean(Ya0( :,1).*0.001.*0.15.*9.8)+offset;
avgrpma0=mean(Ya0(:,2))

Y7=load('runtt1.0.txt');
avgspeed7=mean(Y7(:,3));
avgtor7=mean(Y7( :,1).*0.001.*0.15.*9.8)+offset;
avgrpm7=mean(Y7(:,2));


Ya=load('runttttttt1.0.txt');
avgspeeda=mean(Ya(:,3));
avgtora=mean(Ya( :,1).*0.001.*0.15.*9.8)+offset;
avgrpma=mean(Ya(:,2));


sp=[0;0.1;0.2;0.3;avgspeed1; avgspeed2;  avgspeed3; avgspeed4; avgspeed5; avgspeed6;
avgspeeda0;avgspeed7;avgspeeda]
tor=[0;0;0;0;avgtor1; avgtor2; avgtor3; avgtor4; avgtor5; avgtor6;avgtora0; avgtor7
;avgtora]
rpm=[0;0;0;0;avgrpm1; avgrpm2 ; avgrpm3 ;avgrpm4 ;avgrpm5; avgrpm6;avgrpma0;
avgrpm7;avgrpma ]


% Second Prototype Data Manipulation in Wave Tank


offset1=0.004

Y871=load('run87tt0.4.txt');
avgspeed871=mean(Y871(:,3))
avgtor871=mean(Y871( :,1).*0.001.*0.15.*9.8)+offset1;
avgrpm871=mean(Y871(:,2))

Y872=load('run87tt0.5.txt');
avgspeed872=mean(Y872(:,3))
avgtor872=mean(Y872( :,1).*0.001.*0.15.*9.8)+offset1
avgrpm872=mean(Y872(:,2))
```

```
Y873=load('run87tt0.6.txt');
avgspeed873=mean(Y873(:,3))
avgtor873=mean(Y873( :,1).*0.001.*0.15.*9.8)+offset1
avgrpm873=mean(Y873(:,2))

Y874=load('run87tt0.7.txt');
avgspeed874=mean(Y874(:,3))
avgtor874=mean(Y874( :,1).*0.001.*0.15.*9.8)+offset1;
avgrpm874=mean(Y874(:,2))

Y875=load('run87tt0.8.txt');
avgspeed875=mean(Y875(:,3))
avgtor875=mean(Y875( :,1).*0.001.*0.15.*9.8)+offset1;
avgrpm875=mean(Y875(:,2))

Y876=load('run87tt0.9.txt');
avgspeed876=mean(Y876(:,3))
avgtor876=mean(Y876( :,1).*0.001.*0.15.*9.8)+offset1;
avgrpm876=mean(Y876(:,2))


Y877=load('run87tt1.0.txt');
avgspeed877=mean(Y877(:,3))
avgtor877=mean(Y877( :,1).*0.001.*0.15.*9.8)+offset1;
avgrpm877=mean(Y877(:,2))



sp87=[0;0.1;0.2;0.3;avgspeed871; avgspeed872;  avgspeed873; avgspeed874;
avgspeed875; avgspeed876; avgspeed877 ]
tor87=[0;0;0;0;avgtor871; avgtor872; avgtor873; avgtor874; avgtor875; avgtor876;
avgtor877 ]
rpm87=[0;0;0;0;avgrpm871; avgrpm872 ; avgrpm873 ;avgrpm874 ;avgrpm875;
avgrpm876; avgrpm877 ]

% Analysis of power coefficient curve in Water

  w=(2*pi*rpm)/60;
  P=abs(tor.*w);
  w87=(2*pi*rpm87)/60;
  P87=abs(tor87.*w87);
  D5=D^5;
  RPM=rpm.^3;
  Cp1=P./(1000.*D5.*RPM);
  Cs1=sp./(rpm.*D);
```

```
D6=D1^5;
RPM87=abs(rpm87.^3);
Cp87=P87./(1000.*D6.*RPM87);
rpm87=abs(rpm87);
Cs87=sp87./(rpm87.*D1);
figure
yy1 = smooth(Cs1,Cp1,0.1,'rloess');
[xx,ind] = sort(Cs1);
plot(xx,Cp1(ind),'w.',xx,yy1(ind),'r')
hold on
yy1 = smooth(Cs87,Cp87,0.1,'rloess');
[xx,ind] = sort(Cs87);
plot(xx,Cp87(ind),'w.',xx,yy1(ind),'b')
hold on

% First Prototype Data Manipulation in Wind Tunnel

offset=0.023;

Y1=load('runt1.txt');
avgtor1=mean(Y1(:,1)).*0.001.*9.8.*0.15+offset;
avgrpm1=mean(Y1(:,2));

Y2=load('runt2.txt');
avgtor2=mean(Y2(:,1)).*0.001.*9.8.*0.15+offset;
avgrpm2=mean(Y2(:,2));

Y3=load('runt3.txt');
avgtor3=mean(Y3(:,1)).*0.001.*9.8.*0.15+offset;
avgrpm3=mean(Y3(:,2));

Y4=load('runt4.txt');
avgtor4=mean(Y4(:,1)).*0.001.*9.8.*0.15+offset;
avgrpm4=mean(Y4(:,2));


Y5=load('runt5.txt');
avgtor5=mean(Y5(:,1)).*0.001.*9.8.*0.15+offset;
avgrpm5=mean(Y5(:,2));


Y6=load('runt6.txt');
avgtor6=mean(Y6(:,1)).*0.001.*9.8.*0.15+offset;
avgrpm6=mean(Y6(:,2));

Y7=load('runt7.txt');
```

```
avgtor7=mean(Y7(:,1)).*0.001.*9.8.*0.15+offset;
avgrpm7=mean(Y7(:,2));

Y8=load('runt8.txt');
avgtor8=mean(Y8(:,1)).*0.001.*9.8.*0.15+offset;
avgrpm8=mean(Y8(:,2));

Y9=load('runt9.txt');
avgtor9=mean(Y1(:,1)).*0.001.*9.8.*0.15+offset;
avgrpm9=mean(Y1(:,2));

Y10=load('runt10.txt');
avgtor10=mean(Y10(:,1)).*0.001.*9.8.*0.15+offset;
avgrpm10=mean(Y10(:,2));

Y11=load('runt11.txt');
avgtor11=mean(Y11(:,1)).*0.001.*9.8.*0.15+offset;
avgrpm11=mean(Y11(:,2));

Y12=load('runt12.txt');
avgtor12=mean(Y12(:,1)).*0.001.*9.8.*0.15+offset;
avgrpm12=mean(Y12(:,2));

Y13=load('runt13.txt');
avgtor13=mean(Y13(:,1)).*0.001.*9.8.*0.15+offset;
avgrpm13=mean(Y13(:,2));


Y14=load('runt14.txt');
avgtor14=mean(Y14(:,1)).*0.001.*9.8.*0.15-offset;
avgrpm14=mean(Y14(:,2));

Y15=load('runt15.txt');
avgtor15=mean(Y15(:,1)).*0.001.*9.8.*0.15-offset;
avgrpm15=mean(Y15(:,2));

Y16=load('runt16.txt');
avgtor16=mean(Y16(:,1)).*0.001.*9.8.*0.15-offset;
avgrpm16=mean(Y16(:,2));

Y17=load('runt17.txt');
avgtor17=mean(Y17(:,1)).*0.001.*9.8.*0.15-offset;
avgrpm17=mean(Y17(:,2));

Y18=load('runt18.txt');
avgtor18=mean(Y18(:,1)).*0.001.*9.8.*0.15-offset;
```

```
avgrpm18=mean(Y18(:,2));

Y19=load('runt19.txt');
avgtor19=mean(Y19(:,1)).*0.001.*9.8.*0.15-offset;
avgrpm19=mean(Y19(:,2));

Y20=load('runt20.txt');
avgtor20=mean(Y20(:,1)).*0.001.*9.8.*0.15-offset;
avgrpm20=mean(Y20(:,2));


Y21=load('runt21.txt');
avgtor21=mean(Y21(:,1)).*0.001.*9.8.*0.15-offset;
avgrpm21=mean(Y21(:,2));

Y22=load('runt22.txt');
avgtor22=mean(Y22(:,1)).*0.001.*9.8.*0.15-offset;
avgrpm22=mean(Y22(:,2));

Y23=load('runt23.txt');
avgtor23=mean(Y23(:,1)).*0.001.*9.8.*0.15-offset;
avgrpm23=mean(Y23(:,2));

Y24=load('runt24.txt');
avgtor24=mean(Y24(:,1)).*0.001.*9.8.*0.15-offset;
avgrpm24=mean(Y24(:,2));

Y25=load('runt25.txt');
avgtor25=mean(Y25(:,1)).*0.001.*9.8.*0.15-offset;
avgrpm25=mean(Y25(:,2));

Y26=load('runt26.txt');
avgtor26=mean(Y26(:,1)).*0.001.*9.8.*0.15-offset;
avgrpm26=mean(Y26(:,2));

Y27=load('runt27.txt');
avgtor27=mean(Y27(:,1)).*0.001.*9.8.*0.15-offset;
avgrpm27=mean(Y27(:,2));

Y28=load('runt28.txt');
avgtor28=mean(Y28(:,1)).*0.001.*9.8.*0.15-offset;
avgrpm28=mean(Y28(:,2));

Y29=load('runt29.txt');
avgtor29=mean(Y29(:,1)).*0.001.*9.8.*0.15-offset;
avgrpm29=mean(Y29(:,2));
```

```
Y30=load('runt30.txt');
avgtor30=mean(Y30(:,1)).*0.001.*9.8.*0.15-offset;
avgrpm30=mean(Y30(:,2));

Y30=load('runt30.txt');
avgtor30=mean(Y30(:,1)).*0.001.*9.8.*0.15-offset;
avgrpm30=mean(Y30(:,2));

Y30=load('runt30.txt');
avgtor30=mean(Y30(:,1)).*0.001.*9.8.*0.15-offset;
avgrpm30=mean(Y30(:,2));

Y31=load('runt31.txt');
avgtor31=mean(Y31(:,1)).*0.001.*9.8.*0.15-offset;
avgrpm31=mean(Y31(:,2));

Y32=load('runt32.txt');
avgtor32=mean(Y32(:,1)).*0.001.*9.8.*0.15-offset;
avgrpm32=mean(Y32(:,2));

Y33=load('runt33.txt');
avgtor33=mean(Y33(:,1)).*0.001.*9.8.*0.15-offset;
avgrpm33=mean(Y33(:,2));

Y34=load('runt34.txt');
avgtor34=mean(Y34(:,1)).*0.001.*9.8.*0.15-offset;
avgrpm34=mean(Y34(:,2));

sp=[0 1 2 3 4 5 6.25 6.25 7.1 7.1 8.1 8.1 8.1  10.1 10.1 10.1 10.1 10.1 10.1 10.1 11.0 11.0
11.0 11.0 11.0 12 12 12 12 12 12 12 13.6 13.6 13.6 13.6  ]
tor=[0 0 0 0 0 0 avgtor1 avgtor2 avgtor3 avgtor4 avgtor5 avgtor6 avgtor7  avgtor12
avgtor13 avgtor14  avgtor15 avgtor16 avgtor17 avgtor18 avgtor19 avgtor20 avgtor21
avgtor22 avgtor23 avgtor24 avgtor25 avgtor26 avgtor27 avgtor28 avgtor29 avgtor30
avgtor31 avgtor32 avgtor33 avgtor34 ]
rpm=[0 0 0 0 0 0 avgrpm1 avgrpm2  avgrpm3 avgrpm4 avgrpm5 avgrpm6 avgrpm7
avgrpm12 avgrpm13 avgrpm14 avgrpm15 avgrpm16 avgrpm17 avgrpm18 avgrpm19
avgrpm20 avgrpm21 avgrpm22 avgrpm23 avgrpm24 avgrpm25 avgrpm26 avgrpm27
avgrpm28 avgrpm29 avgrpm30 avgrpm31 avgrpm32 avgrpm33 avgrpm34 ]

 % Plotting Power coefficient curve of First Prototype in Wind

  w=abs((2*pi.*rpm)/60);
  Pm=abs(tor.*w);
  rpm=abs(rpm);
  D5=D^5;
```

```
Cp=Pm./(1.0.*D5.*rpm.^3);
Cs=sp./(rpm.*D);
yy1 = smooth(Cs,Cp,0.1,'rloess');
[xx,ind] = sort(Cs);
plot(xx,Cp(ind),'w.',xx,yy1(ind),'r')
hold on

% Second Prototype Data Manipulation in Wind Tunnel

offset1=0.038;

Y1=load('runtt1.txt');
avgtor1=mean(Y1(:,1)).*0.001.*9.8.*0.15+offset1;
avgrpm1=mean(Y1(:,2));

Y2=load('runtt2.txt');
avgtor2=mean(Y2(:,1)).*0.001.*9.8.*0.15+offset1;
avgrpm2=mean(Y2(:,2));

Y3=load('runtt3.txt');
avgtor3=mean(Y3(:,1)).*0.001.*9.8.*0.15+offset1;
avgrpm3=mean(Y3(:,2));

Y4=load('runtt4.txt');
avgtor4=mean(Y4(:,1)).*0.001.*9.8.*0.15+offset1;
avgrpm4=mean(Y4(:,2));


Y5=load('runtt5.txt');
avgtor5=mean(Y5(:,1)).*0.001.*9.8.*0.15+offset1;
avgrpm5=mean(Y5(:,2));


Y6=load('runtt6.txt');
avgtor6=mean(Y6(:,1)).*0.001.*9.8.*0.15+offset1;
avgrpm6=mean(Y6(:,2));

Y7=load('runtt7.txt');
avgtor7=mean(Y7(:,1)).*0.001.*9.8.*0.15+offset1;
avgrpm7=mean(Y7(:,2));

Y8=load('runtt8.txt');
avgtor8=mean(Y8(:,1)).*0.001.*9.8.*0.15+offset1;
avgrpm8=mean(Y8(:,2));

Y9=load('runtt9.txt');
```

```
avgtor9=mean(Y1(:,1)).*0.001.*9.8.*0.15+offset1;
avgrpm9=mean(Y1(:,2));

Y10=load('runtt10.txt');
avgtor10=mean(Y10(:,1)).*0.001.*9.8.*0.15+offset1;
avgrpm10=mean(Y10(:,2));

Y11=load('runtt11.txt');
avgtor11=mean(Y11(:,1)).*0.001.*9.8.*0.15+offset1;
avgrpm11=mean(Y11(:,2));

Y12=load('runtt12.txt');
avgtor12=mean(Y12(:,1)).*0.001.*9.8.*0.15+offset1;
avgrpm12=mean(Y12(:,2));

Y13=load('runtt13.txt');
avgtor13=mean(Y13(:,1)).*0.001.*9.8.*0.15+offset1;
avgrpm13=mean(Y13(:,2));


Y14=load('runtt14.txt');
avgtor14=mean(Y14(:,1)).*0.001.*9.8.*0.15+offset1;
avgrpm14=mean(Y14(:,2));

Y15=load('runtt15.txt');
avgtor15=mean(Y15(:,1)).*0.001.*9.8.*0.15+offset1;
avgrpm15=mean(Y15(:,2));

Y16=load('runtt16.txt');
avgtor16=mean(Y16(:,1)).*0.001.*9.8.*0.15+offset1;
avgrpm16=mean(Y16(:,2));

Y17=load('runtt17.txt');
avgtor17=mean(Y17(:,1)).*0.001.*9.8.*0.15+offset1;
avgrpm17=mean(Y17(:,2));

Y18=load('runtt18.txt');
avgtor18=mean(Y18(:,1)).*0.001.*9.8.*0.15+offset1;
avgrpm18=mean(Y18(:,2));

Y19=load('runtt19.txt');
avgtor19=mean(Y19(:,1)).*0.001.*9.8.*0.15+offset1;
avgrpm19=mean(Y19(:,2));

Y20=load('runtt20.txt');
avgtor20=mean(Y20(:,1)).*0.001.*9.8.*0.15+offset1;
```

```
avgrpm20=mean(Y20(:,2));


Y21=load('runtt21.txt');
avgtor21=mean(Y21(:,1)).*0.001.*9.8.*0.15+offset1;
avgrpm21=mean(Y21(:,2));

Y22=load('runtt22.txt');
avgtor22=mean(Y22(:,1)).*0.001.*9.8.*0.15+offset1;
avgrpm22=mean(Y22(:,2));

sp=[ 0 1 2 3 4 5 6 7.4 8.45 8.45 8.45 8.45 8.45 9 9 9 10 10 11 11 12 12 12 12 13.6 13.6
13.6 13.6 13.6]
tor=[0 0 0 0 0 0 0 avgtor1 avgtor2 avgtor3 avgtor4 avgtor5 avgtor6 avgtor7 avgtor8
avgtor9  avgtor10  avgtor11 avgtor12  avgtor13 avgtor14  avgtor15 avgtor16 avgtor17
avgtor18 avgtor19 avgtor20 avgtor21 avgtor22 ]
rpm=[0 0 0 0 0 0 0 avgrpm1 avgrpm2  avgrpm3 avgrpm4 avgrpm5 avgrpm6 avgrpm7
avgrpm8 avgrpm9 avgrpm10  avgrpm11 avgrpm12 avgrpm13 avgrpm14 avgrpm15
avgrpm16 avgrpm17 avgrpm18 avgrpm19 avgrpm20 avgrpm21 avgrpm22 ]


% Plotting Power coefficient curve of Second Prototype in Wind

  w=abs((2*pi.*rpm)/60);
  Pm=abs(tor.*w);
  rpm=abs(rpm);
  D5=D1^5;
  Cp=Pm./(1.0.*D5.*rpm.^3);
  Cs=sp./(rpm.*D1);
  yy1 = smooth(Cs,Cp,0.1,'rloess');
  [xx,ind] = sort(Cs);
  plot(xx,Cp(ind),'w.',xx,yy1(ind),'b')
  set(gca,'XLim',[0 1.0])
  set(gca,'YLim',[0 0.01])
  xlabel('Flow Coefficient(Cs)')
  ylabel('Power Coefficient(Cp)')
  title('Power coefficient of Two Prototypes Using Approach A')
  grid
```

Appendix C

C.1 Boost Converter Design

```
% Input parameters to boost converter

f=5000;        % f is switching frequency
rip=0.001;     % rip is the  desired  voltage ripple(del_Vout/Vout)
n=0.8;         % n is the converter expected frequency
Vf=0.7;        % Vf is the diode voltage

% Duty cycle of boost converter

Gain=2.5;
Vin=0:0.5:8.2;          % Vin is the input voltage
Vout=Gain.*Vin;         % Vout is the output voltage
D=(Vout-Vin)./Vout      % D is the duty ratio
T=1/f                   % T is time period
Ton=D.*T                % Ton is on time
Toff=(1-D).*T           % Toff is off time

% Parameters of boost converter

R=50;                          % R is resistor at output
Lmin=(R./(2*f)).*D.*(1-D).*(1-D);  % Lmin is minimum inductance for conduction
model
L=1.2*Lmin;                    % L is inductance to meet design requirement
C=D/(R.*f*rip);                % C is capacitor to eliminate ripple

% Experimental Results

Vin1=[0 1.04 3.04 4.42 5.08 6.49 7.42 8.24];
Vout1=[0 2.17 7.6 11.4 13.01 15.7 18.48 19.79];
In1= [0 0.20 0.89 1.02 1.12 1.31 1.48 1.55];
Iout1=[0 0.06 0.15 0.23 0.27 0.32 0.38 0.41];
Pin1=Vin1.*In1;
Pout1=Vout1.*Iout1;
```

```
% Output parameters of boost converter


Io=Vout/R                  % Io is the output current
Po=Io.*Vout;               % Calculating power
del_I=((Vin)./L).*D*T      % del_I is the peak to peak ripple current
Iavg=Io./(1-D)             % Iavg is the average current in inductor
Imax=Iavg+((del_I)/2)      % Imax is the maximum current
Imin=Iavg-((del_I)/2)      % Imin is the minimum current
figure
plot(Vin,Po,'-*')
hold on
plot(Vin1,Pout1,'-r*')
xlabel('Input Voltage(V)')
ylabel('Output power(W)')
title('Output Power of  DC DC Converter')
grid
figure
plot(Vout,Io,'-*')
hold on
plot(Vout1,Iout1,'-r*')
xlabel('Output Voltage(V)')
ylabel('Output Current(A)')
title('Output Voltage and Current')
grid
figure
plot(Vin,Vout,'-*')
hold on
plot(Vin1,Vout1,'-r*')
xlabel('Input Voltage(V)')
ylabel('Output Voltage(V)')
title('Output Voltage Vs Input Voltage ')
grid
figure
plot(Vout,Po,'-*')
hold on
plot(Vout1,Pout1,'-r*')
xlabel('Output Voltage(V)')
ylabel('Output Power(W)')
title('Output Power Vs Voltage')
grid
n=Pout1./Pin1
figure
plot(Vin1,n,'*')
xlabel('Input Voltage(V)')
ylabel('Output Power(W)')
```

```
title('Output Power Vs Voltage')
grid


% fs=(2*Io*(Vout-Vin+Vf))/(Imin+(Vin/L)*T)
 rip_percent=(del_I./Iavg)*100                    % rip_percent is the percentage of ripple
```

Appendix D

D.1

```
/*
-Start the pwm to the MOSFET  at some set value
-measure the current Input
-measure the voltage of the bus
-calculate the power
-increment the turn on period of the pwm
-measure the current and bus voltage again
-calculate the new power value
-if the power has dropped, reduce the duty cycle of the pwm
-if the power has increased, increase the duty cycle of the pwm
-repeat the steps
*/

#include <16f877.h>
#DEVICE *=16 ADC=10
#use Delay(Clock=20000000)
#use rs232(baud=9600, xmit=PIN_C6, rcv=PIN_C7)

// intialize constants and varibles

  CONST float Vref = 18;
  CONST long d_hill = -1;
  CONST byte in_volt = 0, in_amp = 1, out_volt = 2, out_amp = 3;
  float input_current, output_current, input_voltage, output_voltage;
  float input_power, output_power,old_output_power;
  float gain, g_watts, g_amp, g_volt;
  long u_hill = 1, pwm_max, pwm;
  long boost = 0, boost_gain;
  boolean run;

// Global Variables
boolean meas_done = FALSE, once = TRUE ;
unsigned int8  loops = 0;
unsigned int32 RPM, sensor_pulses = 0;


#int_EXT
EXT_isr(){

 if(!meas_done){
 sensor_pulses++;     // Sensor pulses into PIN_B0
 }
```

```
}

#int_TIMER1
TIMER1_isr(){

 if(loops){
 loops--;
 }
 else if(loops==0){
 meas_done=TRUE;
 }
}

//-----------------------------------------------------------------------
// This function is used to set the duty cycle of the PWM output. It uses the built
// in C compiler function set_pwm1_duty to set the duty cycle.
//-----------------------------------------------------------------------
  void pwm_duty(long pwm_percent, long pwm_maximum) {

  set_pwm1_duty((pwm_maximum/100)*pwm_percent);   // set PWM #1 duty cycle
}

void start_measurement(){

if (once == TRUE){      // only executes once until measurement is complete.

  meas_done=FALSE;
  loops = 19;        // 52.5ms * 19 = ~1000ms(997.6ms)
                // This is the measurement window time

  enable_interrupts(INT_TIMER1);// To create a measurement window
  enable_interrupts(INT_EXT);   // Generate an interrupt every pulse
                        // comming from the sensor
  set_timer1(0);
  once = FALSE;
  }
}
 float input_channel(byte chan) {

  int i,avg_num =30;
  float avg = 0;

  set_adc_channel(chan);
  delay_us(100);
  for (i=1; i<=avg_num; ++i) {
    avg += read_adc();
```

```
    delay_us(100);
  }
  return(avg/avg_num);
}

// Input voltage,current and power

void in_power(){
input_voltage = input_channel(in_volt)*0.01900125;
input_current =((0.0262*( input_channel(in_amp))) -(2.8332));
input_power = input_current * input_voltage;

}

//Output voltage,current and power

void out_power(){
output_voltage = input_channel(out_volt)*0.01922125;
output_current=((0.0258*( input_channel(out_amp))) -(2.8332));
output_power = output_current * output_voltage;
}

void main()
{
 // initialize encoder

  setup_timer_1(T1_INTERNAL | T1_DIV_BY_4);  //interrups every 0.0525088s
  ext_int_edge(H_TO_L);
  enable_interrupts(GLOBAL);

  // initialize hardware

  setup_port_a(ALL_ANALOG);              // set up A/D channels
  setup_adc(adc_clock_div_32);           // start A/D clocks
  setup_timer_2(T2_DIV_BY_4,249,1);      // pwm frequency 5kHz
  setup_ccp1(CCP_PWM);                   // Configure CCP1 as a PWM
  pwm_max = 400;                  // maximum value for PWM based on frequency
  pwm = 0;                  // set pwm to 85% to start
  pwm_duty(pwm, pwm_max);     // set pwm duty cycle to pwm100 value
  output_high(PIN_C3);                // set enable pin on FET driver
  output_high(PIN_C0);              // turn on green led
  delay_ms(1000);                 // delay to get started
```

```
for (;;) {                          // loop forever


start_measurement();

if (meas_done){                 // only updates when measurement is complete.
disable_interrupts(INT_EXT);
disable_interrupts(INT_TIMER1);
RPM = (sensor_pulses * 60)/256;
sensor_pulses = 0;
once = TRUE;
}



in_power();
out_power();

   if (output_voltage> Vref) {
      u_hill =d_hill;
      output_high(PIN_C5);
      }



   else if (old_output_power > output_power) {
      u_hill = -u_hill;
      output_low(PIN_C5);
    }
    old_output_power = output_power;
    pwm+= u_hill;
    if (pwm> pwm_max) pwm= pwm_max;
     else if (pwm < 0) pwm =0;
       pwm_duty(pwm, pwm_max);



      if ((++boost_gain % 10) == 0) {
      pwm_duty(100, pwm_max);
      delay_ms(20);
      g_volt = input_channel(in_volt)*0.01900125;
      g_amp =((0.0262*( input_channel(in_amp))) -(2.8332));
      if (g_amp < 0.05) {
        output_high(PIN_C4);
        output_low(PIN_C3);
```

```
        delay_ms(1000);
      }
       g_watts = g_amp * g_volt;
      gain = input_power /g_watts;
      boost = (long)((gain * 100) - 100);
    }


printf(" %4.2F  %4.2F  %04lu %04lu \n \r"input_power,output_power,RPM,pwm);

 delay_ms(500);
 run=TRUE;
  }                    //end forever loop
}                      //end main
```